The Effects of Silica Support on Kinetic Behavior and Polymer Properties of Heterogonous Metallocene Catalyst

By

Abdulrahman Yousef Ashri

A thesis submitted to the Department of Chemical Engineering

In conformity with the requirements for

the degree of Master of Applied Science

Queen's University

Kingston, Ontario, Canada

(April, 2012)

Abstract

The heterogeneous metallocene catalyst is becoming a very competitive industrially due to its ability to produce tailor-made polymers. The main advantage of the metallocene polymer product is the narrow molecular weight distribution (MWD) and the systematic comonomer distribution along the polymer chains. Therefore, the metallocene polymer product has well-defined mechanical and optical properties. The aim of this thesis is to investigate the effects of the silica support on the reaction kinetics and micro properties of the heterogeneous metallocene catalyst system. These investigations include studying the influence of the pore volume, surface area, particle size distribution, and the surface chemical characteristics of silica support on the catalyst performance.

The experiments showed that the silica type has an influence on the kinetic behavior. For instance, silica with a lower pore volume shows an induction period when compared with higher pore volume silicas. Moreover, the silica type has a clear influence on catalyst activity and polymer morphology. The smallest silica particles produced the highest activity among the other sizes regardless of silica type. The supported catalysts were characterized and linked to the silica type and size in terms of catalyst activity and polymer morphology. Each catalyst in terms of silica type behaved similarly regardless of type of alkylaluminum used in the formulation.

The micro properties of the produced polymers, such as MWD and chemical composition distribution (CCD), were studied to understand the effects of the type and size of silica support and co-catalyst on these properties. The silica types showed no effect on the MWD, but had a slight effect on the CCD. Silica with a high pore volume had a stronger more comonomer response. However, the silica particle size had an influence on the CCD, with less comonomer incorporation observed with smaller silica particles. Finally, triethylauminum was observed to produce polymer with a different MWD when compared with other alkylaluminums. However, all alkylaluminums used in this work had no effect on the CCD of the produced polymer regardless of silica type.

Acknowledgments

I would like it thank both of my supervisors Drs. Timothy F.L. McKenna and João Soares for their support and guidance through my studies. Without them, this work would not have been as focused as it turned out to be.

Many thanks go to my lab mates who have helped me by advising me and giving me some of their time to finish this project.

My continuous thanks go to my parents and my wife for their love, support and incentive. They did their best to encourage me to finish this project.

Table of Contents

List of Tables

List of Figures

Nomenclature

Acronyms

PE - Polyethylene
HDPE - High-density polyethylene
MDPE – Medium density polyethylene
LDPE - Low-density polyethylene
CCD - Chemical Composition Distribution
CEF - Crystallization Elution Fractionation
CRYSTAF - Crystallization Elution Fractionation
DSC - Differential Scanning Calorimetry
GPC - Gel Permeation Chromatography
LCBs - Long chain branches
LLDPE - Linear low-density polyethylene
MAO - Methylaluminoxane
MW - Molecular Weight
MWD - Molecular Weight Distribution
Mn- Number Average Molecular Weight
Mw- Weight Average Molecular Weight
PDI - Polydispersity Index
SCBs - Short chain branches
TCB - Trichlorobenzene
TCE - Terachloroethane
TREF - Temperature Rising Elution Fractionation
TMA - Trimethylaluminum
CSTR- Continuous Stirred Tank Reactor
MFI - Melt Flow Index
FBR- Fluidized Bed Reactor
ZN- Ziegler-Natta
MAO - methyl aluminoxane
TMA - trimethylaluminum
TEAL - Triethyl aluminum
TOAL - Tri-n-octyl aluminum
TIBAL - Tri iso butyl aluminum
Cp2Zr2Cl2 - Bis-Cyclopentadienyl zirconium dichloride
ICP - Inductively coupled plasma
TGA - Thermal gravimetric analysis

Chapter 1

Introduction

This master thesis focuses on the effect of the physical properties of the support on the catalyst performance and microstructure of the product. The motivation for this study is that metallocenes are becoming more commercially competitive, and different technologies are for its use. Metallocenes can be utilized either as homogenous or heterogeneous catalysts in different processes to produce a wide range of polyolefins products. In the case of heterogeneous catalysts, different supports can be used to support the metallocene, and there are many supporting techniques that have been utilized depending on the catalyst system. The focus of the current study was on silica-supported (heterogeneous) metallocene catalysts used in ethylene and ethylene/1-hexene polymerization.

The purpose of this thesis is to investigate the influence of the physical properties of the silica support on the kinetic behavior, process stability, morphology control, and microstructure of the product. Therefore, this research started (chapter 2) with a literature review that discussed the general literature pertinent to the thesis. This will give an overview of the importance of this research and the objectives of the thesis in its entirety.

This thesis is based on an experimental approach to explore each research objective. Chapter 3 will describe the details of the supporting technique utilized to immobilize the metallocene on the silicas. Also, chapter 4 will describe how the general

polymerization procedure was decided upon, and the results collected. Included are the results found with respect to each silica type with different particle size.

Polymer Characterization (Chapter 5) discusses the results from the analysis of the polymers resulting from the previous chapter. This chapter deals with the actual microstructure, which was investigated by using Gel Permeation Chromatography (GPC) to determine molecular weight and molecular weight distribution. Crystallization Elution Fractionation (CEF) was utilized to determine the chemical composition distribution (CCD)

Chapter 2

Literature Review

2.1 An Introduction to Polyethylene and Its Manufacturing

In terms of tonnage, polyethylene is the most widely produced polymer in the world, with production in 2010 being on the order 80 million tones [1]. There are many reasons for the economic importance of polyethylene. PE has good physical and mechanical properties, high chemical resistance, zero toxicity, good bio-acceptability, and has low negative environmental impact. At least as importantly, it is relatively inexpensive to make [2-6].

2.1.1. Types of Polyethylene

High density polyethylene (HDPE) accounted for around 45% of global consumption, followed by linear low density polyethylene (LLDPE) and low density polyethylene (LDPE). HDPE and LLDPE are produced using catalytic processes, and LDPE is made using free radical chemistry at pressures of 1500-2500 bars, and temperatures on the order of 150-275 °C. HDPE is used for blow molding, film/sheet, injection molding, and pipe/conduit applications. Almost all LLDPE is used for film/sheet applications with smaller amounts used for injection molding. Over half of LDPE is used for film/sheet applications, with extrusion coating, wire and cable and injection molding also being important end user applications.

These major families of PE products are often further classified into different subtypes, depending mainly on the amount and type of branching, crystal structure and molecular weight. These include:

- High density polyethylene (HDPE)
- High density cross-linked polyethylene (HDXLPE)
- Cross-linked polyethylene (PEX or XLPE)
- Medium density polyethylene (MDPE)
- Linear low density polyethylene (LLDPE)
- Low density polyethylene (LDPE)
- Very low density polyethylene (VLDPE)
- Ultra high molecular weight polyethylene (UHMWPE)
- Ultra low molecular weight polyethylene (ULMWPE or PE-WAX)
- High molecular weight polyethylene (HMWPE)

With the exception of LDPE, the physical properties of these types of polyethylene are controlled mainly by varying the concentration of hydrogen, which is a chain termination agent used to limit the molecular weight. Different comonomer types and concentrations are used to control the crystallinity; incorporating small amounts of alpha olefins into the backbone of the polymer chain decreases the ability of the macromolecules to form crystals, and since crystalline PE is denser than amorphous PE, this also controls the density. HDPE has essentially no comonomer, where as LLDPE contains up to 10% of a comonomer. In addition, the way in which the PE is extruded after the reaction also has a significant effect on the physical properties of the PE.

2.1.2 Ethylene Polymerization Processes

Polyethylene can be produced industrially by four different processes: solution, slurry, gas phase, and high pressure processes. The first three employ catalysts to promote the polymerization, with a molecular catalyst being used in the solution process, and supported catalysts being used in the other two. In the rest of this thesis, we will focus on catalyzed ethylene polymerization in a slurry processes. For this reason, we will no longer discuss the (commercially important) high pressure process for LDPE, and will briefly mentioned the catalyzed solution processes to contrast them with the use of supported catalysts. The various polymerization processes and reactor operating conditions for catalyzed polymerizations are listed in Table 2.1 [7].

Table 2.1: Process and reactor operating conditions for catalyzed polymerization processes [7] [8]

	Solution	Slurry	Gas-phase
Reactor type	CSTR (1-2 in cascade)	Loop or CSTR (1-3 in cascade)	Fluidized bed (1-2 in cascade)
Pressure, atm	~100	30-35	20-35
Temperature, °C	150-300	85-110	70-120
Polymerization media	Solvent	Solid	Solid
Density range, g/cm^3	0.910-0.970	0.930-0.970	0.910-0.970
MFI, g/10 min	0.5-105	0.01-80	0.01-200

Combinations of reactors are often used in order to tailor the molecular properties of the final product. For instance, fluidized bed reactors can be used in series in order to make a

PE with a bimodal molecular weight distribution (MWD), with the low molecular weight component made in one reactor in the presence of hydrogen, and a high molecular weight component being made in the other reactor containing little to no hydrogen. The following sections will describe each process, and mention some of their advantages and disadvantages.

2.1.2.1 Solution Processes

The reaction is performed relatively at high temperature in the range of 150-300°C, in order to keep the polymer in solution. A homogeneous catalyst, the monomer(s) and polymer all remain dissolved in a hydrocarbon diluent such as cyclohexane. Typically, a low molecular weight polymer is produced with this type of technology, having a density between 0.86 to 0.96 g/cm³. This type of process is the only technology capable to produce high quality LLDPE film resin based on octene-1 comonomer. Gas phase and slurry processes cannot be used for this grade due to high stickiness and ease of dissolution in the continuous phase of the slurry process.

Because of the high reaction rates possible with the molecular catalysts used in these processes, the continuous reactors typically have very short residence times (from 2 up to 30 minutes) which makes it flexible and able to produce a wide range of products, with minimum loss of materials between the grade transitions. However, solution processes suffer from high investment and energy costs, which can be resolved by process simplification, lowering the operating cost [9].

2.1.2.2 Slurry Processes

Slurry processes can be used to produce both polyethylene and polypropylene, using continuous loop(s) or continuous stirred tank reactor (CSTR). The first loop reactor system was developed by Philips Petroleum, and has been exploited commercially since 1970. In an ethylene polymerization process, the reactor contains a dispersion of solid catalyst/polymer particles in a hydrocarbon diluent, typically isobutane or hexane, in which the monomers are dissolved. Polymerization takes place at temperatures between 85-110°C and pressures of up to 30-45 bar. As in the gas phase process, the catalysts are supported on solid particles, typically silica or magnesium dichloride ($MgCl_2$), and the polymer grows inside the pores and on the surfaces of the catalyst particles. Developments in catalyst technology now allow producers to recover the solid particles directly from the reactor and to process them without needing to remove the catalyst residue. The polyethylene produced in a loop reactor usually has a density in the range of 0.93 – 0.97g/cm³ (MDPE and HDPE), with broad MWD suitable for blow molding, film, and pipe applications [9, 10].

The two main process disadvantages of slurry loop reactors are: relatively high investment cost associated with a process which requires many polymer and hydrocarbon recovery steps; the process cannot be used to produce low density materials because of polymer solubility problems in the reactor [9].

In the case of CSTR reactor, the heat of reaction typically is removed through a cooling jacket. The different reactor format means that the CSTR has a much lower surface per unit volume ratio, so less heat can be removed from this type of reactor than can be

removed from the loop. This in turn means that the productivity in a CSTR-based process is necessarily lower than that of a loop process.

2.1.2.3 Gas-phase Processes

Gas phase processes are the most widespread in the polyethylene industry because they are the only processes capable of producing a full range of polyethylene grades having different densities and melt flow indexes (MFI). In gas phase ethylene polymerization, the catalyst and polymer particles are dispersed in a fluidized bed reactor (FBR). The fluidized bed reactor is a large cylindrical reactor filled with polymer resin and catalyst particles. The reactor content is fluidized by a gas flowing through a distributor plate at the entrance to the vertical cylinder. The flow rate must be set carefully since the gas must move fast enough to suspend the bed above the distributor plate, but slow enough to avoid blowing the particles out through the top of the reactor. In order to facilitate this task, the top section of an FBR has a diameter of 2-3 times that of the main section of the reactor in order to reduce the superficial gas velocity, and fine particles to fall back down into the main section of the reactor. The fluidizing gas stream consists of a mixture of monomers and inerts used to adjust the partial pressure of the mixture and improve the heat transfer characteristics of the bed. Nitrogen and propane are the process gases that are most widely used for this purpose. The operating conditions of commercial gas phase reactors are from 85 to 110°C and from 20 to 35 bar pressure, depending on the type of the polyethylene [11].

Gas phase processes have some disadvantages. In particular, heat removal is critical because of the reactor is not properly cooled; agglomeration and chunk formation can result. Moreover, a large amount of off-spec polymer is generated during grade transition, especially for transition from HDPE to LLDPE, or changing from one catalyst to another catalyst type because the reactors typically have residence times on the order of 2 to 3 hours. . Specific details regarding these processes can be found in references [7, 12–14].

2.2 Silica Supports

As mentioned above, a significant fraction of the polyethylene made in the world at the current time uses supported catalysts. The major types of catalysts used commercially include Ziegler-Natta (ZN), metallocene and chromium oxide (also called Phillips catalysts in popular jargon). ZN catalysts used for ethylene polymerization are typically titanium tetrachloride-based active sites, co-crystallized with $MgCl_2$, which serves as the support material and enhances the reaction. Some ZN catalysts can be supported on silica, but with a layer of $MgCl_2$ being first deposited on the silica. Chromium oxide catalysts are more pertinent in terms of the work presented in this thesis, in the sense that they, like metallocenes, are supported on silica. The remainder of this discussion will focus on silica supports in the context of producing metallocenes for ethylene polymerization. For more discussion of how silica is used to support other catalysts, the interested reader is referred to reference [18].

The inherent physical properties of silica make it one of the best supports available for polymerization catalysts. It is considered to be chemically inert, stable at a high temperature, and has high pore volume and surface area that allow us to deposit a large

(commercially viable) quantity of active sites in the particles. Moreover, the physical properties of the silica can be tailored during the synthesis in order to suit the targeted application. In addition, silica is relatively inexpensive, which makes it an appropriate choice for commodity polymer production. There are many forms of silica including anhydrous crystalline such as quartz, tridymite, and critobalite. However, the most common kind used in catalyst supporting is the amorphous form.

The physical properties of the silica play a very important role in controlling the catalyst performance. The pore size, pore volume, and fragility of the silica influence the fragmentation of the support which in turn influences the catalyst activity and polymer morphology (fragmentation will be discussed in more detail below). In addition, the chemical properties of the silica are very important for the catalyst activity, especially in terms of how active sites of the catalyst are anchored on the surface of the pores. This is generally controlled by the level of silanol groups on the silica's surface. Furthermore, since silica is a hydrophilic material, the hydroxylated silica can easily adsorb moisture. The quantity of hydroxyl groups needs to be controlled in order to avoid catalyst deactivation. Moreover, in case of supporting metallocenes using methyl aluminoxane (MAO), free trimethylaluminum (TMA) in solution with MAS that can react with the absorbed water to produce free MAO, which in turns could react in a homogeneous form causing reactor fouling. For this reason, silica is treated thermally and chemically before use as a catalyst support (this will be discussed in more detail in Chapter 3, where the supporting method used for our catalysts is presented). In all, the thermal and chemical treatments should leave approximately 1 OH group per nm^2 left on silica.

It should be noted that care must be taken during thermal treatment since at around 900 C, the amorphous silica starts to sinter and the pore structure begins to collapse. If this happens, the support loses its high surface area as the small pores begin to fuse together forming larger pores. Sintering can also be promoted by the alkali metals which will enhance the formation and the breakage of Si-O-Si bonds, and also leads to a reduction of the pore size [15, 16].

2.2.1 Silica Manufacturing

The silica used as a catalyst support is a synthetic amorphous gel that is highly porous with pore volume in the range of 1.0-2.5 ml/g SiO, and high surface area 200-600 m^2/g SiO. The shape, size, porosity, and surface area are very important as they can be used to control the activity and morphology of the final polymer particles. In addition, the silica particles should have optimum mechanical strength to keep its shape during catalyst preparation, handling and feeding, yet have enough fragility to be able to fragment during polymerization.

The surface area, pore volume, pore size, and shape of the silica can be controlled during its manufacturing, or can be modified after this step. Typically, the silica gel is produced in a pipeline mixing process by reacting sodium silicate and a mineral acid. Usually, when the sulfuric acid is used silichydroxide and $NaSO_4$ are produced. During the acidification, the solution starts condensing until polymeric micelles are formed. The degree of polymerization increases with the increase of the solution concentration, and more importantly with decreasing the pH of the solution. The size of the micelles can be

adjusted by changing the pH of the solution. At higher pH, the micelles are larger which can decrease the final surface area and pore volume of the silica [17, 18].

Afterwards, the micelles (hydrosol) will start coalescence and three dimensional networks are formed through hydrogen bridges between the hydroxyl groups on the surface of the micelles. The hydrogel is a network of condensed primary colloidal particles, which are usually a few nanometers in diameter. During this step the pH and temperature of the solution are very important in controlling the hydrogel formation time. The degree of cross-linking of these hydrogels will affect the fragility of the final silica and so must be accurately controlled. Smaller particles are dissolved and reprecipitated on the larger particles (Ostwald ripening), and this will reduce the surface area of the particles as shown in Figure 2.1. These steps are very important for supports used for polyolefin catalysts because this is what gives the catalyst its mechanical strength, which is very important in fragmentation (see below in Section 1.3.1) [17, 18].

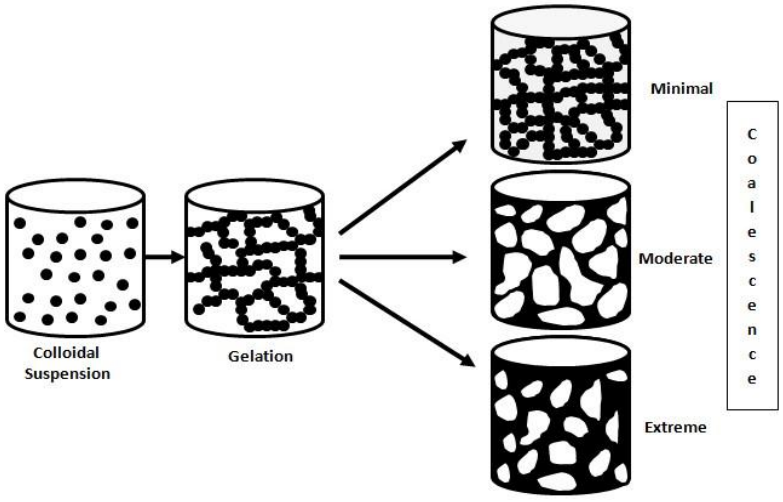

Figure 2.1: Silica gel formation

The resulting silica gel needs to be washed in order to remove the dissolved salts from the silica matrix. The residual salts in the final silica can influence the thermal and electrical properties. The thermal stability of the silica strongly depends on the level of the salt which is controlled by the degree of washing. High Na_2O concentrations reduce the melting point of the silica, which will strongly decrease the surface area and pore size due to increased sintering of the silica at high calcination temperatures.

The final step in silica manufacturing is drying. During this step the pore volume of the silica particles decreases drastically due to the shrinkage of the silica particles. Usually, the pore volume before drying is around 4-5 ml/g SiO_2, but the drying normally drops it to about 1-2 ml/g SiO_2. The final mean pore diameter is typically in the range of 10 to 30 nm. As a general rule, the faster the drying occurs, the larger the pore volume. Therefore, if small pores and high porosity is targeted, the silica needs to be dried quickly. Emulsification can also be used as an alternative drying technique with the silica gel [18, 19].

As mentioned above, the physical properties of the silica can be also modified after manufacturing. There are many techniques (chemical or physical) that can be implemented on the silica to mainly change the surface area, pore volume, pore size, and pore size distribution. The more important ones include the use of an alkaline aging agent, hydrothermal treatment, or the use of a fluxing agent. The use of an alkaline aging agent has relatively similar affect as the aging step in silica manufacturing. Where the average pore diameter tends to increase at first, but then it begins to decrease again with

severe ripening. The use of an alkaline agent will affect the surface curvature of the silica particle, which can be changed from highly convex to concave with primary particle coalescence. Thus, alkaline aging is another mean to initiate fusion of primary particles within the silica gel matrix. This can be done by soaking the silica in an ammonium hydroxide solution with of pH 10 [17, 19, 20].

Hydrothermal treatment is another method that can be used to fuse the primary particles and thus reinforce the silica gel network. It consists of treating the silica, even in its dried state, with steam or water vapor at high temperatures; the surface area decreases markedly with increasing severity of the hydrothermal treatment. Pore volume also declines, although not quite as severely, and pore diameter increases as a function of the severity of the hydrothermal treatment [17, 21].

Still another way of lowering the surface area through fusion of particles is the treatment of the dried silica with a fluxing agent such as sodium, potassium, or other group 1 metal ions before calcination. Such metals are known to act as a flux during calcinating, catalyzing the creation, and breaking of Si-O-Si bonds. Thus, with high calcination temperature and high metal loading, more sintering will occur due to the reduction in melting temperature. This drastically lowers the surface area due to primary particle fusion.

There are a variety of commercial silicas available in the market that are made by many different process technologies (e.g.pyrogenic silicas, precipitated silicas, colloidal

silicas). Silica gels used for polyolefin catalysts, desiccants, and chromatography are usually produced by precipitation. It should also be noted that given the complexity of the steps in the manufacturing process, the same silica type from different manufacturers will have different responses to the process parameters.

2.2.2 Silica Dehydration

One of the crucial steps in immobilization of the precursor on the support surface is calcination. Since the silica is a hydrophilic material it is capable of absorbing water rapidly from the moisture in the air. The existence of any trace of water on the silica surface will reduce the catalyst activity dramatically. In the silica dehydration (calcination) process, the physically adsorbed water will be removed simply by heating the silica to 100-200 °C. However, most of the geminal and vicinal hydroxyl groups still remain on the silica surface at this temperature. The level of hydroxyl groups can be controlled by heating the silica to 600-800 °C, and that will be reflected directly on the catalyst activity. This will produce silica that is almost completely dehydroxylated, with essentially only isolated silanol groups remaining, as illustrated in Figure 2.2.

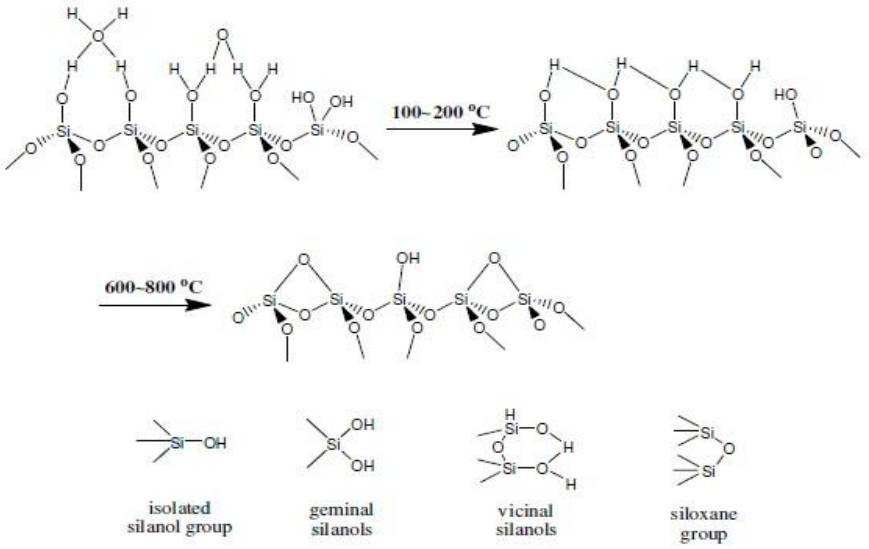

Figure 2.2: Demonstration of the dehydration of a silica surface [23]

Support homogeneity is another important point which needs to be ensured during catalyst preparation. This includes the distribution of isolated hydroxyl groups (vicinal or geminal) on the silica support, which may affect the supporting mechanism leading to a variety of active of sites (non-single site behavior) [24, 25]. All of the silica particles in a batch need to be exposed to the same conditions in terms of temperature, nitrogen or air flow.

2.2.3. Metallocene Supporting on Silica

Many supporting techniques have been used to immobilize metallocene on silica.. The supporting techniques shown in Table 2.2 are an overview of the better known techniques described in the open literature. Then can be divided into two main methods; physical absorption and chemical methods. All rely on some sort of activator (in addition to the support itself and the active site), the most common of which is methyl aluminumoxane

(MAO). Before describing the different supporting methods, it is important to understand the role of the activator.

Table 2.2: Method for supporting metallocene on silica

Supporting Method	Physical absorption	Chemical
Method-A	SiO2 + Metallocene + Activator	SiO2-OH + Metallocene + Activator
Method-B	SiO2 + Activator + Metallocene	Si-O-Si + Metallocene + Activator
Method-C	SiO2 + (Metallocene + Activator)	

2.2.3.1 The Role of Co-catalyst or Activators

The role played by the co-catalysts or activators in metallo-organic catalyst systems is very important. Activators are essential to produce active sites, and the catalyst precursor must be contacted with an effective activator during catalyst supporting or/and polymerization. The activator type is very important if we are to achieve high catalyst activity, and specific activators are generally matched with a specific catalyst system. Typically, during the activation step, the co-catalyst will become an anion, which is very important in catalytic active cation-anion ion pair. The electronegativity of the catalyst system may have a significant influence on polymerization characteristics and polymer properties. Many studies have been conducted in this area with different catalysts and co-catalysts, including both homogeneous and heterogeneous systems. For a review of these studies, the interested reader is referred to reference [26]. In what follows we will

present a brief overview of the subject in order to put the work done in the following chapters into perspective.

An aluminoxane is a compound produced from an alkyaluminium under controlled hydrolysis. There are many types of aluminoxane available on the market, including ethylaluminoxane and isobutylaluminoxane. However, the consensus from the literature and from polymer producers is that the highest activity could be obtained with methylaluminoxane as a co-catalyst for most metallocene polymerizations. Despite the importance and relatively widespread use of MAO in metallocene polymerizations, and even with the extensive research done in this area, the exact composition and structure of the MAO is still unknown [27, 28]. MAO is produced by hydrolyzing trimethyl aluminum under controlled conditions. This reaction will produce a compound in which aluminum and oxygen are arranged alternatively and the free valences are saturated with methyl groups. Some of the proposed structures of the MAO in the literature [29, 30] are shown in Figure 2.3.

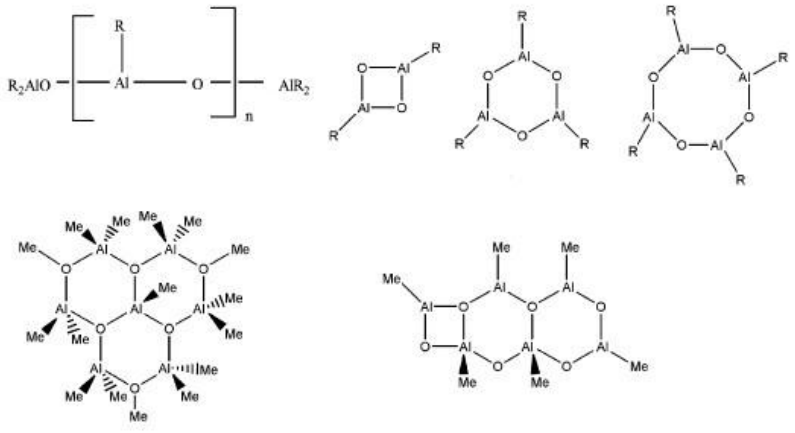

Figure 2.3: Some of the possible structures of MAO [31]

The three and four coordinate Al structures are the most probable structures, based on several NMR studies [32]. The structures are possibly created by a reversible methyl exchange between MAO and metallocene. Therefore, the molecular weight of the MAO probably varies between 1100 and 1600 g/mol.

One of the problems associated with MAO is its instability during storage, when it is diluted, and this might lead to change in its molecular weight and real concentration due to agglomeration [29, 30]. Nevertheless, despite its instability in solution, MAO is still a very effective co-catalyst in metallocene polymerization. The difficulty in determining the exact structure could be related to the multiple equilibriums between the residual trimethylaluminum (TMA) in the MAO solution. The equilibrium in MAO solution is unstable due to the partial hydrolysis during the manufacturing [33]. Furthermore, free or unreacted TMA in the MAO solution has a negative effect on the polymerization. For instance, high levels of TMA during ethylene polymerization with zirconocene tend to reduce both the activity of the catalyst and molecular weight of the polymer [34, 35, and 36]. In addition to the instability problem, MAO is expensive. In order to overcome these problems, many researches were conducted to find out another activator that could produce a high activity with better shelf life and lower cost. However, MAO still has the best performance as a co-catalyst in homogenous metallocene system. For this reason, we have chosen to begin working with MAO as the initial co-catalyst/activator in the work presented below, but will explore the role of different types of alkyl aluminums as scavengers during the polymerization reaction.

2.2.3.2 Physical Absorption Methods

Supporting methods relying on physical absorption are commonly used due to their simplicity and lower cost [37, 48]. As mentioned above, the hydroxyl groups on the silica surface are very important for the catalyst activity, so the concentration of hydroxyl groups needs to be carefully maintained during the calcination step to avoid a significant reduction in the catalyst activity.

In Method-A (Table 2.2), shown in Figure 2.4, the metallocene compound will be deposited first on the silica, and then reacted with an activator such as methylaluminoxane (MAO). This method is highly dependent on the prior thermal treatment as that will control the hydroxyl density on the silica surface. Alternately, the hydroxyl groups on the silica surface could be treated chemically via a dehydroxylation agent such as hexamethyldisilazine, which will form functional groups and produce an active catalyst [38]. Regardless of how it is done, an increase in the number of reactive siloxane groups will lead to active immobilized metallocene sites [39].

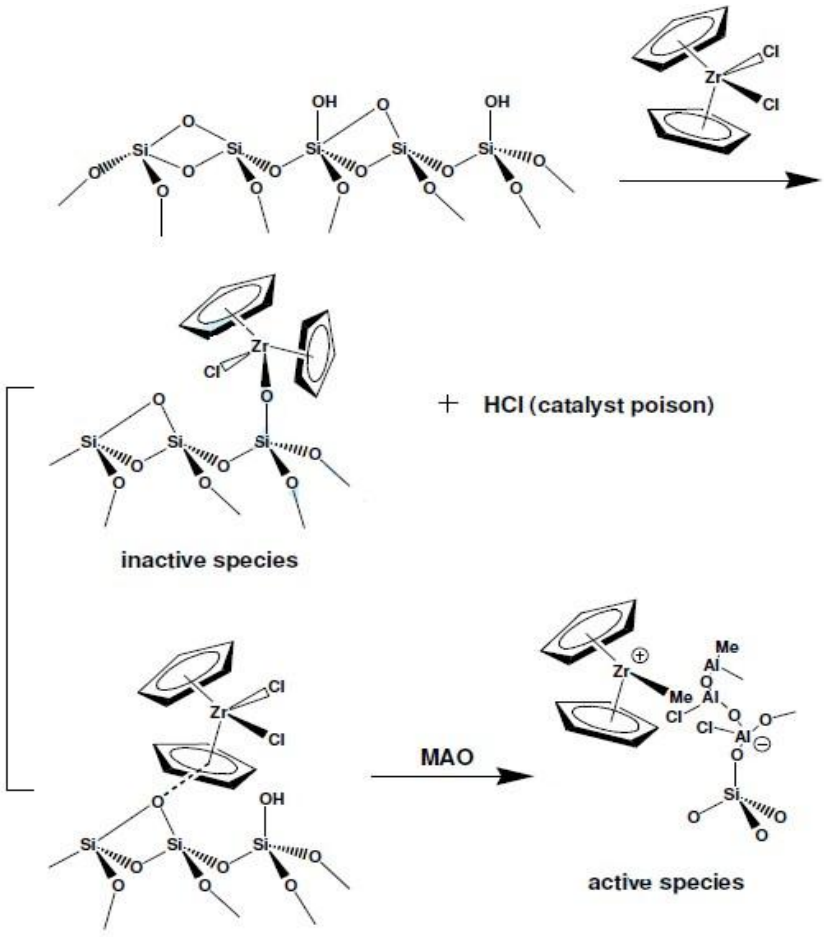

Figure 2.4: Physical supporting Method-A with thermal-treated silica [40]

In the second physical supporting technique (Method-B) the silica is treated with an activator like MAO, then washed with a solvent such as toluene and dried to remove any unanchored activator, followed by impregnation with metallocene. Trimethyl aluminum or a mixture of alkyl aluminums could also be used instead of the MAO. However, TMA needs to be contacted directly with adsorbed water on the silica surface (no need for thermal treatment) and will generate in-situ aluminoxanes as shown in Figure 2.5.

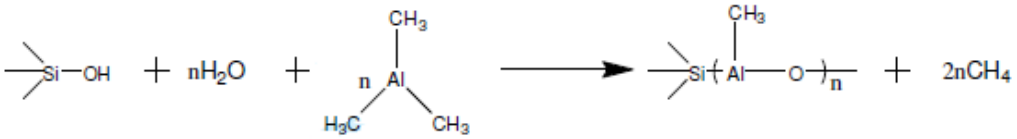

Figure 2.5: Physical supporting Method-B (Reaction of TMA with silica to form in-situ MAO) [41]

In the third method of physical absorption (Method-C), the metallocene and activator are mixed together in solution. The solution is then contacted with the dehydrated silica for a certain time. The final catalyst needs to be washed with a solvent to remove any unanchored catalyst components (to avoid any reactor fouling during polymerization). This method has certain advantages, such as reducing the number of reaction steps and less solvent usage [42]. For this reason we chose to use this method in the research presented in subsequent chapters.

However, it is important to mention here that leaching of the active sites during polymerization can be a problem with the physical absorption methods. The leaching problem typically produces polymer particles with very bad morphology, or agglomerations leading to reactor fouling, and reactor shut down in both slurry and gas phase processes. The problem of leaching can be overcome by using the chemical supporting methods, where a covalent chemical bond is formed between the catalyst and the support [43, 44].

2.2.3.3 Chemical Supporting Methods

In Method A in Table 2.2, and as shown in Figure 2.6, a functional group is added the metallocene ligand in order to react with other functional groups on the support surface creating a strong chemical bond.

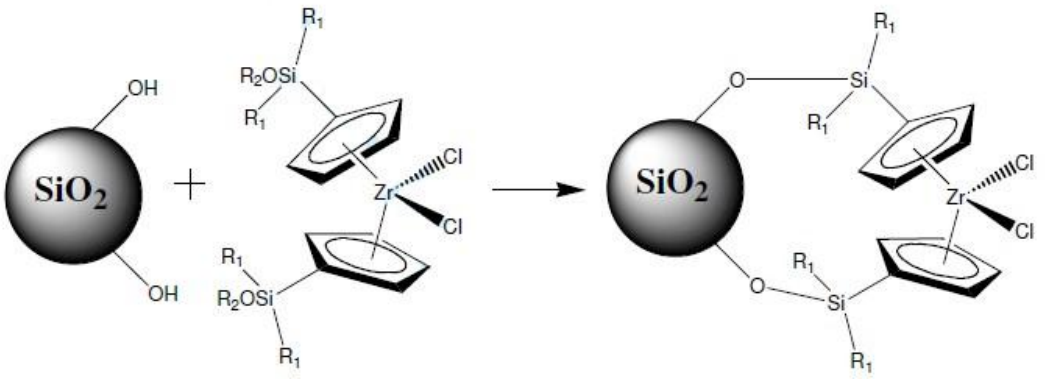

Figure 2.6: Metallocene supporting by chemical method-A by reacting the hydroxyl groups on the silica surface with functional groups in the metallocene ligands [45]

The major disadvantage of this method is the possibility of side reactions between metallocene ligands, such as chlorine and silica. These side reactions produce inactive sites and other byproducts such as water and hydrochloric acid that is known as catalyst poisons [46, 47, and 48].

In the second chemical supporting method (Method B), siloxane groups on the silica surface react with other functional groups on the metallocene ligands to produce supported metallocene [40], as shown in Figure 2.7. This method is considered as a modification of the previous Method A, but it eliminates the production of byproducts during catalyst supporting.

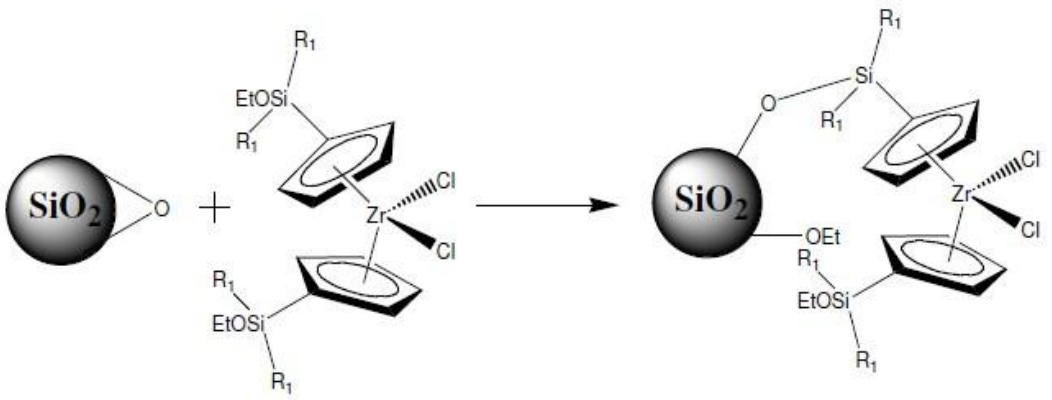

Figure 2.7: Metallocene supported by chemical Method-B using siloxane groups [49]

Another chemical supporting technique involves the synthesis of the transition metal complex directly on the silica surface. Side reactions could be eliminated with this method, however at the current time; it shows very low activities that make it unattractive for commercial applications. This problem of low activity could be overcome by using a spacer group, where the spacer group will reduce the electronic charge and effect the steric hindrance between the support and catalyst [50].

2.3 Impact of Support Properties on the Polymerization

In addition to interacting with the active sites during the supporting step, as discussed in the previous section, the physical properties of silica can also influence the manner in which the reaction progresses once the catalyst is injected into the reactor. The pore size and the structure of the pore network can have an influence on the rate of mass transfer of monomer towards the active sites, the physical strength of the bridges between the substructures of the particle will have an impact on how the support breaks up during the

reaction, and the overall size of the particle can influence how heat and mass are exchanged between the surface of the particle and the surrounding reactor environment.

2.3.1 Support Fragmentation

Fragmentation refers to the step during the reaction when the catalyst[1] particle breaks up into tiny pieces, held together by the polymer produced during the initial moments of the reaction, and that is when the monomer diffuses into the pores of the catalyst particle and reacts at the active sites on the surface of the support to produce polymer. The buildup of the polymer chains inside the catalyst particle will start to generate stress. When this stress exceeds the local mechanical resistance of the support, the bridges between the substructures of the silica particle break. Progressive rupture of these bonds throughout the catalyst particle leads to the fragmentation of the catalyst support. However, it is very important that fragmentation occurs in a well-defined manner. The particle needs to maintain its integrity (i.e. one catalyst particle should give one polymer particle), rather than breaking up into many fine pieces that are detrimental to reactor operation. In other words, fragmentation should not be too rapid. On the other hand, if catalyst particle does not fragment, polymer will block the pores, producing undesired hollow particles with low bulk density, or ultimately leading to the extinction of the reaction in the particle [51].

[1] Note that from now on we will use the term catalyst (or catalyst particle) to refer to a support particle upon which the active sites have been somehow anchored.

The fragmentation step has a direct effect on catalyst activity and final morphology. Controlled fragmentation will generate enough porosity that monomer can continue to arrive at the active sites inside the particle during the polymerization, and should ideally, allow the polymer particle to grow uniformly by expansion leading to a well-defined, preferably spherical shape.

It is widely accepted that the fragmentation of a catalyst is governed by the competition between the buildup and relaxation of stresses in the particle that is due to the production of polymer at the active sites. Several parameters mainly influence the catalyst fragmentation in the early stages of the polymerization, e.g. the nature of the catalyst (the physical properties of the support material and the active sites distribution). The size and size distribution of the pores can also influence how the fragmentation proceeds in a particle. It has been shown that the fragmentation tends to take place at the larger pores first followed by smaller ones until it reaches the very small pores where the hydraulic pressure build up by the polymer is insufficient to break up the support until much later in the process [17, 18].

A number of analytical techniques have been used to study fragmentation with different reaction conditions and different supports. These include Laser Scanning Confocal Fluorescence Microscopy [43, 51], Energy Dispersive X-ray analysis, Melt Microscopy [52], X-ray Micro tomography [53–56] and video-microscopy and Infrared imaging [40, 51]. In addition, special stopped flow reactors have recently been used to look at slurry [57] and gas phase polymerizations [58] at very short times.

The general conclusions from these studies were that two types of fragmentation mechanisms observed, and mainly depend on the nature and structure of catalyst support. First, layer-by-layer fragmentation mechanism is mostly observed with catalysts supported on silica having small mean pore size, with a uniform pore size distribution. Second [59], a sectioning fragmentation mechanism that proposes that fragmentation occurs first on large pores, then on smaller ones, and so on until the support has completely broken up. In fact, it appears that a combination of layer-by-layer and sectioning mechanism could take place on a silica support that has few large pores, as shown in Figure 2.8, then a relatively homogeneous set of substructures inside the particle. It has been shown in one study that medium pores on the order of 100 nm in diameter were the most favorable pore size that dominated the initial fragmentation, and the smaller pores were involved afterwards [60].

The schematic representation of these fragmentation mechanisms are shown in Figure2.8.

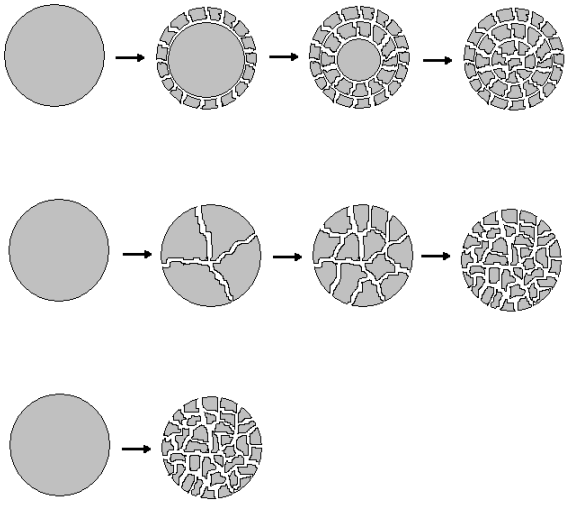

Figure 2.8: Presentation of the supported catalyst fragmentation mechanisms;

(a) layer-by-layer, (b) sectioning

Finally, other factors effecting the fragmentation mechanisms such as the co-catalyst distribution on the support, the type of monomer used, and the polymerization conditions applied without ignoring the physical aspects of the support [61].

2.3.2 Impact of Pore and Particle Size

As mentioned above, the pore volume, pore shape, and pore size distribution are very important for catalyst performance and product micro properties. These physical properties control the adsorption and distribution of the active sites, and the activator distribution on the support. They can therefore directly influence the fragmentation of the support during polymerization. In general, the shapes of the polymer particles produced by catalyst with higher porosity will have better morphology compared with the less porosity catalyst. Despite its importance, only a very small number of papers focused on the direct effect of the porosity of the support [17, 18, 59, 60].

The pore sizes are classified into three different families: micropores with a diameter less than 2 nm, mesopores with diameters of 4 to 200 nm, and macropores with diameters greater than 0.1 μm. The number and distribution of these types of pores in the support are very important in mass transfer and fragmentation behavior. As mentioned pore size and pore distribution could be controlled during and after the manufacturing [62, 63].

Some studies showed that as the pore volume of the support increase the catalyst activity will increase. Catalyst support with large pore size will allow the active sites and the activator to be anchored through the catalyst particle, and enhance the monomer's diffusion. For instance, the critical pore size estimated in Chromium catalyst supported

on silica was found to be between 100 to 1000 Å. Where, 1000 Å is considered the maximum measured value and controlled by the design of the catalyst [64]. In terms of the impact of the porosity of the support on the rate of reaction, catalysts with high porosity will have higher rates of monomer diffusion into the pores of the catalyst particle and a more even distribution of monomer within the particle. This will lead to faster polymerization with less induction time compared with the compacted particle in the case of catalyst with lower porosity. However, other investigations [65, 66] led to observations that a support with large pore diameter had lower activity as well as with small pore diameter less than 2 nm (it might be necessary to correct this for the relative surface area since the support with large pores will have a lower specific surface area and therefore fewer active sites per gram of support). However, the effect of pore size disappeared with reactions at high temperatures. These behaviors were observed in silica and in molecular sieves in both gas and slurry polymerizations.

There are a few papers that have been published about the effect of the silica particle size. One of these investigation showed that the diameter of the silica support has an effect on the kinetics behavior with metallocene/MAO [67]. The smaller particles showed a shorter induction period at the beginning of polymerization, and higher reaction rate compared with larger particles. One of the explanations that was proposed for this behavior is due to more surface area available with smaller particles with the same catalyst loading [68]. Also, smaller particles will have less mass transfer limitations and that leads to faster fragmentation at the same time. However, these explanations need more investigations, because the amount of MAO and metallocene loading may vary with different particle sizes, and additional elemental analysis is required.

2.4 Conclusions

This chapter presented a rapid overview of the literature on the subject of the polymerization of ethylene using metallocene catalysts supported on silica. It is clear that the physical properties of the support have an impact on the way in which the active sites are anchored to the surface of the silica supports, and how fragmentation and particle expansion occur. However, despite the importance of this subject, much still remains to be done to define the role of the pore size on metallocene catalyzed polymerizations. Therefore, it has been decided to examine the polymerization kinetics and particle morphology obtained using three different silica supports, which will first be characterized, then tested in reaction conditions.

As a review of the literature showed that MAO is the most pertinent choice for activator/co-catalyst in commercial metallocene systems, it was decided to limit ourselves to this product in order to invest more time in exploring the impact of the physical properties of the supports.

Chapter 3

Metallocene Supporting

3.1 Introduction

As discussed in the introduction, the pore structure of the silica used as a support in the polymerization of ethylene using metallocene catalysts can be important. For this reason, it was decided to investigate the impact of three different types of porous silica in order to study the effects of the catalyst support on kinetics and molecular properties.

3.2 Experimental

3.2.1 Support Characteristics

Two of these silicas were produced by Grace Davison (SYLOPOL 955 and 2408HT). While the third one (ES-70) was supplied by INEOS. All of three silicas were white, free flowing powders and had similar optical properties. However, the physical properties of these silicas are different and the details of these silica supports are shown in Table 3.1, 3.2.

Table 3.1: The physical properties of silicas supplied by Grace

		2408HT		955W	
Property	Unit	Min.	Max.	Min.	Max.
Pore Volume (H2O)	ml/g	1.4	1.7	1.55	2.00
Surface Area (BET)	m^2/g	280	355	280	355
Total Volatile	%		10		10
SiO_2 (dry basis)	%	99.3		99.3	
FeO_3 (dry basis)	%		0.05		0.05
Na (dry basis)	%		0.12		0.12
SO_4	%		0.10		0.10
Mg (dry basis)	%		0.20		0.20
Ca (dry basis)	%		0.15		0.15
Al_2O_3 (dry basis)	%		0.20		0.20
Sum of Na_2O + Mg + Ca (dry basis)	%	12	0.32		0.32
Particle Size					
D (10%)a	µm	12		10	
D (50%) a	µm		80	35	45
D (90%) a	µm				97
> 125 µm (Screen Analysis)	%		0.5		0.5

[a] Measured with Malvern Mastersizer

Table 3.2: The physical properties of silica ES-70

Silica type	ES-70
Supplier	INEOS
Pore diameter A°	180
Pore Volume cm3/g	295
Surface Area m2/g	1.48

Each of the three silicas mentioned above was sieved to five different cuts as and the weight fractions of each cut are presented in Figure 3.1. ES-70 had higher average particle size compared with 955W and 2408HT, and 955W has relatively smaller particles.

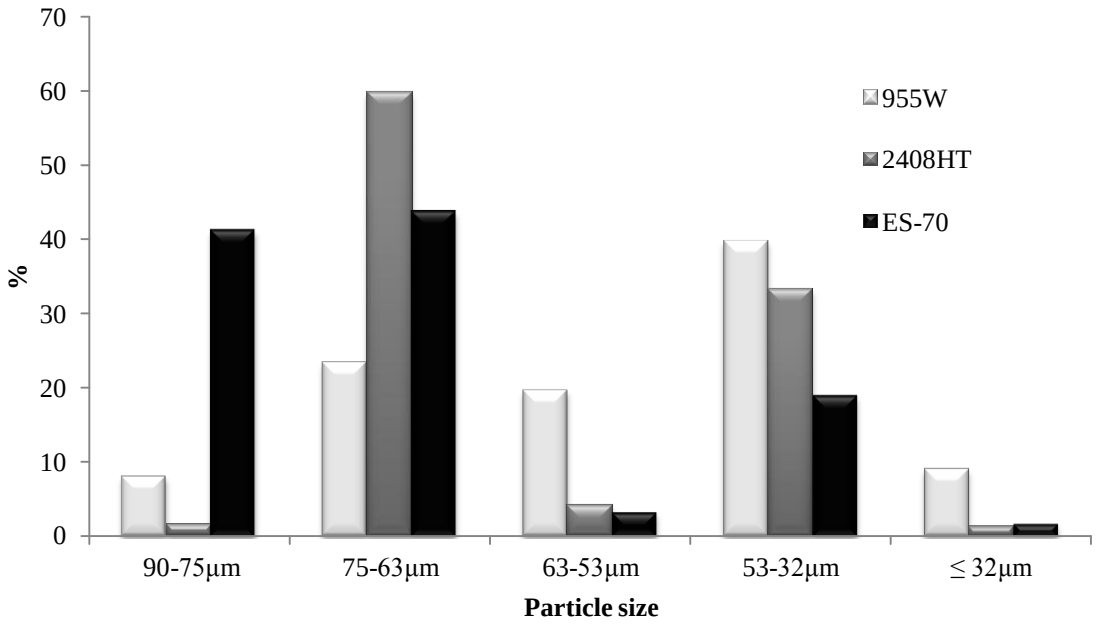

Figure 3.1: Particle size distribution of the utilized silicas 955W, 2408HT, and ES-70

The surface area and pore volume of each cut of the Grace 955W were measured to find out if is there were differences as a function of particle size[2]. The same BET technique was used to measure the surface area and pore volume. The analysis shown in Figure 3.2 revealed that there is no significant difference between the cuts, with the exception of the smallest cut (≤32µm) which had lower surface area and pore volume. This reduction in

[2] N.B. This was only done for the Grace 955W as it was observed later in the study that there was no significant difference at this level between the cuts, and because the differences between the three major products was slight

surface area and pore volume might have an effect on the metal loading during the catalyst supporting step by limiting the diffusion of the activator and/or catalyst precursor, and providing a lower surface area per gram, thereby eventually leading to fewer active sites per gram of support. Therefore, the metal loading in the catalyst batches which were used in these silica cuts need to be investigated.

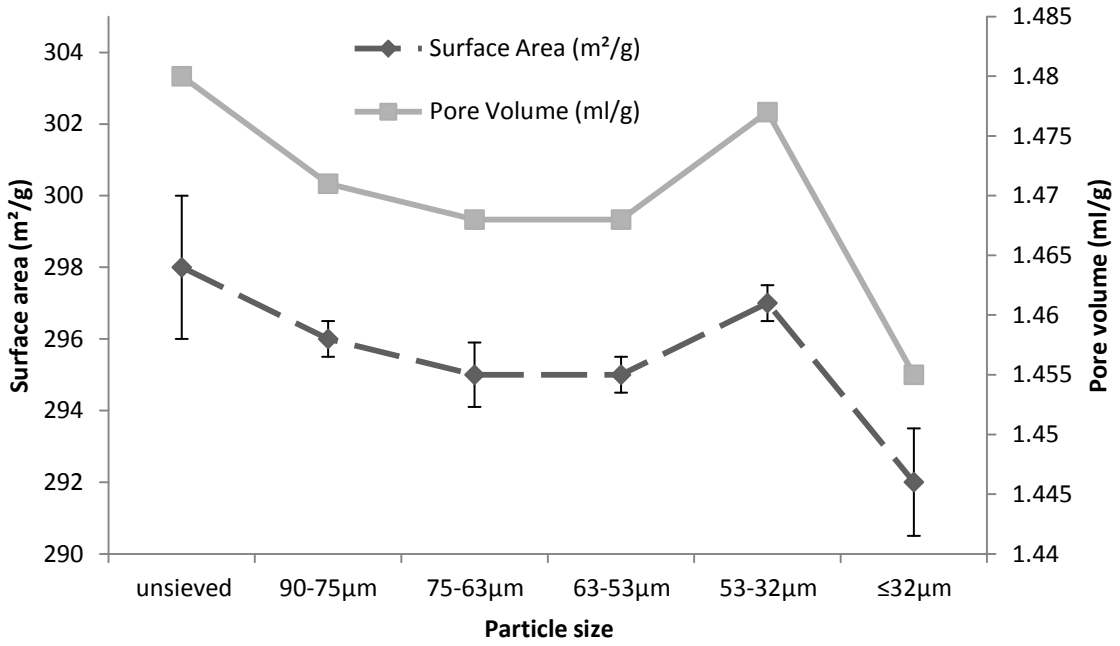

Figure 3.2: Pore volume and surface area of silica 955W with different particle size cuts

3.2.2 Calcination Method

The first step in catalyst supporting starts by taking one gram of the required silica and placing it in a calcination tube under an atmospheric environment. The calcination tube is then placed in a tube furnace, and the furnace was heated to 200 ºC. It typically takes around 30 minutes for the temperature to reach 200C. After that, the silica will be kept for 24 hours at 200 ºC. The hot silica was subsequently transferred carefully to a 20 ml

dry vial, and quickly covered with dry paper tissue and caped. The vial was placed inside the evacuation chamber of the glove box and 5 extensive nitrogen pressure/vacuum cycles were performed to remove any air inside the vial. Finally, the dried silica was stored inside the glove box before being used as a catalyst support.

3.2.3 Catalyst Supporting Process

One of the most important aspects of this research was to study the supporting of the metallocene (Cp_2ZrCl_2) on the silica support. As mentioned above, each of the three silicas mentioned above was sieved to five different cuts, and the same supporting technique was implemented to all of the silica cuts.

For each catalyst batch one gram of the targeted silica was dehydrated for 24 hours at 200 ºC under air environment, as described in the previous section. The same supporting technique was implemented to all the silica types and sizes.

Different chemicals were used in the supporting reactions as shown in Table 3.3. Due to the sensitivity of all of the materials to air, very careful handling was needed and all the steps were implemented under positive nitrogen pressure to avoid any deactivation during the supporting, storing, and transferring.

Table 3.3: Materials used in catalyst supporting

Name	Formula	Grade	Supplier
Nitrogen	N_2	UHP	PRAXAIR
MAO	$(CH_3)_2Al(OAlCH_3)NAlCH_3$	19 wt% in toluene	Aldrich
Polymeric MAO (PMAO)	$(CH_3)_2Al(OAlCH_3)NAlCH_3$	13 wt% Al in toluene	Akzo Nobel
Silica	SiO_2	SYLOPOL 955W	Grace Davison
Silica	SiO_2	SYLOPOL 2408HT	Grace Davison
Silica	SiO_2	ES-70	INEOS.
Toluene	$CH_3C_6H_5$	99.9%	Sigma-Aldrich
Bis-Cyclopentadienyl zirconium dichloride	$Cp_2Zr_2Cl_2$	99%	Aldrich

All of the materials used were of a high purity and were used as received, with exception of the toluene. Toluene was used as a solvent mainly in catalyst supporting, and also tested as a polymerization solvent. Since the quality and the purity of the toluene are very important for catalyst activity, and because of the sensitivity of the catalyst to any impurities (even at the level of ppm), toluene was purified by distillation to remove any air or moisture. A standard set-up was used for this task, and consisted of a two neck 4 L round bottom flask (3.5 L useful volume) connected to a collection flask connected by a three way valve. A condenser cooled by water and nitrogen supply was connected to the top of the main flask and attached to an oil bubbler at the outlet. Several granules were added to smooth the boiling of the liquid, and 2 to 3 cylindrical beads of solid metallic sodium were also added to the large round bottom flask. Due to the sensitivity of the sodium beads to air they were stored in oil and were rinsed in toluene prior to use. The toluene set-up was purified to remove any air or moisture by purging the system with dry

nitrogen. Next, 20 ml of n-butyl lithium and 20 ml of distilled styrene were transferred into the system via a transfer needle through the second neck in the large round bottom flask which was sealed with a rubber septum. The styrene was purified before use by vacuum distillation to remove the inhibitor (4-tert-butylcatechol) present in the reagent as supplied. After the entire components were added to the system, the rubber septum was replaced with a glass stopper.

The mixture was heated by an electrical heater which was placed under the round bottom flask and the solvent was refluxed for around 24 hours. After heating, the solvent color turned to deep orange, indicating that the system was free of oxygen. In case the color was not as desired, additional butyllithium and styrene were be added. A low flow of dry nitrogen was supplied to the top of the condenser, to prevent any air accessing into the system at all times.

3.2.4 Supporting Technique

Many supporting techniques were tested during the initial phases of the research project to identify the technique that provided the best balance of catalyst productivity, reactor fouling, and resin morphology. Different Al/Zr ratios were tested to check its direct effect on the catalyst activity. Also, a wide range of supporting temperatures and supporting times were examined to explore their effects on the catalyst performance. The outcome of this initial exploration led to the adoption of a hybrid technique that was implemented in all of the experiments reported here. First, the incipient wetness method [69] was used to contact polymeric methyl aluminumoxane (PMAO) with dehydrated silica, then the

physical absorption (method-C) which was mentioned in section 1.2.3.2 was used to support the catalyst precursor [42].

In the first step in the process of catalyst supporting, 0.25 gram of dehydrated silica was transferred to a very clean and dry 20 ml vial. 0.5 gram of polymeric methyl aluminumoxane in toluene (PMAO) with 13 wt% Al in toluene was added. The used PMAO was supplied by Akzo Nobel and it is chemically similar to MAO, but has a better shelf life than MAO. Another advantage of PMAO that it had higher aluminum content than the MAO available in the market that had only 4.7 wt% supplied by Aldrich. The MAO was used as an activator in catalyst supporting , but unfortunately it produced lower activity compared with PMAO which had the highest activity and good morphology control. Another disadvantage of MAO that a sort of agglomeration occurred when it was stored in the glove box, which made the aluminum concentration unknown. Therefore, more precaution was taken to avoid the agglomeration problem by storing the MAO and PMAO inside a refrigerator under low temperature.

A small magnetic stirrer was placed in the vial to mix the catalyst components, and then the vial was sealed tightly with a cap with a polytetrafluorethylene-lined rubber septum.

0.015 gram of bis- cyclopentadienyl zirconium dichloride (Cp_2ZrCl_2) was transferred into another hypo vial, and then quickly 0.5 gram of 13 wt% PMAO was added to the 0.015g Cp_2ZrCl_2, and tightly sealed with the same type of cap. All of these steps were performed under nitrogen environment inside a glove box. The two vials were then removed from the glove box for the next steps.

The vial which contains the silica and PMAO was placed in an oil bath set at 50C and left to be mixed for one hour with a small magnetic stirrer. During this time approximately 130 ml of dried toluene was transferred to a 150 ml round bottle sealed with rubber septum which had previously been well purged with nitrogen. The toluene was then purged with nitrogen through the transfer needle for 15 minutes. After one hour, the contents of the vial with 0.015g Cp_2ZrCl_2 and 0.5 PMAO was transferred by a nitrogen pressure through a transfer needle to the dried toluene. An additional 20 ml of dried toluene was used to rinse catalyst vial to ensure that all the contents were transferred. At this stage, the vial containing the toluene and catalyst mixture was placed back in the hot oil bath, and left to be mixed for one more hour at 50 ºC.

After this, the catalyst supporting on silica is completed, but the catalyst needed to be washed three times with dried toluene to remove any unanchored Cp_2ZrCl_2 and PMAO, if not it will lead to reactor fouling. Around 10 ml of toluene was added to the catalyst vial and placed back in the hot oil bath, and to be mixed for 5 minutes. Then, the mixer was switched off to let the solid particles settle down and when clear two phases are formed, the vial was pressurized with nitrogen. Then, slowly a transfer needle was inserted to remove most of the liquid. After that, around 20 ml toluene was added to the vial, then placed back in the hot oil bath and left to be mixed for 5 minutes. The same steps above were repeated twice. Finally, after decanting most of the liquid phase, the catalyst particles were dried by passing a low nitrogen flow through the catalyst vial which was paced in the oil bath at 50 ºC. Typically, the drying step took around 25

minutes. The final catalyst is a free flowing powder with a pinkish color. At this stage, the catalyst is ready, and needs to be placed inside the glove box to avoid deactivation.

3.2.5 Inductively Coupled Plasma

Inductively coupled plasma (ICP) is an analytical technique used for detection of traces of metals, and so can be used to analyze our supported catalysts. ICP works by exciting atoms and ions and causing them to emit electromagnetic radiation. The emission occurs when the species are excited to higher electronic states and shortly after excitation they go through a process of relaxation that produces ultraviolet and visible line spectra that can used for qualitative and quantitative elemental analysis. Each element will emit a certain wavelength, and the intensity of the emission is proportional to the concentration of the element within the sample [70, 71]. An inductively coupled plasma atomic emission spectroscope manufactured by Teledyne-Leeman Laboratories was used in this work. Emission spectrometry offers several advantages compared to more the traditional flame and the electrothermal adsorption methods; in particular a lower inter-element interference is observed because it employs significantly higher temperatures. It can therefore be used for the simultaneous detection of dozens of elements under the same set of excitation conditions, and the detection of low concentrations of elements that tend to form refractory compounds.

The set-up used here consists of two parts: the ICP itself and the optical spectrometer. The ICP torch is made of 3 concentric quartz glass tubes and typically argon is used to create the plasma. Plasma is an electrical conducting gaseous mixture containing a

significant concentration of cations and electrons with a net charge approaching zero. Usually, argon is used to create a plasma having ions capable of absorbing adequate power to form an external source. The temperature is therefore maintained around 7000 K for further ionization to maintain plasma for the targeted test.

Ionization of flowing argon is initiated by a spark from Tesla, and the resulting ions interact with the fluctuating magnetic field produced by the induction coil on top. This interaction causes the ions and electrons within the coil to flow via closed annular paths. A sample is introduced into this flow by pumping it from a sample container with a peristaltic pump. A special pneumatic nebulizer is used with liquid samples that run through the central quartz tube in order to convert the liquid sample into a fine spray or mist for spraying the chamber, and remove any droplets bigger than 8 μm in diameter. The mist is then introduced directly into the plasma flame. The sample immediately collides with the electrons and charged ions in the plasma and is broken down into charged ions. The different molecules will break up into their respective atoms. The excited atoms will lose electrons and recombine repeatedly in the plasma, emitting radiation at certain wavelengths of the elements involved.

To be able to measure the metal content in the metallocene immobilized on silica support, metals must be in an ionic form. The supported catalyst was therefore first digested by strong acids to decompose the catalyst components. The following procedure was used to prepare the samples for ICP analysis. In the first step, 0.028 g of the supported catalyst was placed in a clean Teflon container. 3.0 ml of high purity hydrochloric acid (37 - 38% conc.) was then added to the container, followed by addition of 1 ml of high purity nitric

acid (69 - 70% conc.). 1 ml of sulfuric acid (95 - 98% conc.) was subsequently added (very carefully) to the mixture. Finally, the Teflon container was placed in a boiled water bath, and left to be mixed with Teflon coated magnetic stirrer for 30 minutes. The change in the mixture color from a yellowish color to colorless indicates that the sample was dissolved. Afterwards, the mixture was transferred to a clean graduate cylinder, and was diluted with de-ionized water to a total volume of 20 ml. All the samples were filtered before the ICP analysis.

3.3 Results and Discussion

3.3.1 Effect of Calcination

Before examining the results of the polymerization studies, it is important to understand the eventual effects that the supporting procedure on the silica. To this end, the surface area and pore volume of the three silicas were measured with a Micromeritics Gemini VII porosimeter using the BET method [72]. Table 3.4 shows the results of the measurements comparing the manufacturers' specifications on the raw silica calcination, and measurements after dehydration at 200 ºC.

Table 3.4: Surface area and pore volume of the silica used in this work

Silica type	Surface Area (m^2/g)		Pore Volume (cm^3/g)	
	Supplier info.	**Measured after drying**	**Supplier info.**	**Measured after drying**
955 W (G/D)	280 - 355	300	1.55 – 2.00	1.49
2408HT (G/D)	280 - 355	300	1.4 – 1.7	1.49
ES-70 (INEOS)	295	242	1.48	1.21

Dehydration of the ES-70 silica at 200 °C for 24 hours reduced the surface area and pore volume more than the other silicas, which may be related to the differences in the physical properties such as salt residuals and pore size distribution [18, 19]. On the other hand, the structural characteristics of 955W and 2408HT were not affected by the calcination at 200 °C step. In general, ES-70 has lower surface area and pore volume compared with 955W and 2408HT.

3.3.2 Metal Loading

In addition, ICP was used to measure the Aluminum (coming from PMAO) and Zirconium (coming from Cp_2ZrCl_2) content in the supported catalyst batches with different silica types and different particle sizes. This was done in order to see if any of the physical properties impact the metal loading during the supporting under similar conditions. Before performing the analysis, two calibrations curves for Al and Zr were made. Four standards were used for Zr, and six for Al with different concentrations. These calibration curves are very important in order to create precise measurements. All the ICP measurements had very high accuracy, and the average standard error was very low; 0.016 ppm with Zr and 0.56 ppm with Al based on 3 runs.

The analyses showed that the metal loading varied with changing the silica support type and size. As shown in Figure 3.3, the Al and Zr loading in the catalyst supported on ES-70 appeared to be lower than 955W with 20% (Al) and 34% (Zr). This may occurred because ES-70 silica has less pore volume and surface area than 955W, which may limit the diffusion of catalyst components with high molecular weight such as MAO and Cp_2ZrCl_2. The differences in metal loading matched with the pore volume and surface

area of these silicas after calcination, as shown in Table 3.4. While these differences appear slight, we will see below that they are reflected in the value of the activity measured on each of the catalysts; in other words, the metal loading and the physical properties of the silica support will influence on the catalyst performance as it will be discussed in Chapter 4.

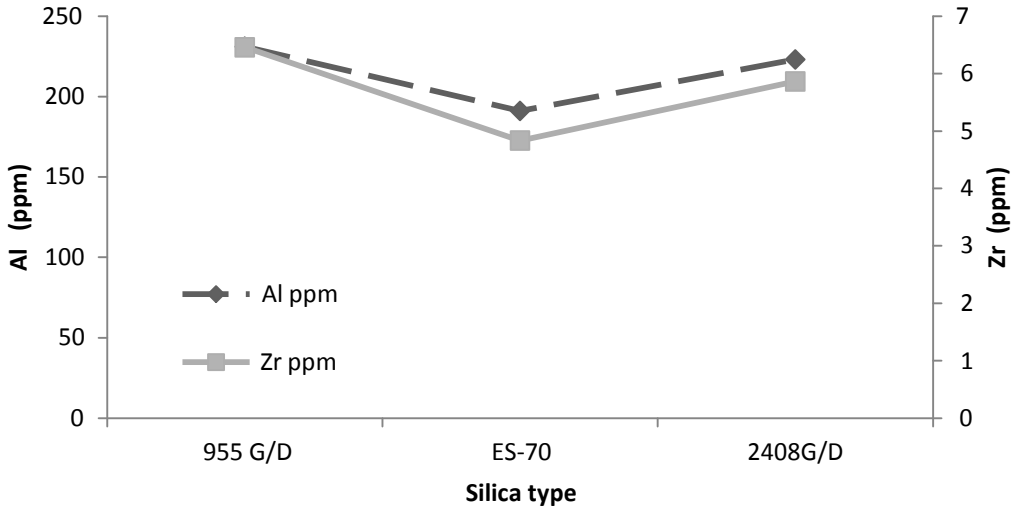

Figure 3.3: The effect of the silica type on metal loading in supported catalysts

The second part of the ICP analysis was to explore the effects of the particle size of the silica support on the metal loading during the supporting process. Six batches of catalyst supported on 955W with different particle sizes (each of the five cuts and an unsieved batch) were prepared similarly using the method described above. The results in Figure 3.4 show that metal loading varies slightly from cut to cut, but the variation is not likely to be significant.

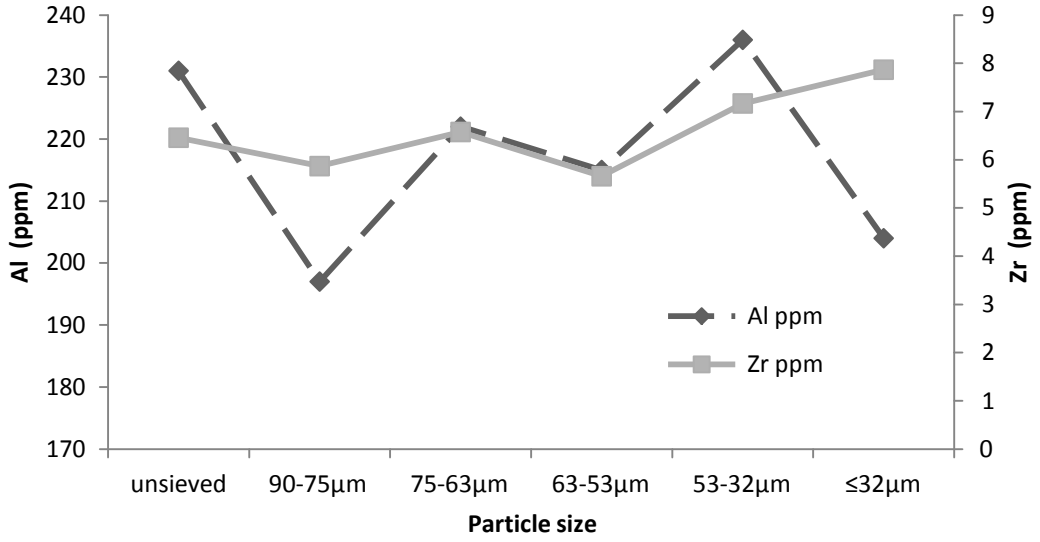

Figure 3.4: The effect of the different particle size of silica 955W on metal loading

3.3.3 Characterization of the Silica Surface

The surface area characterizations of the silica support are very important in the catalyst supporting process. The silica surface has a combination of different hydroxyl groups and siloxane groups, as discussed in Chapter 2, and the residual concentration of these different groups depends on the calcination conditions. We therefore evaluated the concentration of hydroxyl groups on each of the silicas used in this work after the calcination step. Thermal gravimetric analysis (TGA) allows us to measure the weight change of a sample as a function of temperature, and was used to measure the hydroxyl left after the dehydration at 200 ºC.

The TGA results had indicated that the different silica types used in this research, had different levels of hydroxyl groups, as shown in Figure 3.5. Figure 3.6 shows the weight loss vs. temperature curves, and we can see that some weight is lost from 30 to 100 ºC,

indicating the removal of the physically absorbed water, a plateau from 100 to 300 ºC, followed by second transition between 300 to 800 ºC, representing the removal of the hydroxyl groups. The amount of hydroxyl groups left in each silica after dehydration at 200 ºC was determined by calculating the weight percentage difference of the sample between 200 C and 800 ºC. The results suggest that the weight loss with silica 2408HT between 200C to 800 ºC was higher than the others, but the difference is still within the experimental error. As a result, the difference in the OH levels in the silicas after the Dehydration might lead to different catalysts activity.

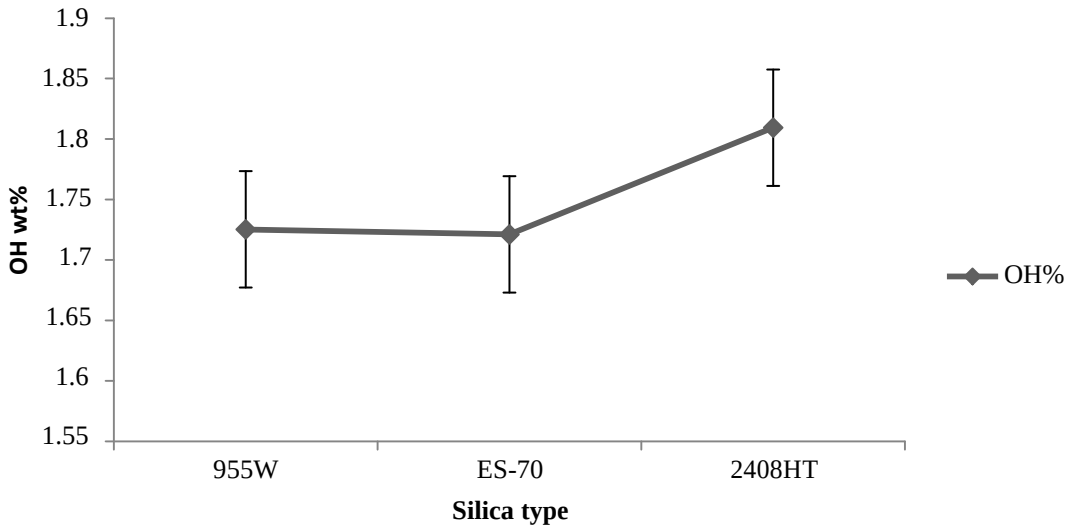

Figure 3.5: The mount of hydroxyl groups removed from different silica types at temperature 200-800 ºC preformed under N_2. Errors reported for 3 replicate runs.

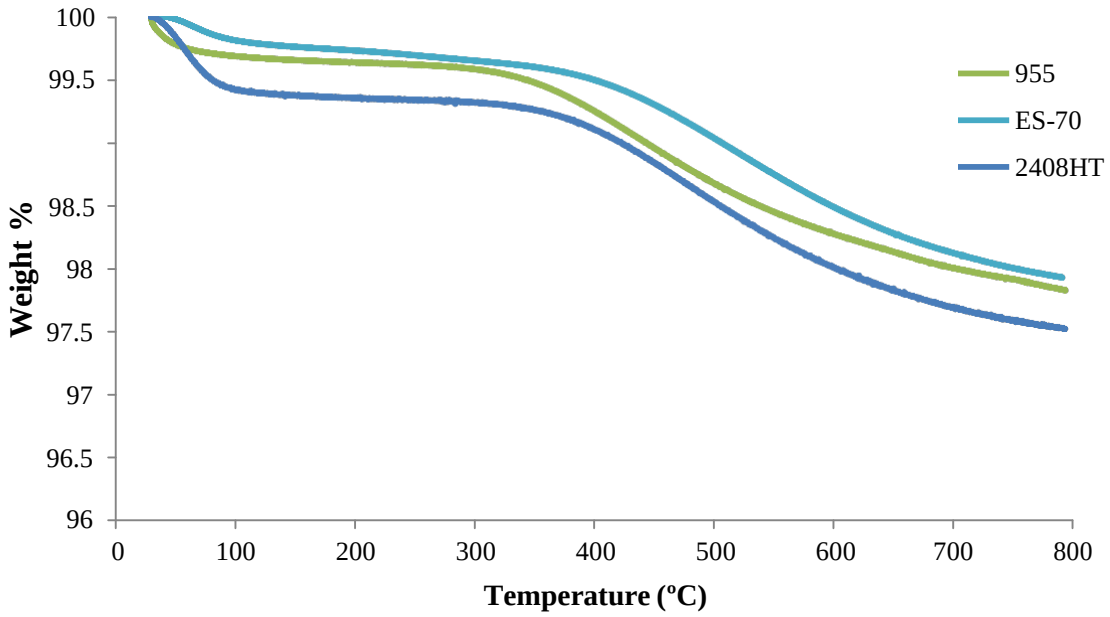

Figure 3.6: TGA profiles of different silica type preformed under N_2 at temperature 30 – 800 ºC

It has been found that even the differences in the physical properties in terms of pore volume, surface area, and particle size distribution influence the dehydration mechanism. As shown in Figure 3.6, results showed that silica ES-70 with the lowest pore volume and surface area lost its OH groups at a slower rate than 955W and 2408HT. However, the silica particle size did not point out a clear difference in the amount of the OH groups removed between 200 C and 800 °C. Also, there was no observed trend in the loss of OH groups due to the changes in particle size, as shown in Figure 3.7. Moreover, the dehydration mechanisms of all of the cuts of the 955W had relatively comparable behaviors, as shown in Figure 3.8. As a result, these findings may explain the reason for most of the 955W cuts in having similar activities.

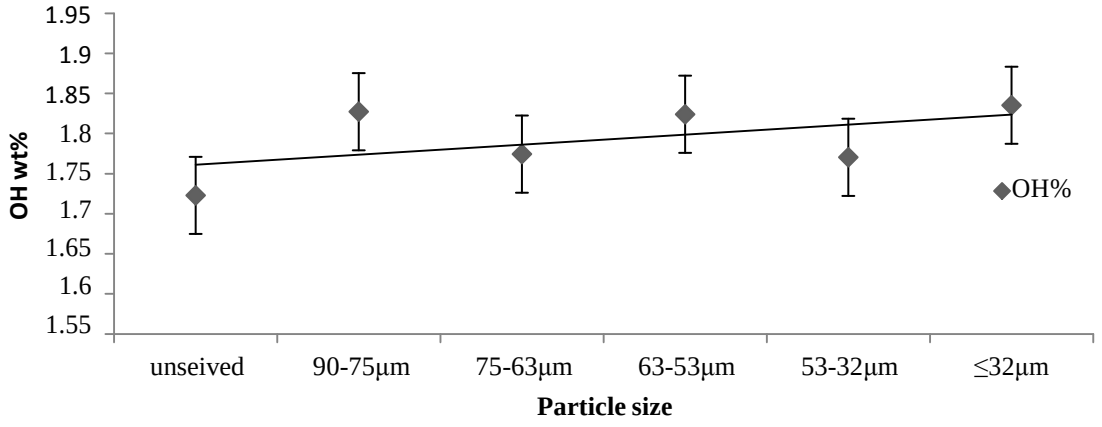

Figure 3.7: The mount of hydroxyl groups removed from different particle size from 955W silica at temperature 200 - 800 ºC preformed under N_2

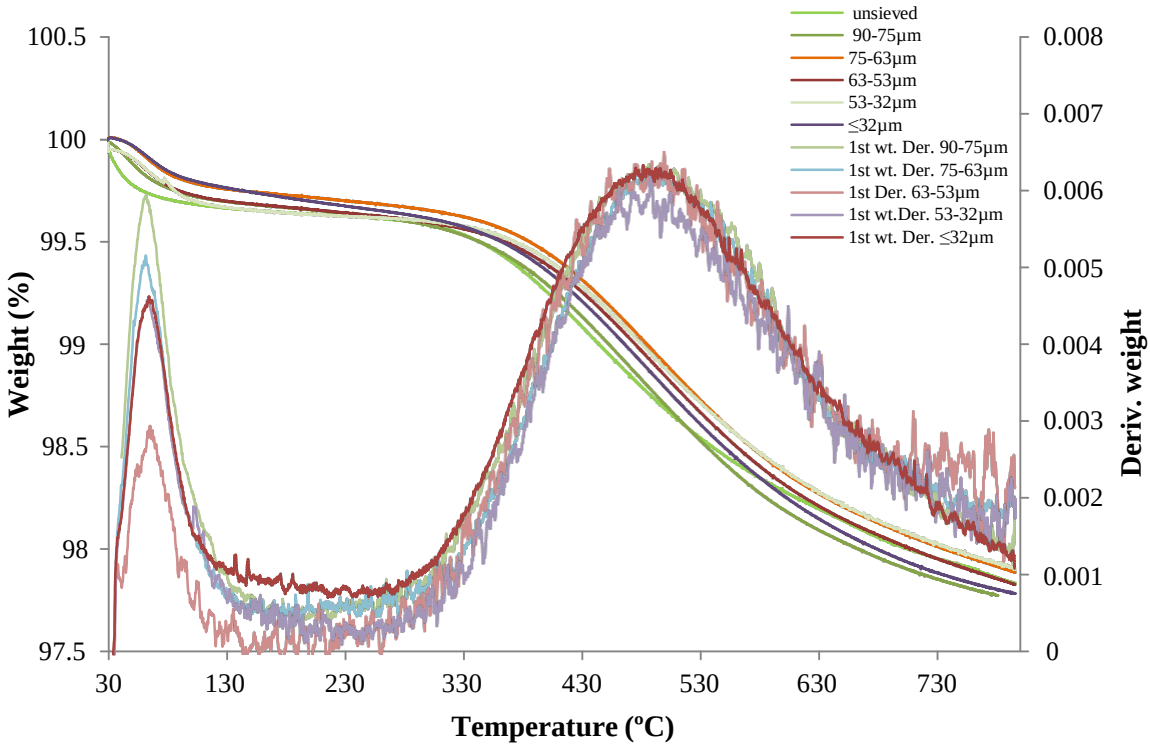

Figure 3.8: TGA profiles of different particle sizes of silica 955W performed under N_2 at temperature 30 – 800 ºC

3.4 Conclusion

Three silica types were utilized, and each silica was sieved to five different particle cuts in order to be used as support. The three silicas have different particle size distributions, and while the pore volume and surface area of the two products from Grace were similar, the third ES-70 had a lower pore volume and surface area, and appeared to be the only one slightly influenced (in terms of these structural parameters) by the calcination step.

The metal loading in the catalyst was measured by the ICP in order to understand the effects of the silica type and size on it. The ICP results showed that the loading of Zr and Al on the different supports was reasonably reproducible. Some variability in these values was noted, and we will try to link them to activity data later on in this work.

Finally, the hydroxyl level in each silica was measured using TGA. Once again, residual hydroxyl concentrations varied from 1.72 to 1.82 % (with respect to pre-calcination values. Detailed studies on cuts of the silica Grace 955W show that the rate of hydroxyl removal was essentially independent of particle size.

Chapter 4

Polymerization

4.1 Introduction

The three different silicas presented in Chapter 3 were used to produce two different materials: HDPE pure homopolymer with a density at least 0.94 kg/m^3, and medium density polyethylene (MDPE) copolymers with a low content of 1-hexene with a density range of 0.926 to 0.940 kg/m^3.

The objective is to attempt to identify differences in the polymerization kinetics and product quality (this will be presented in Chapter 5) due to the different particle and pore sizes, as well as the impact of different scavenger types on the polymerization.

Before presenting the results we obtained from our experimental work, a detailed description of the reactor set-up will be presented.

4.2 Experimental

4.2.1 Materials

The materials that were used in polymerizations and their purity are shown in Table 4.1.

Table 4.1: Materials used in polymerization

Name	Formula	Grade	Supplier
Ethylene	C_2H_4	CP	PRAXAIR
Hexane	C_6H_{14}	95%	J.T. Baker
1-hexene	C_6H_{12}	97%	Aldrich
Ethanol	C_2H_5OH	85 %	VWR
Nitrogen	N_2	UHP	PRAXAIR
Methyl aluminumoxane (MAO)	$(CH_3)_2Al(OAlCH_3)_NAlCH_3$	10 wt% in toluene	Aldrich
Polymeric Methyl aluminumoxane (PMAO)	$(CH_3)_2Al(OAlCH_3)_NAlCH_3$	13 wt% Al in toluene	Akzo Nobel
Tri methyl aluminum (TMA)	$(CH_3)_3Al$	2.0 M in hexane	Aldrich
Triethyl aluminum (TEAL)	$(C2H_5)_3Al$	1.0 M in hexane	Aldrich
Tri-n-octyl aluminum (TOAL)	$(CH_3(CH_2)_6CH_2)Al$	25 wt% in hexane	Aldrich
Tri iso butyl aluminum (TIBAL)	$(C2H_3)_3Al$	1.0 M in hexane	Aldrich

All the feed streams used in polymerization were of a high purity grade. However, nitrogen and ethylene fed to the reactor were passed through purification beds to remove any tiny traces of oxygen or water. Each stream passed first through molecular sieves (4A and 13x) to remove any moisture. They then passed through a deoxygenating bed (CuO on alumina) for removing any trace of oxygen. A schematic of the purification loop is shown in Figure 4.1.

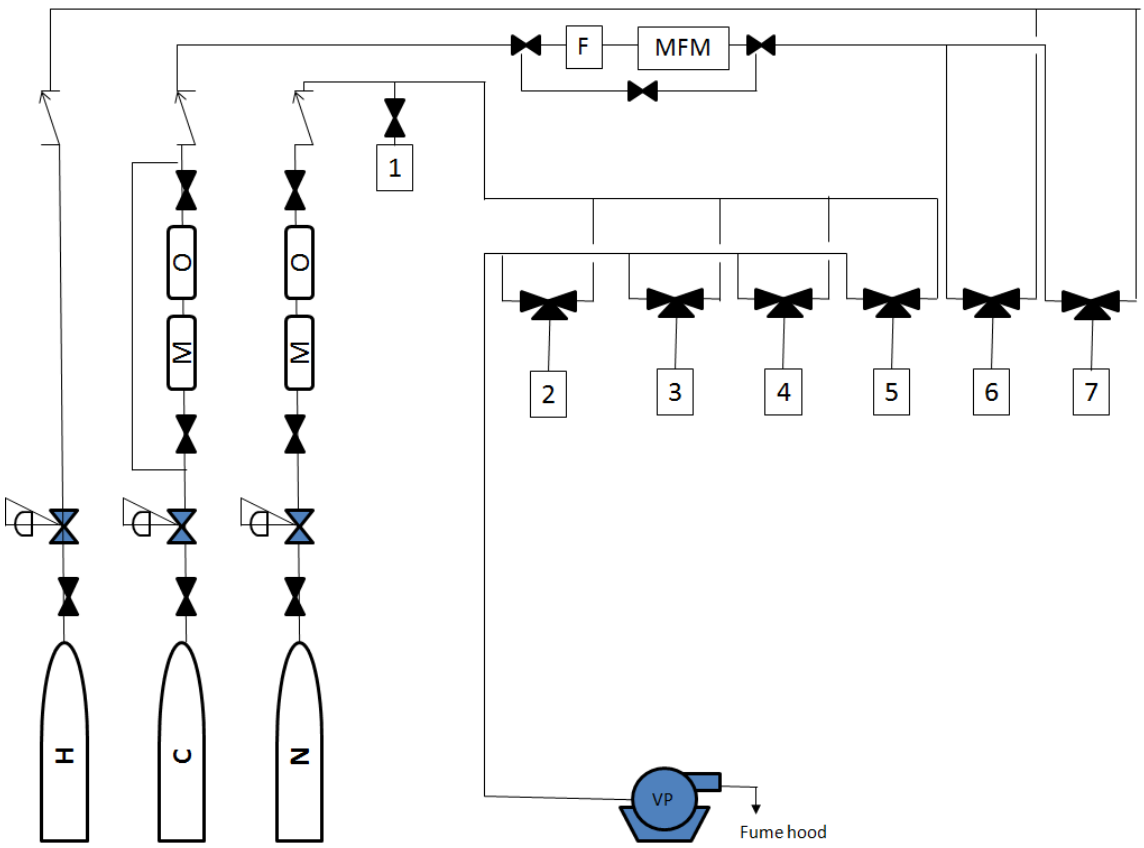

1. N2 supply toluene
2. N2 vacuum supply to toluene
3. General N_2 / vacuum supply
4. General N_2 / vacuum supply
5. N_2 / vacuum supply autocalve
6. C_2H_4 / H_2 supply from manifold
7. $C2H_4$ / H_2 supply from manifold

C. C_2H_4 supply

F. 7µm inline filter
H. H_2 supply
M. Molecular sieves (4A and 1x)
N. N_2 supply
O. Deoxygenation bed (CuO on alumina)
VP. Vacuum pump
MFM. Mass flow meter

Figure 4.1: General supply manifold for autoclave reactor

Both hexane (reaction solvent) and 1-hexene (comonomer) were purified by contacting them with activated 4A and 13X molecular sieves in a sealed glass bottle. The bottle was pressurized with UHP nitrogen and the rubber septum used to close it was secured tightly onto the glass bottle with a thin wire cable to avoid any leaks. Typically, the activation of the molecular sieves was achieved by heating the sieves in air at 250 ºC for 24 hours.

Before the hexane or 1-hexene were put in contact with the sieves, they were bubbled with nitrogen for at least 15 minutes in the original bottles to remove any air or moisture since any traces of moisture will be absorbed into the molecular sieves.

4.2.2 Reactor Description and Preparation

All of the polymerization experiments in this research study were performed in a 300 ml autoclave reactor, a schematic of which is shown in Figure 4.2. During the polymerization, the reactor pressure was maintained constant and by feeding a controlled quantity of monomer in semi-batch mode. The reactor was equipped with a magnetic stirrer with four pitched blades. In addition, a J-type thermocouple was positioned between the cooling coil and reactor wall to measure the internal temperature of the contents, and was connected to a data acquisition system. The temperature was controlled using LabView® software, running on a 150 MHz Pentium PC. A proportional-integral controller was used to maintain the temperature with an on/off technique. An external heater jacket was used to increase the reactor temperature, while the cooling source was cold tap water passing through a cooling coil, the flow of which was controlled by an on/off solenoid valve. The reactor temperature was controlled to within ± 0.3 ºC of the set point.

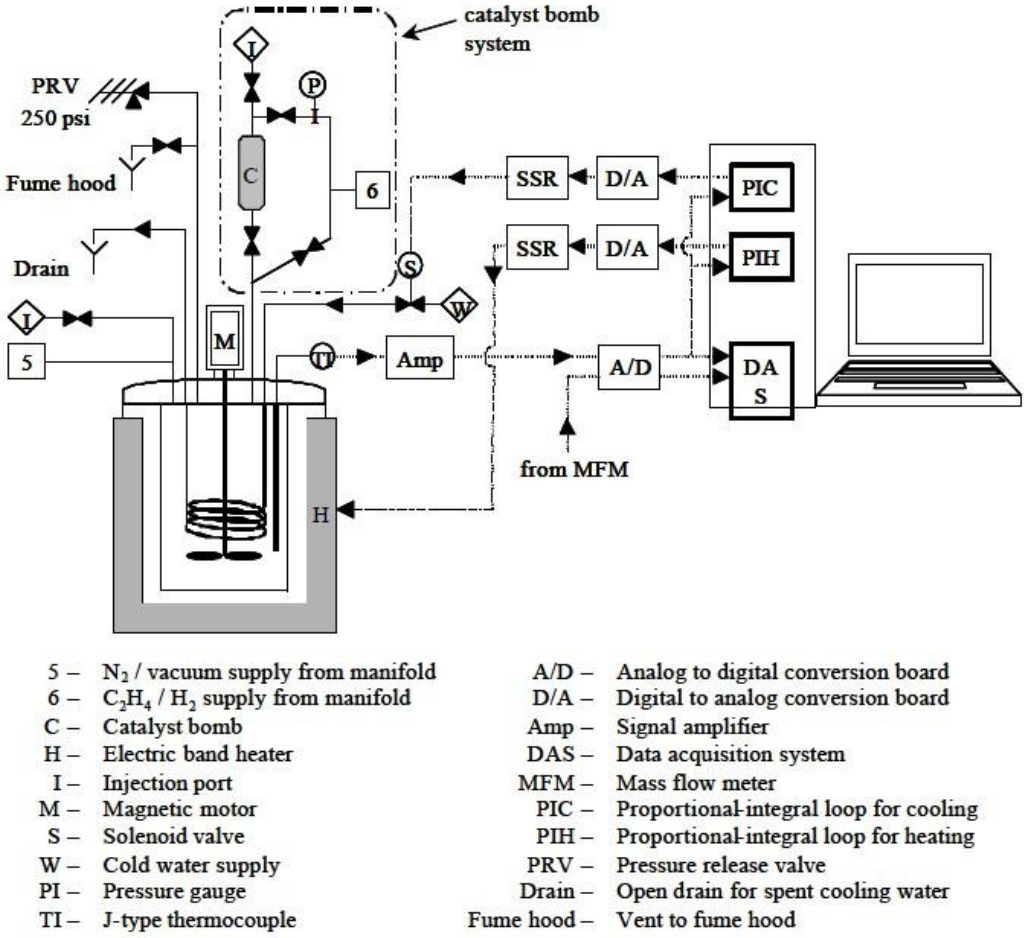

Figure 4.2: Semi-batch 300 l Parr autoclave reactor including control and data acquisition system

The reactor was run in isobaric mode by fixing the ethylene pressure, which was set manually by a regulator on the gas cylinder. The ethylene flow was measured by an on-line mass flow meter (Brooks 5860CE), and was connected to a PC for recording. The reactor body and impeller must be totally free of polymer left from the previous run in order to avoid any contamination. Thus when they were not in use, they were kept in a high temperature oven at approximately 97 °C.

A high-pressure catalyst injection port connected to the top of the reactor was used to introduce the catalyst into the rector. The catalyst injection port consists of a three way connecter with an isolation valve (used to transfer solvent and catalyst) at the top, and a quick one direction connecter (used for all gases supply to the reactor) attached to the top of 20 ml high pressure cylinder. An isolation valve connected to the bottom of the cylinder controlled all the feeds to the reactor. In addition, all the tubing and catalyst cylinder have a smooth surface to avoid any catalyst and polymers build up during catalyst transfer.

Since the polyolefin catalysts are very sensitive to poisons such as oxygen, carbon monoxide and moisture, the catalyst preparation and transfer to the reactor needs to be done under a nitrogen condition avoid deactivation. Before polymerization, all the reagents, catalysts and scavengers used were weighed inside the glove box in 20 ml vials, and sealed tightly. All the vials and caps were placed in a high temperature oven for a short period before use in order to insure that they are completely dry. They were then moved to the small chamber of the glove box for five pressure purge cycles, to get rid of any air before they are moved inside the glove box. Two vials were prepared for each run; the first one was used for alkyl aluminum, or co-catalyst. The second one was used for the solid catalyst. Solvent and comonomer were also prepared ahead of time and left under positive nitrogen pressure. Hexane and 1-hexene were contacted at least one day in advance with dried molecular sieves and bubbled with nitrogen for 30 minutes to remove any traces of water and impurities and maintained under nitrogen pressure.

The first step in polymerization is assembling the reactor and making sure it is sealed well without any leaks. Next, the feed and vent lines were connected to the reactor via quick connecters connection. Then, the heating jacket was placed in its position. Finally, the cooling water was made available and the reactor was ready for use.

The reactor was purged alternately with vacuum and nitrogen for three times in order to remove the air inside the reactor. Then, the reactor temperature was set at pre-heating mode where the temperature will increase up to 125 °C. During the heating cycle the reactor was pressurized and evacuated three to five times to remove any trace of oxygen and moisture. Once the reactor temperature reached 125 °C, the reactor was automatically cooled down to 35 °C to avoid any loss of solvent during transferring. At this point the reactor was ready for the solvent transfer. As described previously, the solvents were prepared by distillation in case of toluene, or dried and purged in case of hexane.

The solvent transfer was initiated by pressurizing the solvent source with 10 psig of nitrogen. A transfer needle was inserted into the solvent bottle, but not in to the solvent, to let it purge for one minute in order to remove any air trapped within. The free end of the needle from the solvent vessel was then inserted into a sealed and purged round flask (250 ml), which was calibrated to 150 ml. A vent needle, which was connected to a bubbler, was inserted into the round flask to be purged for one to two additional minutes. 150 ml of solvent was transferred into the round flask just by dipping the needle end into the solvent then pushed with nitrogen. After transferring the desired amount of solvent, it was bubbled for one minute with the same transferring needle from the source vessel.

Next, the vent needle was removed, followed by removal of the transfer needle from the source vessel. This was done in such a way to make sure that a positive pressure was maintained in all vessels all of the times.

A measured amount of scavenger (0.2 – 1.2 g) was prepared inside the glove box in a sealed vial, and was then transferred and mixed with 150 ml of the solvent. This was performed by pressurizing the vial with 10 psig nitrogen and purging with nitrogen for 10-30 seconds. During the purging, extra caution was needed to avoid any aluminum alkyl splash, which is very dangerous. After that, the small amount of aluminum alkyl was transferred to be mixed with the solvent. Mixing was done by gently bubbling with nitrogen for two minutes in order to remove any fumes generated by the reaction through the vent needle. At this point the solvent was ready to be transferred into the reactor. This was done by pressurizing the round bottle with nitrogen, then connecting the transfer needle from the round flask to the top valve of the catalyst injection port. During the transfer, the vent line in the reactor needed to be opened in order to create a pressure difference that allowed the solvent to be transfer to the reactor. Around 20 ml of the solvent was left in the round flask to be used in the catalyst transfer later on.

After the 130 ml of solvent was transferred into the reactor, the transfer needle was removed. Both the reactor and the solvent flask were kept under a positive nitrogen pressure. In case of copolymerization, 6 ml of purified 1-hexene was transferred from 20 ml vial into the reactor. It was done by pressurized vial with 10 psig nitrogen, and then a clean transferred needle was inserted into the vial, but not into the 1-hexene and let it

purge for 10 – 20 seconds. Then, the second end of transferred needle was connected to the top valve of the catalyst injection port. Since, the reactor was under the same pressure, a pressure difference needs to be created to allow the transfer of the 6 ml of 1-hexene. This was performed by venting the reactor very gently through the vent valve, then the transferred needle was lowered into the 1-hexene and the transferring was started. After all the 1-hexene amount was transferred the reactor vent valve was closed, then the transferred needle was removed and quickly the isolation valve was closed. The isolation valve between the catalyst injection port and the reactor was closed to prevent any back pressure generated by the solvent vapor pressure. The reactor was then heated up to the desired reaction temperature, and pressurized with ethylene to the desired reaction pressure which was maintained with a pressure regulator. At this point, the data acquisition system automatically started and the run number was saved in the data acquisition software.. At this point, the reactor is ready for catalyst charging.

As mentioned above, the solid catalyst was measured (0.01to 0.025g) and prepared inside the glove box in a 20 ml vial and sealed. Catalyst transfer started by pressurizing the round bottle with nitrogen, then the transfer needle was inserted and purged for a short while. The second end of the transfer needle was inserted into the catalyst vial. Another transfer needle was inserted close to the bottom of the catalyst cylinder, through the top valve with septa, and purged for 20-30 seconds. After that, the other end of the transfer needle was connected to the catalyst vial. The solvent was transferred into the catalyst vial gradually and mixed. The transfer was accomplished by dipping the transfer needle into the solvent source vessel, and was removed when the catalyst vial was half full.

Next, the mixture in the vial was transferred to the catalyst port with continuous hand mixing during the transfer. The step was repeated two to three times until all of the catalyst solution was transferred into the catalyst port. During the transfer, a needle valve connected to a bubbler was connected to the top of the catalyst port in order to create a pressure difference, and allow the solvent and catalyst to be conveyed.

All the transfer needles were removed from the catalyst port and isolated. The nitrogen valve was closed and the ethylene was lined up to the catalyst port. Just before injecting the catalyst into the reactor, a positive nitrogen pressure was imposed to ensure the transfer of all of the catalyst. Finally, the catalyst was injected into the reactor by just opening the isolation valve between the catalyst port and the reactor vessel.

The reaction begins rapidly once the catalyst is injected into the reactor. The beginning of the reaction is characterized by a high ethylene flow rate, and a slight decrease in the reactor temperature due to the solvent injected with the catalyst. This is then followed by minor increase in the reactor temperature (± 2 °C) due the reaction start. The reactor stabilized within one minute. However in case of reactor fouling (due to catalyst leaching) or a sluggish controller overshoot (due to a poorly tuned controller), and subsequent oscillations will occur. Nevertheless if care is taken to avoid leaching and properly tune the controller, the temperature control was generally good, and any slight oscillations observed (± 0.2 °C) should have minimal if any effect on the catalyst activity or polymer properties. Reaction time and ethylene consumption were recorded. Total

yield was obtained from the total amount of ethylene fed to the reactor, and the polymerization rate was the value of the instantaneous monomer flow rate.

When the polymerization time finished, the data acquisition system stopped, the mixing stopped, heating jacket removed, ethylene flow stopped, and reactor was vented. All of these steps need to be performed very quickly. Then, the reactor was dismantled and all its contents (polymer and solvent) were transferred to a beaker containing ethanol and acid traces to deactivate any catalyst or co-catalyst that was still active. Finally, the reactor was cleaned very well for the next run.

A magnetic stirrer was used to agitate the ethanol mixture containing the reactor powder. The product was then filtered with filter paper and dried for overnight inside the fume hood. The net weight of the product was calculated in order to determine the catalyst activity. At this point, the final product was ready for any analysis and characterizations.

4.3 Result and Discussion

A preliminary screening study was performed to identify the most appropriate reaction conditions for this catalyst system. A wide range of reaction temperatures (60 – 85 °C) and ethylene pressure (100 -190 psi) were tested. The experiments showed that 75 °C was the best temperature in terms of obtaining the highest catalyst activity and reactor stability. This temperature is in the range of those used for commercial production, so the data generated will be useful in an industrial context. An ethylene pressure of 190 psi produced the highest activity

with no deleterious effects on the reactor stability. The results of these experiments are not presented here for the sake of brevity.

4.3.1 Identification of Reference Conditions

Once the appropriate reaction conditions were identified, we began by studying the impact of different activators or co-catalysts, including Trimethyl aluminum (TMA), Tri ethyl aluminum(TEAL), Trisobutyl aluminum (TIBAL), Tri n-octyl aluminum (TOAL) , Methyl aluminumoxane (MAO), and polymeric Methyl aluminum oxane (PMAO). The type of alkyl aluminum used as an activator had a strong impact on the reaction, as shown by the results in Figure 4.3.

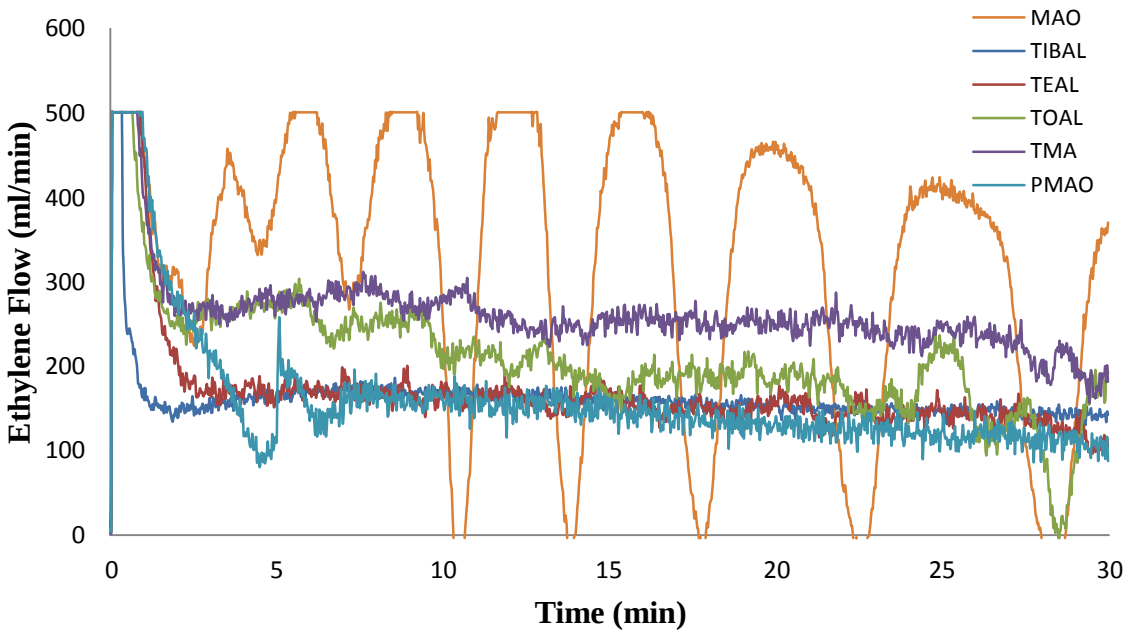

Figure 4.3: Kinetic profile of catalyst Cp_2ZrCl_2/PMAO supported on ES-70 silica with different co-catalysts [Rxn Temp.: 75 ^oC, C2 Press.: 190 psig]

MAO certainly gave the highest activity, as expected, but with very bad morphology and reactor fouling due the leaching problems, and also led to fluctuations in the reactor temperature and ethylene flow, as shown in Figure 4.4. When leaching occurred a thin polymer layer would coat the reactor wall, impeller, and the thermocouple. The polymer fouling on the reactor temperature element will lead to poor temperature control. As a result, the fluctuation in temperature will be directly reflected on the ethylene flow due to the fluctuation of the changing pressure (solvent vapor pressure) in the reactor. At the same time, the high polymerization rate with MAO made the temperature control difficult especially at the beginning of the reaction. The rest of the co-catalysts had lower activity compared with MAO, but with less level of leaching. TIBAL and TEAL showed the best performance in terms of morphology control and produced spherical particles at the end of the reaction , with almost no leaching or reactor fouling, and reasonable activity (but lower than that obtained with MAO). Since, the product morphology is very important for this research, TIBAL was selected to be used in all of the experiments as a co-catalyst and scavenger, because it had the best performance in general.

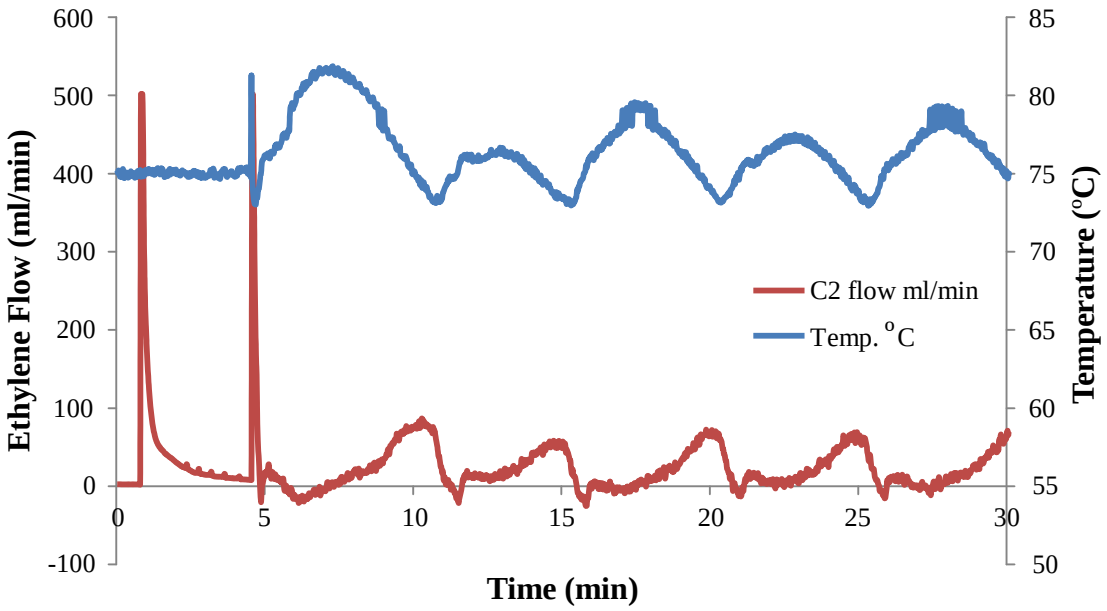

Figure 4.4: Kinetic profile of catalyst Cp_2ZrCl_2/PMAO supported on 2408HT silica with MAO as scavenger

Two types of solvents (toluene and hexane) were also tested in polymerization. Hexane was selected because it had less leaching (as would be expected), better morphology control, and a similar activity as was obtained with toluene.

These experiments allowed us to set a reasonable set of reference conditions, summarized in Table 4.2, that were used in the remainder of the experiments presented below.

Table 4.2: Reaction conditions applied with all of the polymerization experiments

Solvent	Hexane
Temperature (°C)	75
C_2 Pressure (psig)	190
Reaction time (min)	30
Mixing speed (RPM)	500
Catalyst	(Cp_2ZrCl_2/PMAO) supported on silica
Supported catalyst amount (g)	0.025
Co-catalyst TIBAL (g)	0.6

4.3.2 Reproducibility

The catalyst preparation and polymerization experiments showed good reproducibility. The reproducibility of the catalyst supporting was tested by producing three batches using the unsieved 2408HT silica and Cp_2ZrCl_2/PMAO with the same method. These three batches (Cat.A, Cat.B, and Cat.C) were polymerized under the same exact conditions, and showed good reproducibility, as shown in Figure 4.5. Then, three replicate polymerizations (Cat.A-1, Cat.A-2, and Cat.A-3) were performed with one of these catalyst batches, showing reasonable reproducibility.

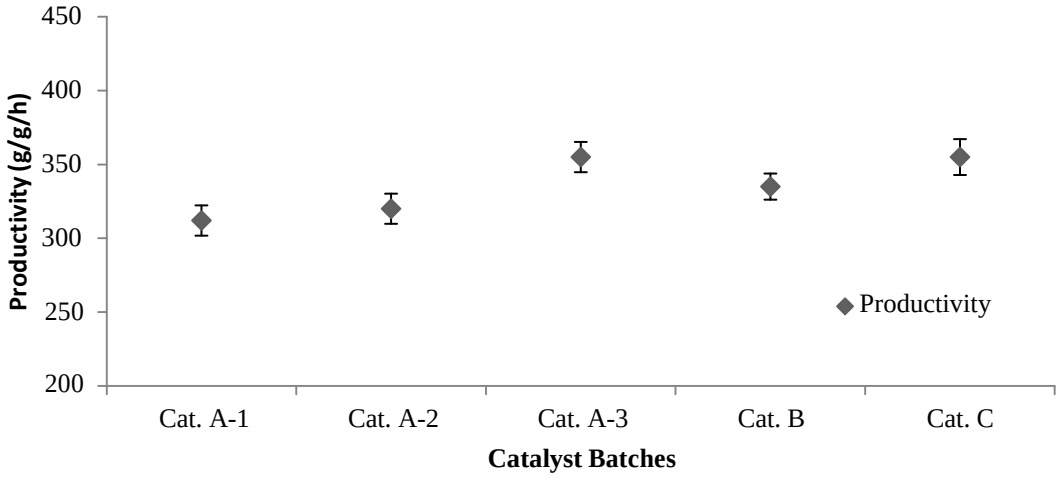

Figure 4.5: Reproducibility of three catalyst (Cp_2ZrCl_2/PMAO, with TIBAL as scavenger) batches supported on unsieved 2408HT silica with same techniques on the same silica and polymerized under the same reaction conditions

4.3.3 The Effect of Silica Support on Kinetics

The next step in this research was preparing the three catalyst batches with three different silica supports. For that purpose, SYLOPOL 955 and 2408HT from Grace Davison and ES-70 from INEOS were used to support the catalyst precursor Cp_2ZrCl_2. Each one of these silicas has different physical properties in terms of surface area and pore volume, as described in Chapter 3.

One of the first observations was that there was a small difference in the average catalyst activity as a function of the silica support type, as shown in Figure 4.6. However, the difference was within the experimental error, so additional experiments were conducted using different particle sizes to confirm these results. This will be discussed below. In addition, the effect of the silica support type was also reflected on the product morphology which will be discussed in the next section 4.3.4. The rates of

polymerization obtained using catalysts based on each of the three supports are shown in Figures 4.7, 4.8, and 4.9. The rates of both 955W and 2408HT (Grace Davison) in Figures 4.8, 4.9 have very similar kinetic profiles. On the other hand, the shape of the rate curve using the catalyst supported on ES-70 silica, shown Figure 4.7 is slightly different from the other two. It decays to a local minimum more rapidly than the two catalysts supported on the Grace silicas, increases slightly to a local maximum, and then decays very slowly after 6-7 minutes of polymerization. It is possible that the different pore size and volume, as well as the slightly different levels of residual hydroxyl groups discussed in Chapter 3 is at the origin of the different profiles as seen in these three figures.

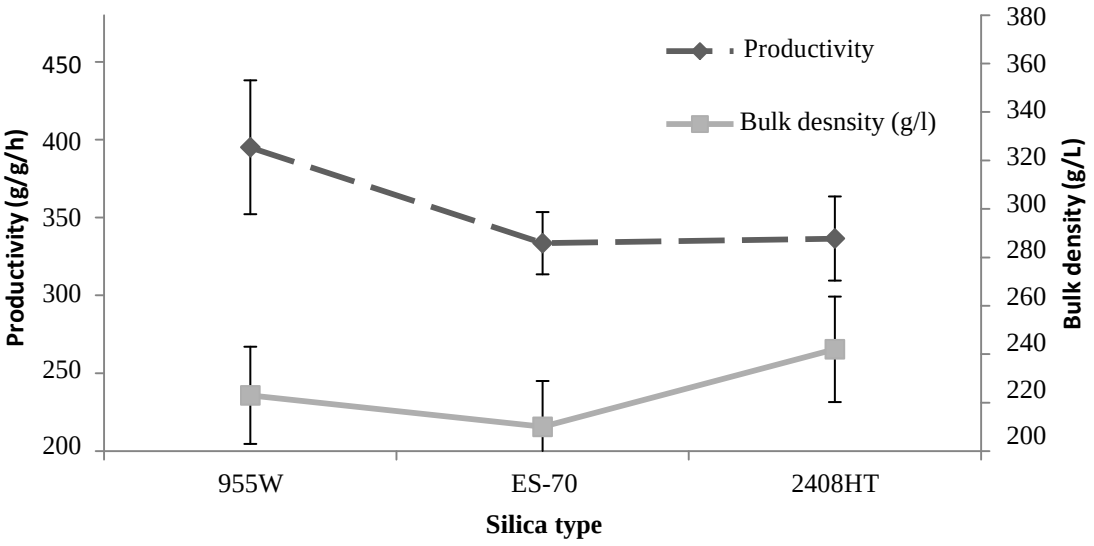

Figure 4.6: The effect of the silica type on productivity and bulk density

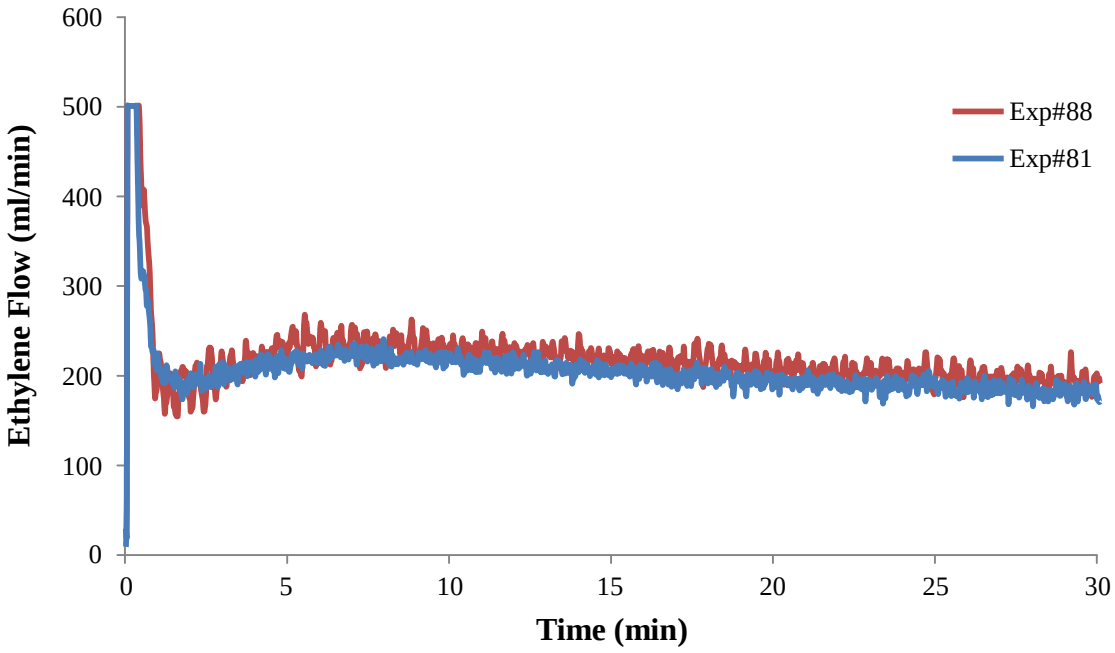

Figure 4.7: Kinetic profile of two replicate runs for catalyst (Cp_2ZrCl_2/PMAO, with TIBAL as scavenger) supported on ES-70 silica

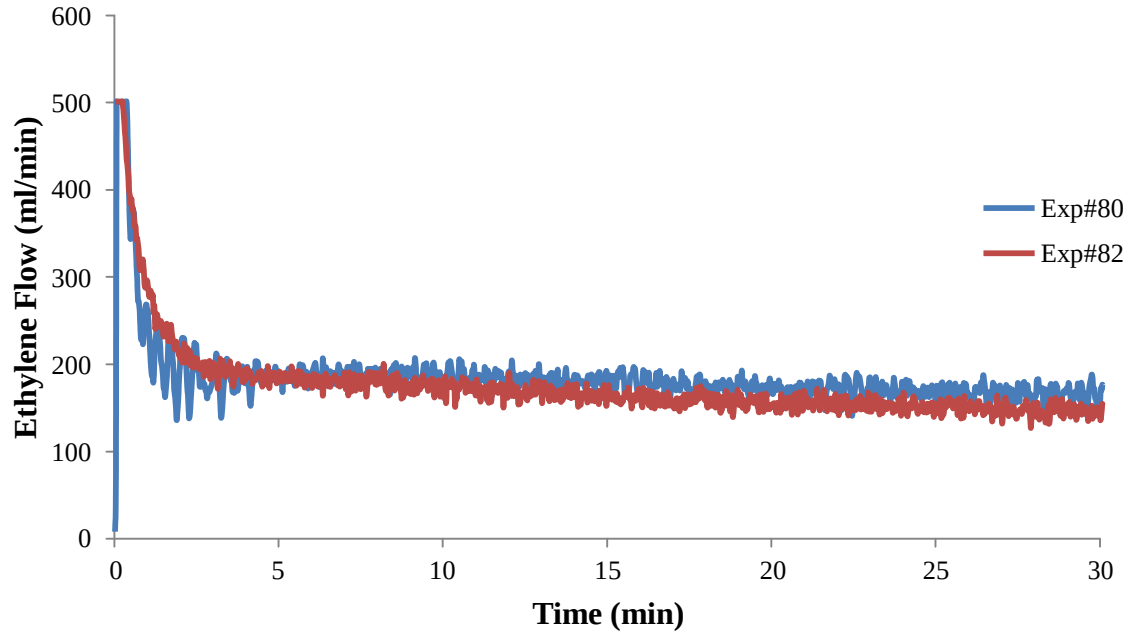

Figure 4.8: Kinetic profile of two replicate runs for catalyst (Cp_2ZrCl_2/PMAO, with TIBAL as scavenger) supported on 955W silica

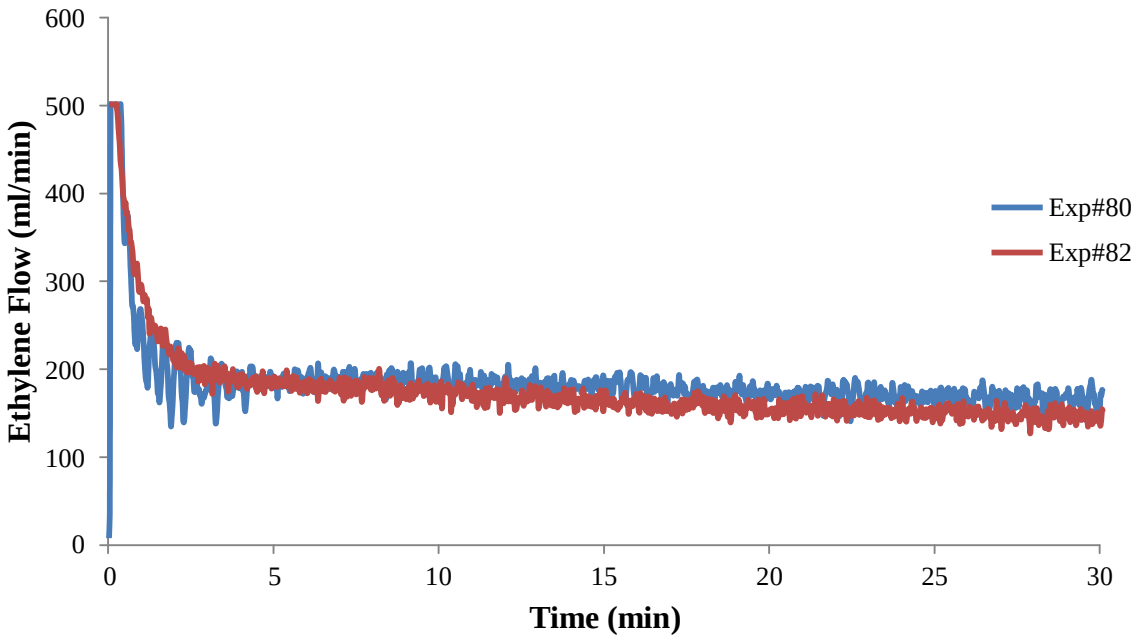

Figure 4.9: Kinetic profile of two replicate runs for catalyst (Cp_2ZrCl_2/PMAO, with TIBAL as scavenger) supported on 2408HT Silica

Copolymerization experiments were conducted under the same reaction conditions and 1-hexene was used as comonomer. The main purpose of copolymerization was to get more understanding about the effect of the silica support type and size on the chemical composition distribution, and molecular weight distribution. At the screening stage, different levels of 1-hexene were used to find out the best set of conditions in terms of reactor fouling and morphology control. High levels (8 ml) of comonomer produced sticky polymer leading to reactor fouling, and bad morphology. Therefore, 4, 6, and 8 ml of 1-hexene equivalent to (0.21 mol/L, 0.32 mol/L, 0.43 mol/L) concentration respectively were tested and 6 ml led to reasonable performance without fouling and comparable morphology with homopolymer. All the homopolymerization experiments with the different silica types (955W, 2408HT, and ES-70) and different particle sizes

were redone with 6 ml of 1-hexene, to study the effect of the support on comonomer incorporation, CCD, and MWD. The kinetic results indicted almost similar activity between the homopolymerization and copolymerization. Even with the addition of the comonomer all of the kinetic profiles remained unchanged. However, more fluctuation in ethylene flow was observed with copolymerization experiments than the homopolymerization, as shown in Figures 4.10 and 4.11.

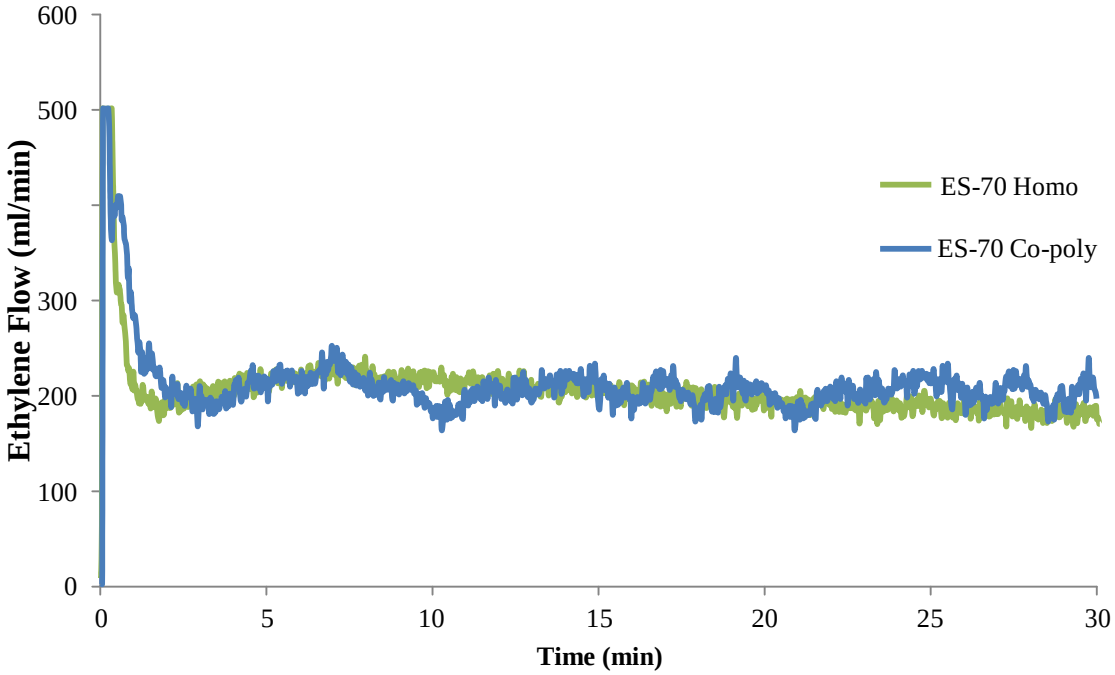

Figure 4.10: Kinetic profiles of homo-polymer and copolymer (6 ml of 1-hexene) of catalyst (Cp_2ZrCl_2/PMAO, with TIBAL as scavenger) supported on ES-70

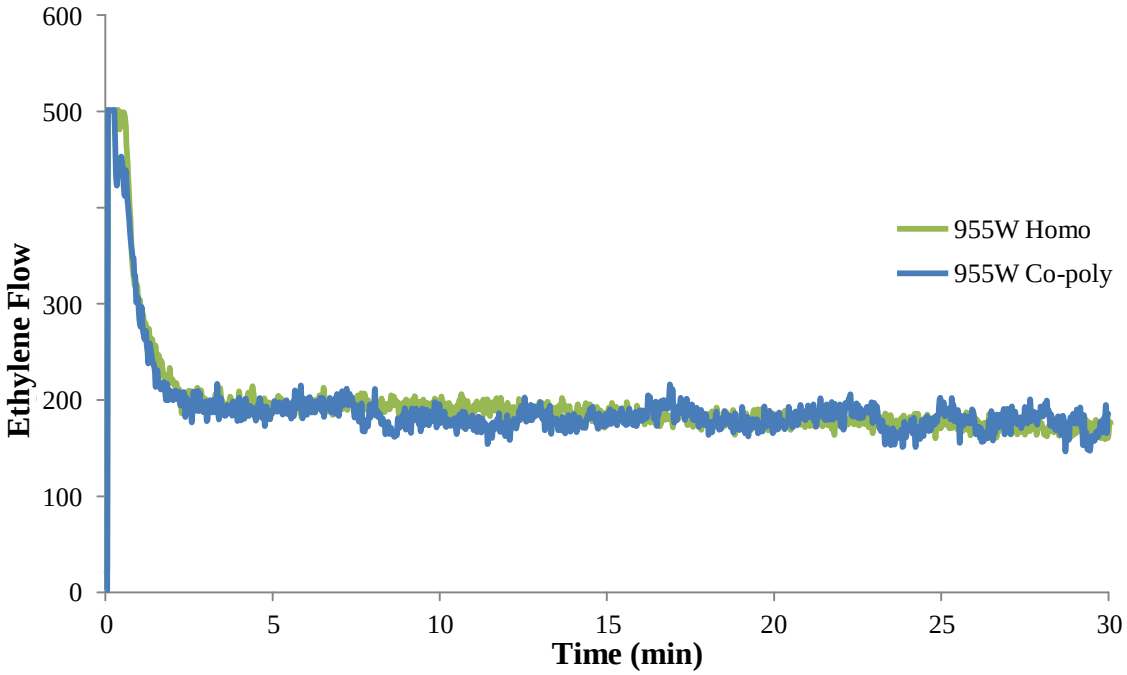

Figure 4.11: Kinetic profiles of homo-polymer and copolymer (6 ml of 1-hexene) of catalyst (Cp_2ZrCl_2/PMAO, with TIBAL as scavenger) supported on 955W

4.3.4 Morphological Effects of the Silica Type and Particle Size

Perhaps more striking that the impact on the rate, was the influence of the support type on the morphology of the polymer particles produced on the different silicas. For example, 2408HT produced higher fine level than the other silicas that was indicated during the bulk density measurements which was performed in a small beaker with known volume, then filled with polymer powder and measure the net weight of the polymer occupying that volume. Also, the SEM results as shown in Figure 4.14 confirm that 2408HT resin had more fines. Thus, the 2408HT products had the highest bulk density and that was common with all products of the 2408HT cuts compared with products of the other silicas cuts, as shown in Figure 4.16. SEM images of the resulting reactor powders illustrated

that there was a clear effect from the silica type on the morphology of the polymer particles, as shown in Figures 4.12, 4.13, and 4.14.

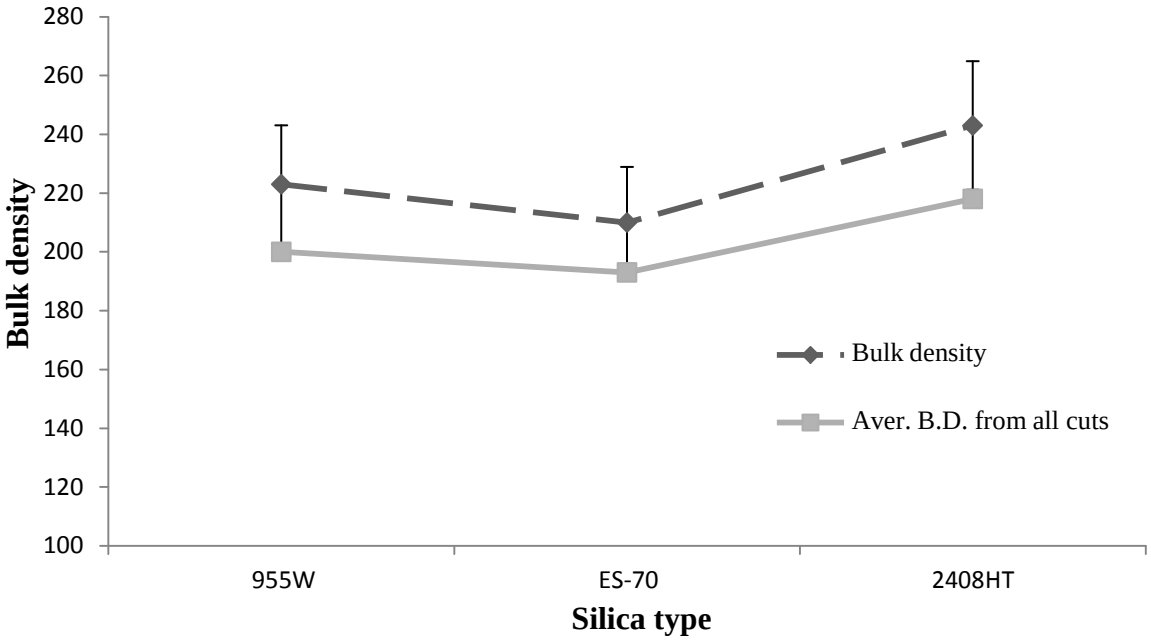

Figure 4.12: The effect of the silica type on the bulk density of the final polymer for unsieved silica supports and average bulk density of all of the cuts from each of the silica

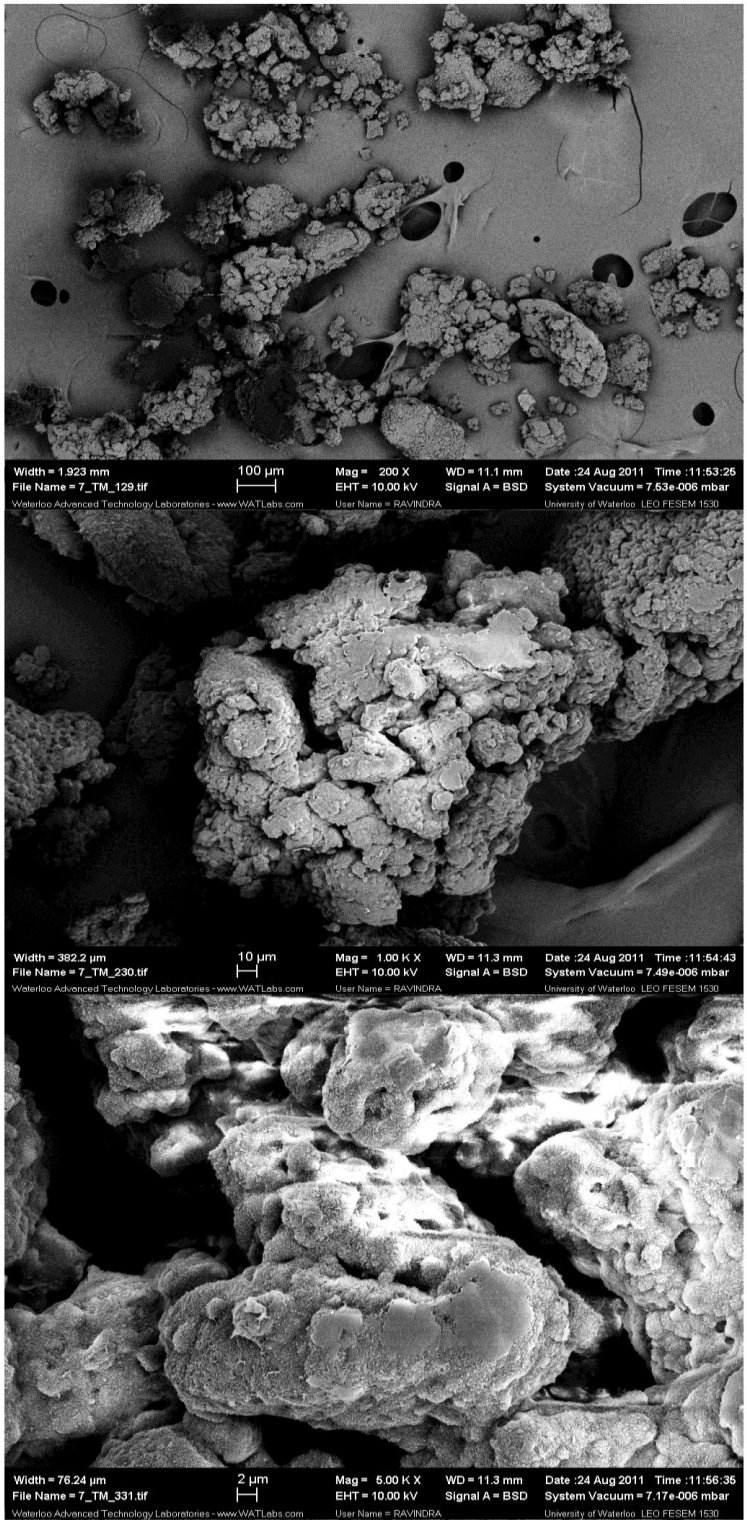

Figure 4.13: SEM images for homo-polymer produced with TIBAL and 955W silica

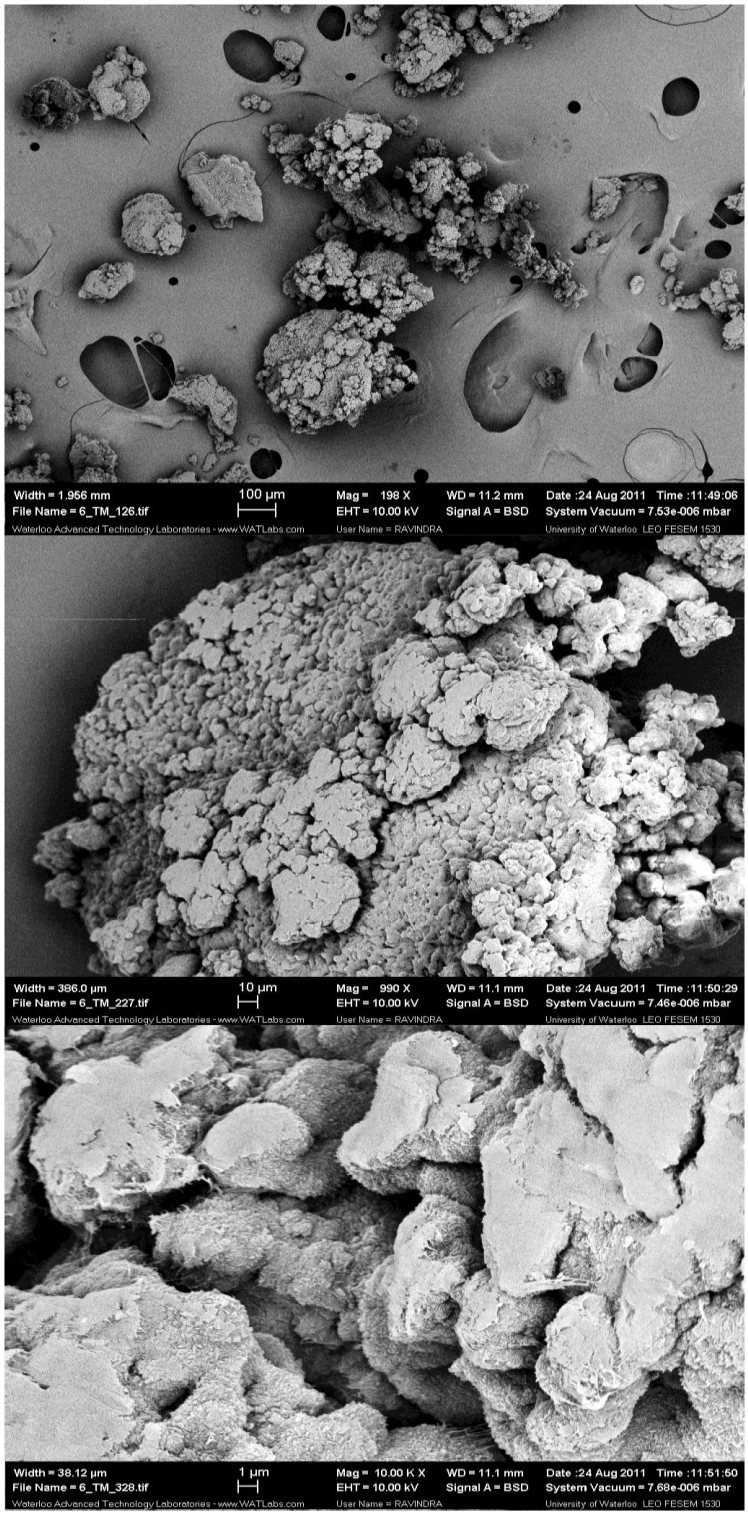

Figure 4.14: SEM images for homo-polymer produced with TIBAL and ES-70 silica

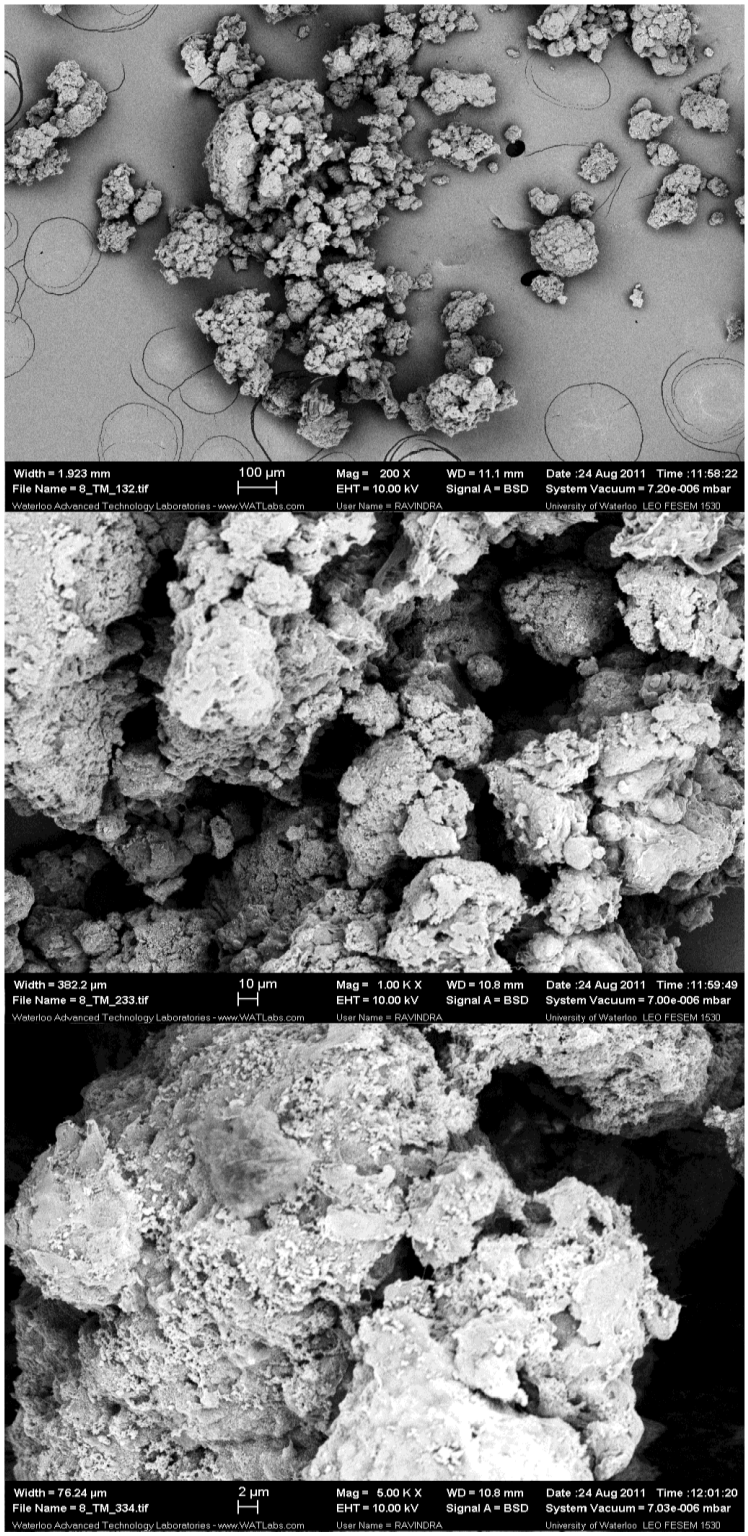

Figure 4.15: SEM images for homo-polymer produced with TIBAL and 2408HT silica

4.3.5 Studies on Fractionated Supports

After looking rapidly at the behavior of catalyst made from original batches of the product, each silica was sieved to five different particle size cuts, as discussed in Chapter 3. Each of the cuts from each of the silicas were used to support the same catalyst (Cp_2ZrCl_2) with the same procedure described previously. Each of the catalyst batches were then polymerized under the same reaction conditions to find out how the silica size might affect the catalyst activity, morphology, and microstructure of the product. As shown in Figure 4.16, and as mentioned above, catalysts supported on 955W showed a higher overall activity than both ES-70 and 2408HT. The same figure also shows that for any given silica, particle cuts greater than 53 μm showed comparable levels of productivity. The smaller particles, especially for the smallest cut, had notably higher yields than the others. Moreover, as shown in Figure 4.15, the average bulk density of the resin from ≥32μm cut showed the same trend (silica to silica) as seen without sieving, but had a slightly higher value for each of the silicas. It is possible that these results can be explained by the difference in pore volumes noted in Chapter 3. Silica 955W had a slightly higher pore volume than the others, with slightly higher levels of Zr loading on the support. While it is difficult to prove that the results in Chapter 3 are statistically significant based on the number of experiments run, the observed rate data presented in this Chapter is coherent with these trends.

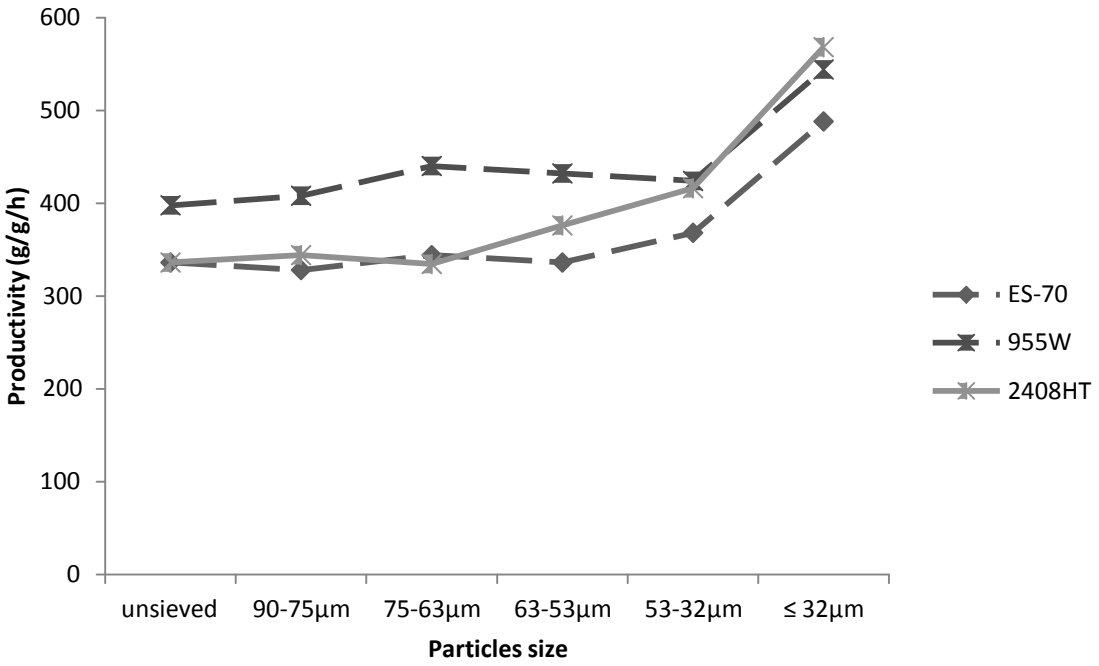

Figure 4.16: Catalyst (Cp_2ZrCl_2/PMAO, with TIBAL as scavenger) productivity with different silica types having different particles sizes

The rate profiles obtained from each of the cuts of each support are shown in Figures 4.17, 4.18, and 4.19. The profiles show that the rates for each of the cuts as a function of time confirm the summary in Figure 4.16: the rate of polymerization is consistently higher on the smallest cut for each of the supports, with the difference between the cuts decreasing as the size of the cut increased. In addition, the results of Figure 4.19 confirm the shape of the curves seen in Figure 4.7 for support ES-70.

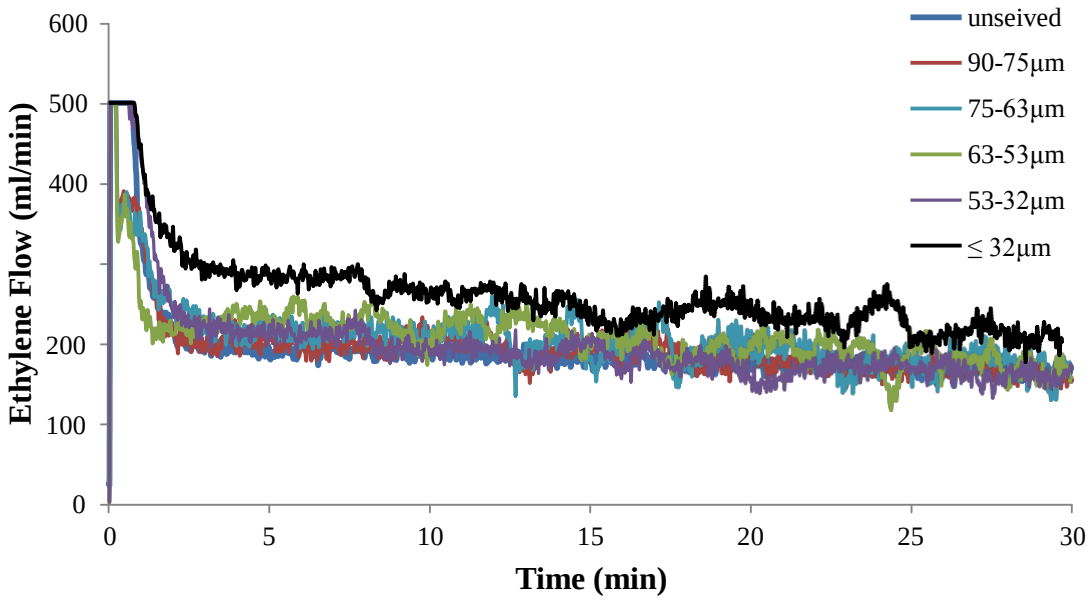

Figure 4.17 : Kinetic profile of catalyst (Cp_2ZrCl_2/PMAO, with TIBAL as scavenger) supported on 955W silica with different particle size cuts

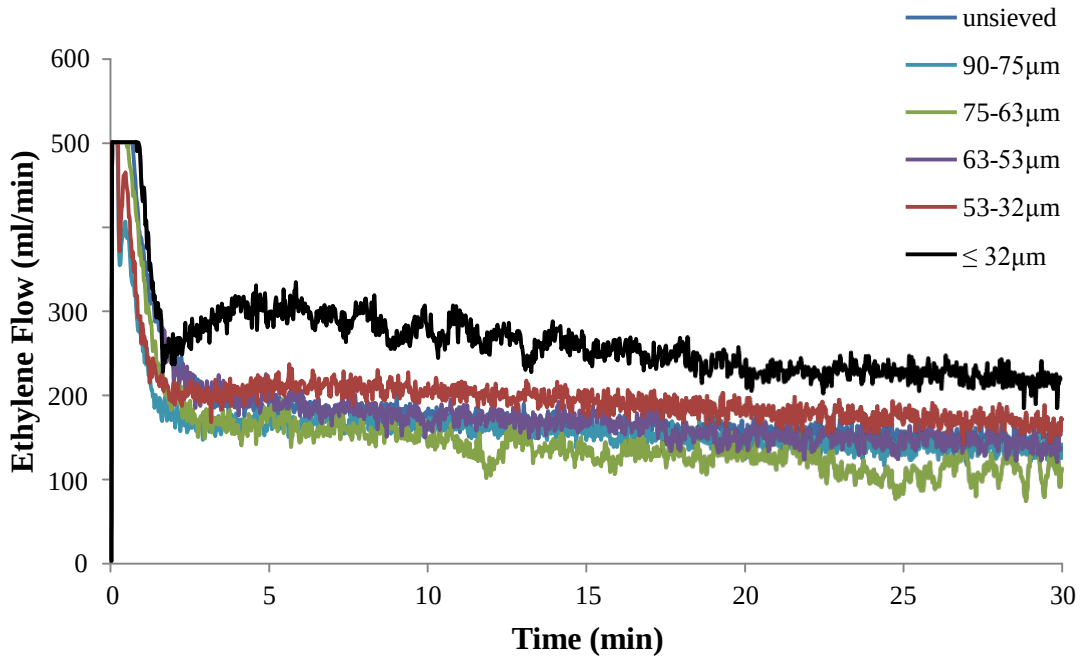

Figure 4.18: Kinetic profile of catalyst (Cp_2ZrCl_2/PMAO, with TIBAL as scavenger) supported on 2408HT silica with different particle size cuts

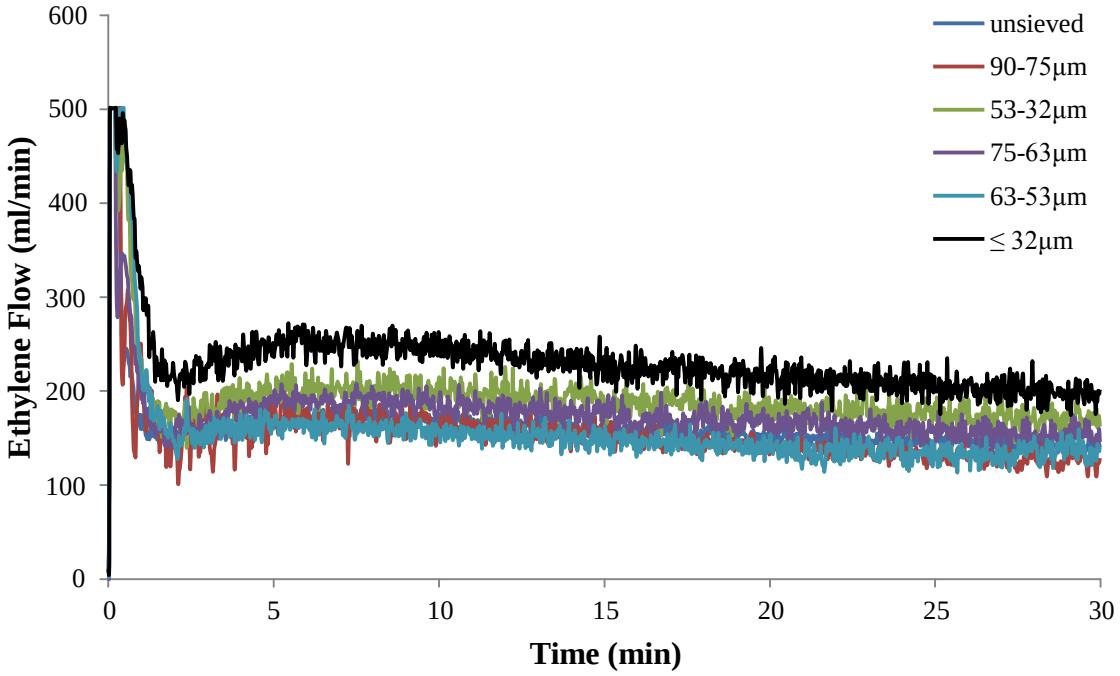

Figure 4.19: Kinetic profile of catalyst (Cp_2ZrCl_2/PMAO, with TIBAL as scavenger) supported on ES-70 silica with different particle size cuts

4.3.6 Effect of Co-catalysts or Scavengers

As mentioned above, the co-catalyst or scavenger used for the polymerization reaction will have an impact on the kinetic behavior and catalyst activity. Further investigations were conducted with different co-catalysts in polymerization with different silica types and different particle sizes. All the catalyst batches were prepared with same method, then reacted under the same polymerization conditions. The Al/Zr ratio in polymerization was also maintained with same level with all of the co-catalysts, as shown in Table 4.3. The co-catalysts used in these experiments were Trimethyl aluminum (TMA), Tri ethyl aluminum (TEAL), Trisobutyl aluminum (TIBAL), Tri n-octyl aluminum (TOAL), Methyl aluminumoxane (MAO), and polymeric Methyl aluminumoxane (PMAO). The purpose of investigation was to study the effect of the co-catalyst with different silica

supports on the catalyst activity, product morphology, and micro properties of the produced resin.

Table 4.3: Amount of co-catalyst/scavenger used in polymerization experiments

Co-catalyst type	Grade	Amount (g)
TIBAL	1.0 M in hexane	0.6
TMA	2.0 M in hexane	0.6
TEAL	1.0 M in hexane	0.6
TOAL	25 wt% in hexane	1.26
MAO	10 wt% in toluene	0.5
PMAO	13 wt% AL in toluene	0.18

The choice of the co-catalyst has little impact on the average rate over the course of 30 minutes reaction, as shown in Figure 4.20. In the initial investigation MAO produced the highest activity, but with very poor morphology, as shown in Figure 4.22 with very bad rector temperature control and severe reactor fouling. PMAO was also used as an activator in the catalyst supporting since it has more aluminum (13 wt% compared with 4.7 wt% in MAO), and along with MAO, both were tested as a scavenger in polymerization. While PMAO produced lower activity, and lower reactor fouling than MAO, both led to severe reactor fouling. All of the other co-catalysts in Table 4.3 produced very little, or no leaching compared with MAO and PMAO. Both TMA and TOAL had more leaching than TIBAL, and TEAL that had almost no leaching. That was simply determined visually at the end of each reaction when the reactor was opened for cleaning, and the higher the degree of leaching the more it was difficult to clean the reactor from the polymer build up. As was the case above, the highest activities were

obtained using 955W silica-supported catalysts regardless of the type of co-catalysts, while catalysts supported on ES-70 and 2408HT silicas were not significantly different.

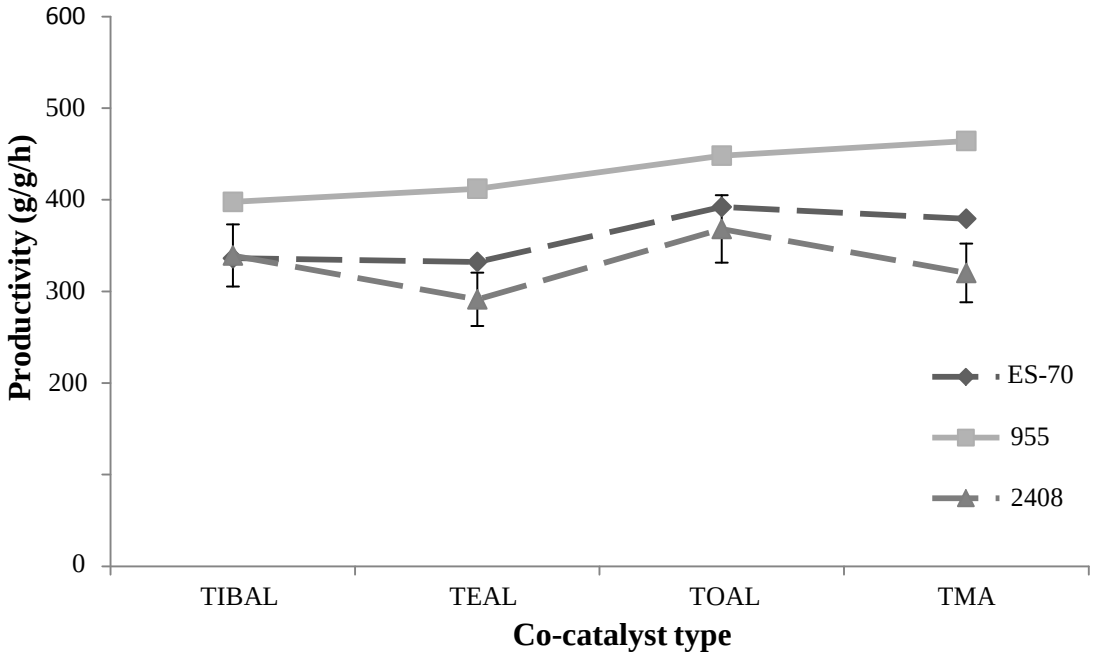

Figure 4.20: Effect of the co-catalysts on productivity with different silica types

Changing the co-catalyst type had a clear effect on the morphology of the final polymer, and that was reflected on the bulk density of the produced polymer. A clear trend was found with different co-catalyst types on the bulk density with different silica support types, as shown in Figure 4.21. It shows that TMA and TOAL led to lower bulk densities than TEAL and TIBAL did. It is possible that this is due to the fact that TMA and TOAL had higher activity, producing bigger, less well defined particles with no sphericity.

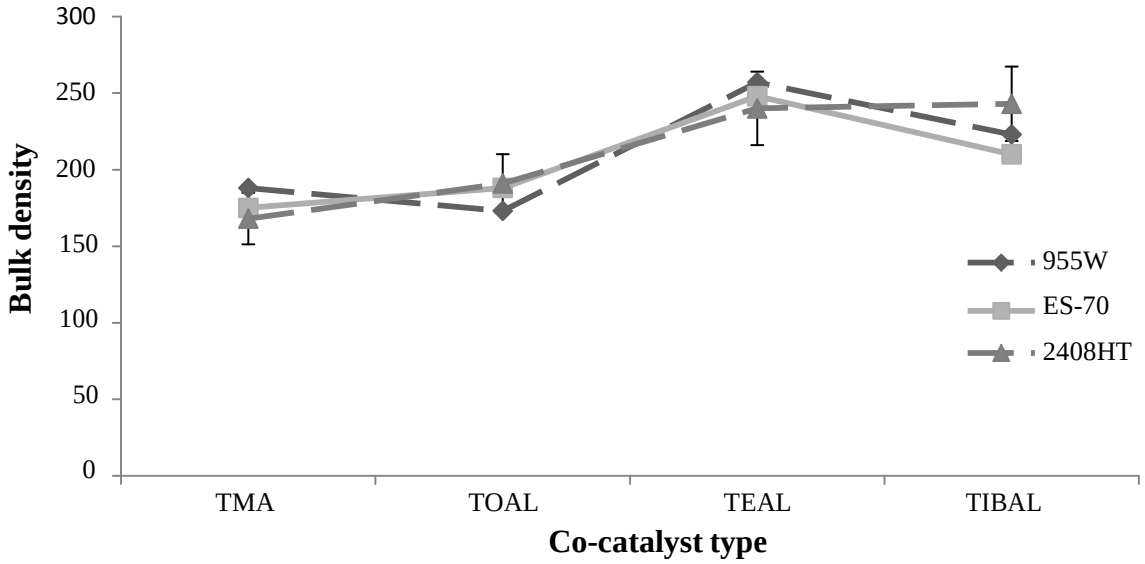

Figure 4.21: Effect of co-catalysts on the bulk density with different silica types

For instance, the images of particles made with TOAL as the co-catalyst in Figure 4.24 shows how that the resulting particles had rough surfaces and were irregularly shaped. In addition, some of the active sites leached from the silica surface as inferred from the high level of reactor fouling obtained with TOAL.

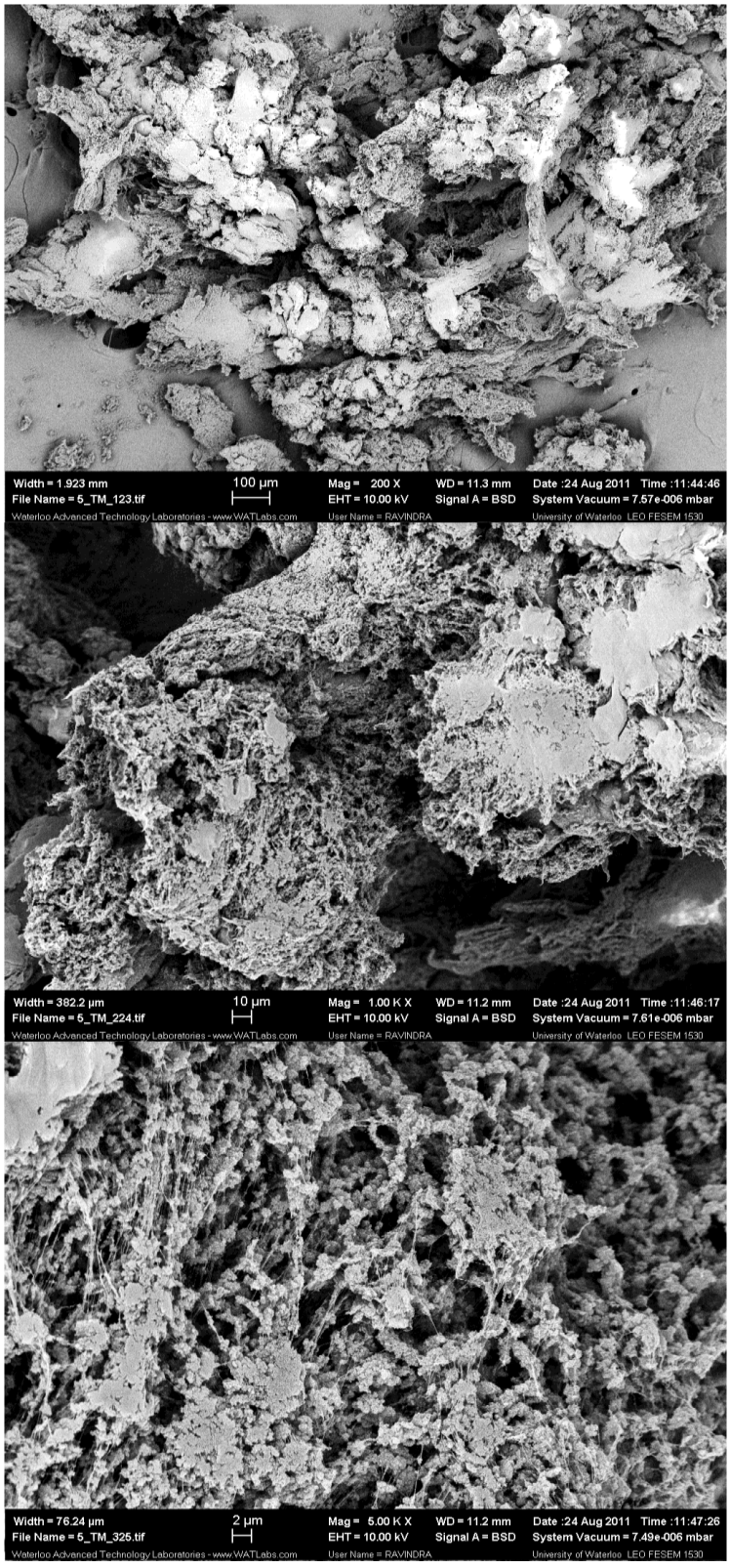

Figure 4.22: SEM image for homo-polymer produced with MAO with ES-70 silica

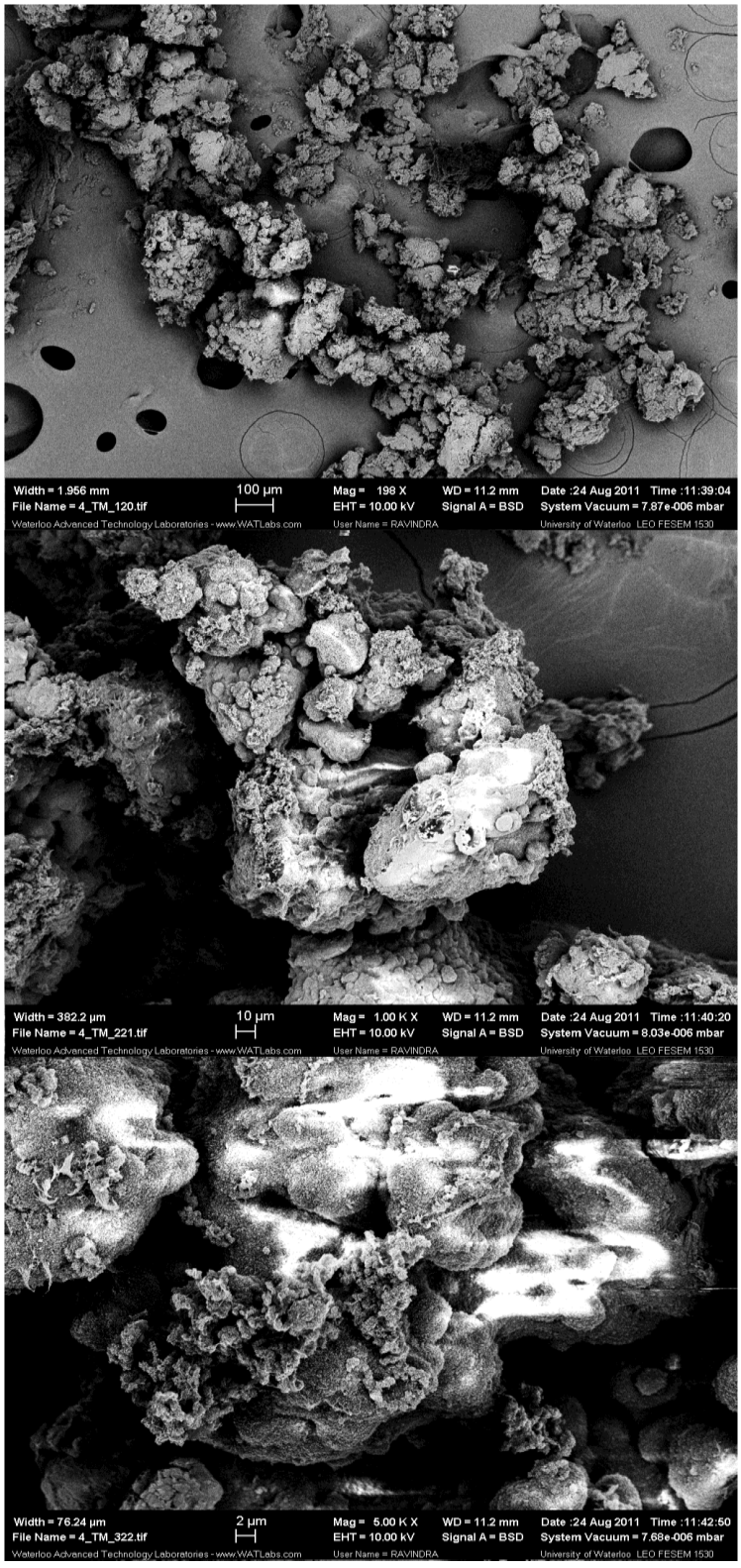

Figure 4.23: SEM images for homo-polymer produced with PMAO and ES-70 silica

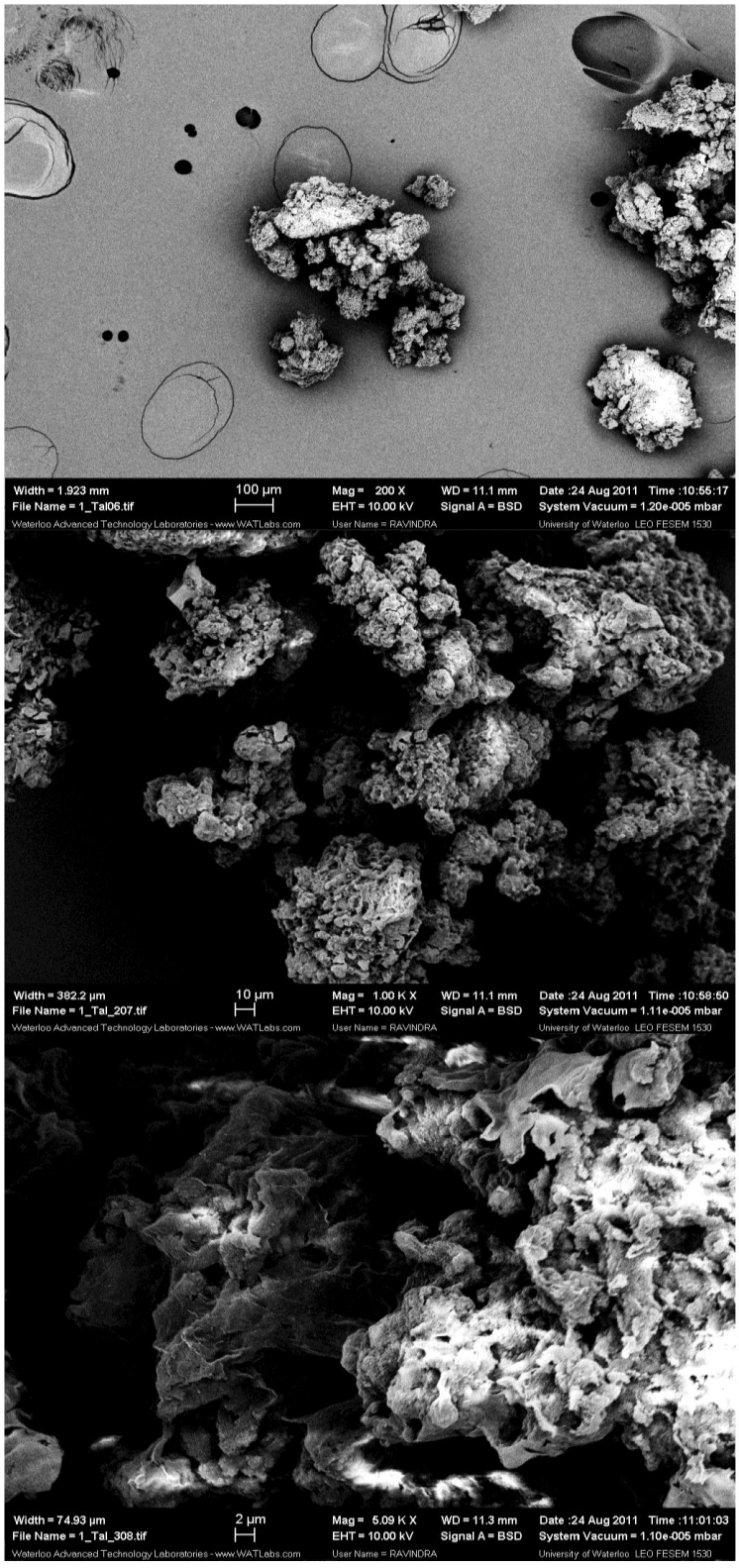

Figure 4.24: SEM images for homo-polymer produced with TOAL and ES-70 silica

When TEAL was used with ES-70, it tended to produce smaller particles, as shown in Figure 4.25. The SEM images show that TEAL had good morphology control that produced particles with a more regular surface and more spherical shape compared with TOAL and TMA products. No leaching was observed with TEAL either. Furthermore, the product obtained with TEAL had a higher bulk density than those made with TMA or TOAL, once again suggesting that these products have a more regular shape.

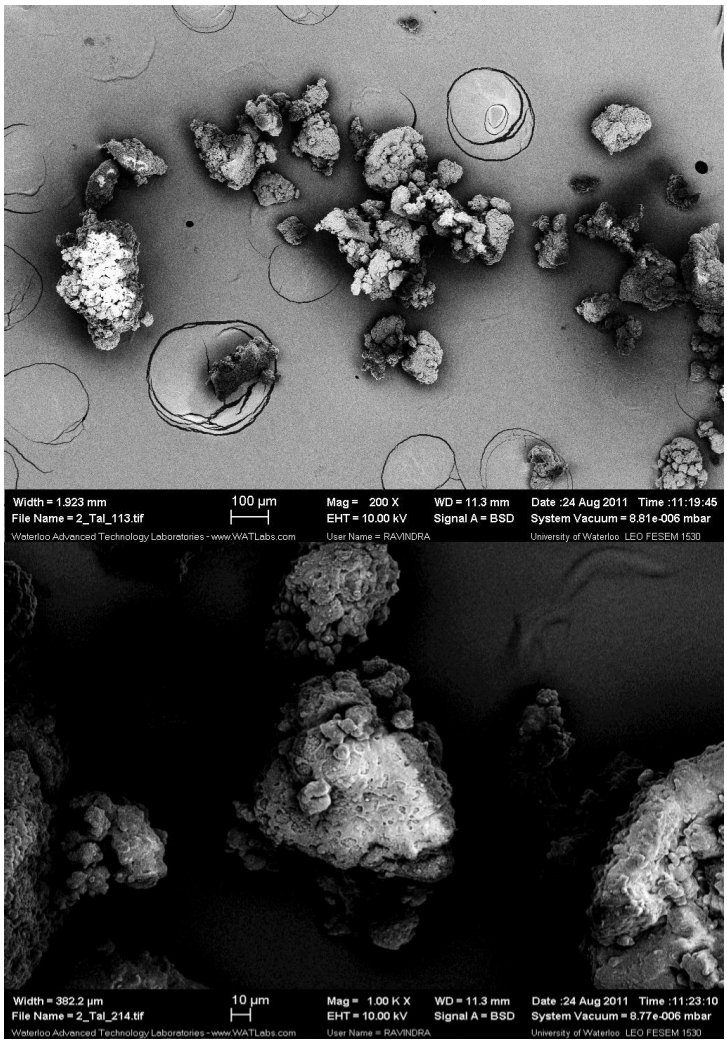

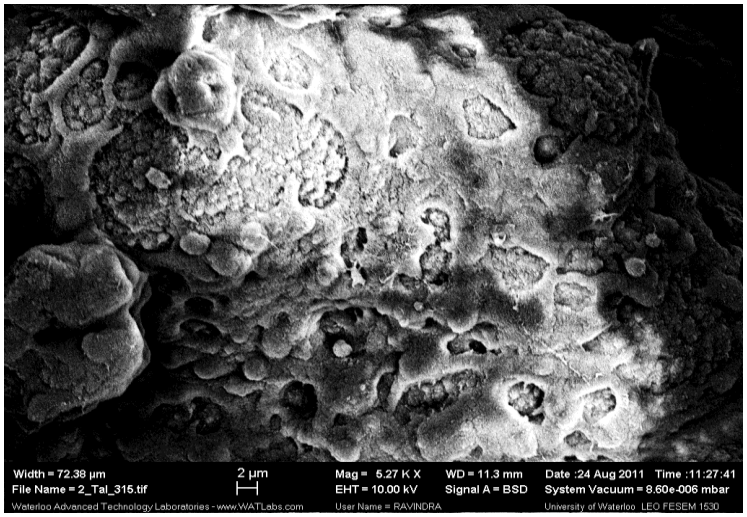

Figure 4.25: SEM images for homo-polymer produced with TEAL and ES-70 silica

TMA and TOAL seem to lead to particles with similar morphological properties, with slight differences. Both powders had rough surfaces and not uniform particles as shown in Figures 4.24 and 4.26, which, combined with noticeable reactor fouling, imply that leaching was a problem for both types of co-catalyst. Moreover, TMA and TOAL showed high activity and low bulk density.

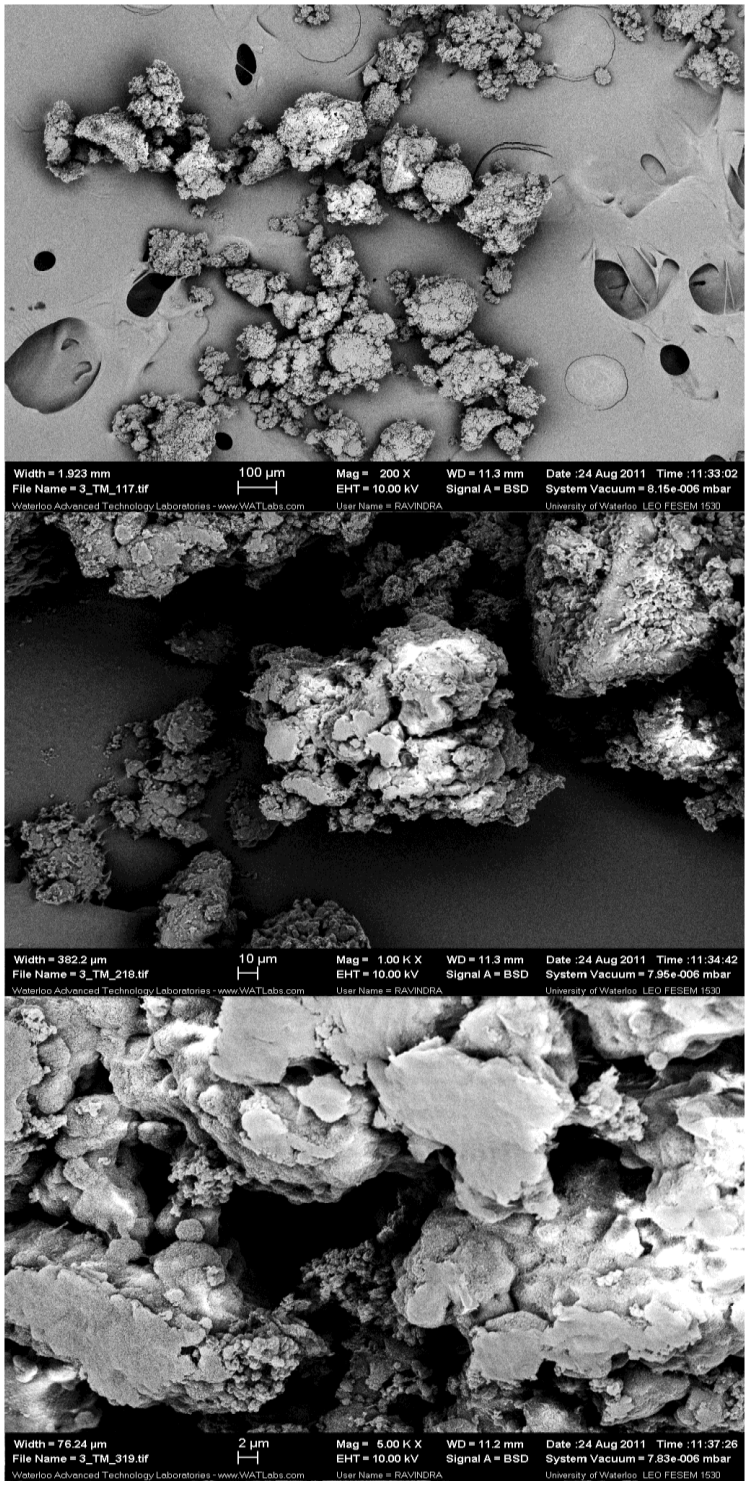

Figure 4.26: SEM images for polymer produced with TMA and ES-70 silica

4.4 Conclusion

Different silica supports led to catalysts that exhibited different kinetic profiles. The shape of the rate profiles for both sieved and unsieved catalysts made from ES-70 showed a different shape of rate curve than did catalysts supported on 955W and 2408HT. Catalysts supported on silica with higher pore volume and surface area (955W) tended to have higher activities than the others. All of the different particle size cuts of the 955W silica had this higher activity, lending credence to this idea.

Different co-catalysts or scavengers were used with a heterogeneous metallocene supported on different silica types. The type of alkyl aluminum had a clear effect on the morphology control. MAO gave the highest catalyst activity, but very poor morphology control. Both TMA and TOAL produced higher activity than TEAL and TIBAL, but with poor morphology and lower bulk density.

The morphological analysis showed that TEAL produced the most regular morphology with the highest bulk density. All the silica types responded similarly to each type of co-catalyst.

Chapter 5

Polymer Characterizations

The wide range of applications of polyethylene resins results from the diversity their microstructural distributions. It is, therefore, important to characterize the microstructure of the polymers made in Chapter 4 in order to determine whether changing support types had an impact on the polymer molecular architecture.

5.1 Materials and Methods

Gel permeation chromatography (GPC) and crystallization elution fractionation (CEF) were used to analyze the MWD and CCD of the polymers, respectively. The materials used in the analyses are listed in Table 5.1.

Table 5.1: Materials used in CEF and GPC analyses

Name	Formula	Grade	Supplier
Nitrogen	N_2	UHP	PRAXAIR
Irganox 1010	N/A	N/A	CIBA-GEIGY
1,2,4 TCB	$C_6H_3Cl_3$	99%	Sigma-Aldrich
n-heptane	$CH_3(CH_2)_5CH_3$	99%	Sigma-Aldrich

For both GPC and CEF, the polyethylene samples were first dissolved in 1,2,4-trichlorobenzene stabilized with Irganox 1010 at 140 ^oC for at least 2 hours. Irganox 1010 is a hindered phenol antioxidant used to scavenge radicals that may degrade the polymer.

5.1.1 Gel Permeation Chromatography

A high-temperature gel permeation chromatographer (Polymer Char, Valencia, Spain) equipped with a Viscotek differential viscometer an infrared mass detector was used for MWD determination. The universal calibration curve was used to calibrate the GPC. Samples were prepared by placing approximately 9 mg of polyethylene powder without any additives in a clean 10 ml vial, 9 ml of TCB, and one drop of n-heptane to serve as a reference peak. The vial was placed in the GPC auto sampler and heated to approximately 140 C for a couple of hours before injection in the GPC columns. Three PLgel 10 µm mixed-B columns (Polymer Labs) were used for the fractionation.

5.1.2 Crystallization Elution Fractionation (CEF)

Crystallization elution fractionation (CEF) was used to determine the CCD of the samples because it is the faster and highest resolution technique for polyolefins today. The schematic diagram of the CEF apparatus from Polymer Char (Valencia, Spain) is shown in Figure 5.1.

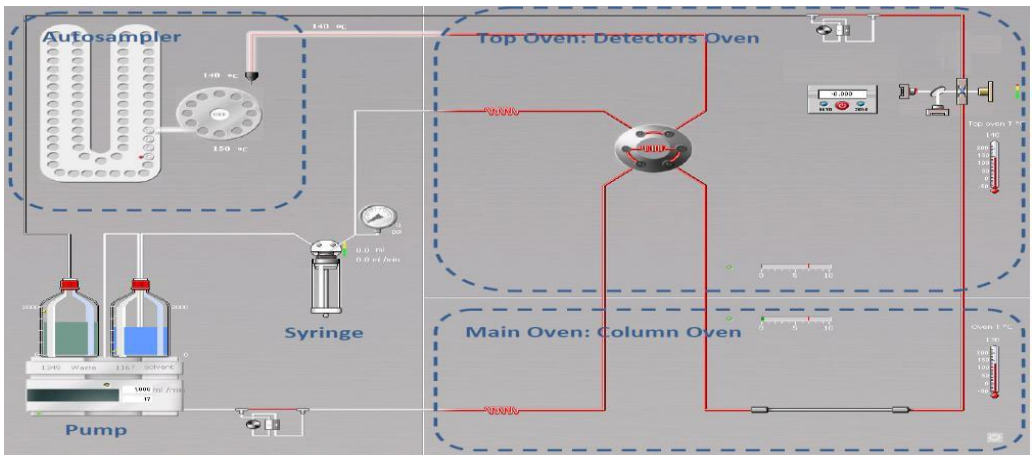

Figure 5.1: Schematic diagram of CEF instrument

The samples were first dissolved in 10-ml size vials in 8 ml of 1,2,4 trichlorobenzene (TCB). The dissolutions were carried out at the instrument's autosampler. The sample concentrations were 0.5 mg/ml. The dissolution temperature was 160 °C and the dissolution time was 1 hour. At the end of the dissolution period, the samples were transferred from the autosampler to the injection loop using a dispenser. The content of the loop (0.4 ml) was injected into the CEF column using an isocratic pump. At the column, the polymers were fractionated according to their "crystallizabilties" using two temperature cycles. During the crystallization cycle, the column temperature is decreased under continuous TCB flow within the limits of the column. This solvent flow rate is calculated from the column volume, cooling rate, and the difference between the first and the last temperatures in the cooling cycle. At the end of the cooling cycle, the temperature is kept constant for few minutes and the solvent flow rate is increased to the elution flow rate value to allow the soluble polymer to leave the column and reach the detector. The deposited fractions are then dissolved as the temperature increases during the elution cycle using a continuous TCB flow that allows the fractions to move from the column to the detector in order to measure their concentrations. The infrared detector is located at the instrument's top oven and is kept at constant temperature. At the end of elution cycle, the column is cleaned with fresh solvent in order to be ready for the injection of the next sample. All of the experiments were performed under the same conditions listed in Table 5.2 which is considered the standard conditions used for polyolefins with High density polyethylene [73, 74].

Table 5.2: CEF running conditions for all the experiments

Parameters	Run conditions
CR (°C/min)	1
ΔT_c (°C)	120-35
F_c (ml/min)	0.02
HR (°C/min)	1.5
F_e (ml/min)	0.5
ΔT_h (°C)	140-35

5.2 Results and Discussion

5.2.1 GPC Analyses

The GPC profiles shown in Figure 5.2 reveal that the type of silica used to support the catalyst had a negligible effect on polymer MWD, either for homo-or copolymers. This finding is not unexpected, since the catalyst used to make the polymer was the same for all the silica supports. Therefore, we may conclude that, at least from a MWD point of view, the influence on the support on catalyst behavior was very minor, if any.

In this study, three different types of silica (955W, 2408HT, and ES-70) were utilized to understand the effect of the silica support on the microproperties of the produced polymers. The GPC results indicated that the silica type and size have no clear effect on the MWD of the produced homo-polymers and copolymers, and the Cp_2ZrCl_2 supported on different silicas produce similar polydispersity index (PDI), as shown in Figure 5.2. However, The results in table 5.3 showed that the silica type might influence on the response of the catalyst to the comonomer, which could be indicated between the

difference PDI of the homo-polymer and copolymer of the same silica. For instance, the polymer produced with Cp_2ZrCl_2 supported on silica 955W has the highest difference in PDI between homo-polymer and copolymer compared with other silicas, but the difference is not profound.

However, the *Mn* results in table 5.5 support the idea that the silica type with different physical properties does effect comonomer incorporation. The polymer produced with Cp_2ZrCl_2 supported on silica 955W showed a clear difference between the homo-polymers and copolymers in *Mn*. Catalysts supported on 2408HT had the same effect, but lower than 955W. This reduction in *Mn* with copolymers might be related the comonomer chain transfer effect. Other factor may support this idea, that both silicas 955W and 2408HT had more pore volume and surface area than ES-70 which may allowed more comonomer diffusion lead to this reduction in *Mn*, and that will broaden the DPI and create the differences between the homo-polymers and copolymers, as shown in Figures 5.3, 5.4, and 5.5.

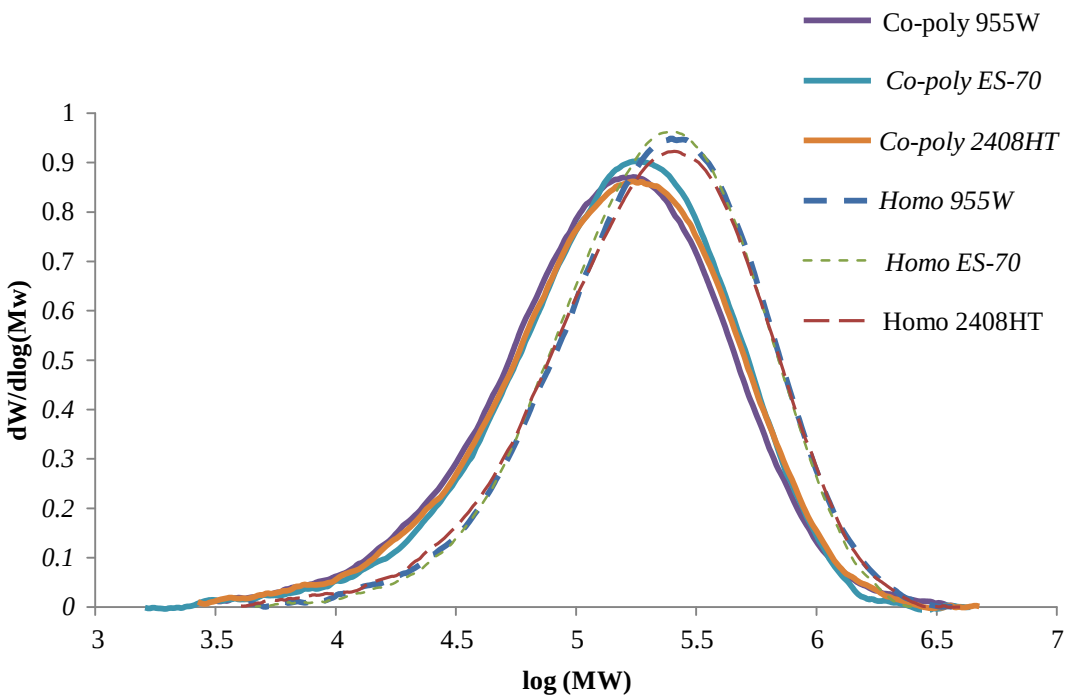

Figure 5.2: MWD of homo-polymers and copolymers produced from catalyst Cp_2ZrCl_2/PMAO supported on different silica type

Table 5.3 : PDI of homo-polymers and copolymers produced from Cp_2ZrCl_2/PMAO with different silica types

Cuts (PDI)	2408 Homo	2408 Copoly	ES-70 Homo	ES-70 C0poly	955W Homo	955W Copoly
N/S	2.8	3.3	2.5	2.8	2.6	3.3
(90-75µm)	3.1	2.9	2.8	2.7	2.7	3.3
(75-63µm)	2.9	3.3	2.8	3.0	2.7	3.1
(63-53µm)	2.7	3.3	2.7	2.8	2.7	2.9
(53-32µm)	2.9	2.9	2.8	2.9	2.6	3.2
(≤32µm)	2.6	2.7	2.6	2.9	2.6	2.9
Average	2.8	3.1	2.7	2.8	2.6	3.1
% diff. Between H&C	8.8		5.7		18.0	

Table 5.4: *Mw* of homo-polymers and copolymers produced with different silica types

Cuts	2408 Homo	2408 Copoly	ES-70 Homo	ES-70 Copoly	955W Homo	955W Copoly
N/S	314000	237000	310000	235000	235000	233000
(90-75μm)	347000	225000	302000	274000	330000	248000
(75-63μm)	316000	225000	300000	236000	330000	227000
(63-53μm)	352000	246000	293000	278000	360000	243000
(53-32μm)	318000	215000	249000	244000	310000	207000
(≤32μm)	352000	253000	310000	281000	319000	210000
Average	333000	233000	294000	258000	328000	228000
% diff. Between H&C	42.7		13.8		44.0	

Table 5.5: *Mn* of homo-polymers and copolymers produced with different silica types

Cuts	2408 Homo	2408 Copoly	ES-70 Homo	ES-70 C0poly	955W Homo	955W Copoly
N/S	112000	73000	126000	84000	123000	71000
(90-75μm)	114000	78000	109000	100000	124000	74000
(75-63μm)	110000	68000	109000	80000	122000	73000
(63-53μm)	129000	74000	109000	99000	135000	84000
(53-32μm)	110000	74000	110000	85000	120000	64000
(≤32μm)	133000	92000	117000	98000	124000	74000
Average	118000	76000	113000	91000	125000	73000
% diff. Between H&C	54.6		24.2		70.4	

The GPC results in Tables 5.3, 5.4, and 5.5 show that the size of the silica support does not have an appreciable effect on M_w and M_n. This is an indication that the differences in polymerization rates reported in Chapter 4 were due to differences in the number of active sites per unit surface area and not due to mass transfer limitations during the polymerization. If mass transfer limitations were significant, one would expect that the particle size cuts that had the highest polymerization rates would also have the highest M_w and M_n values.

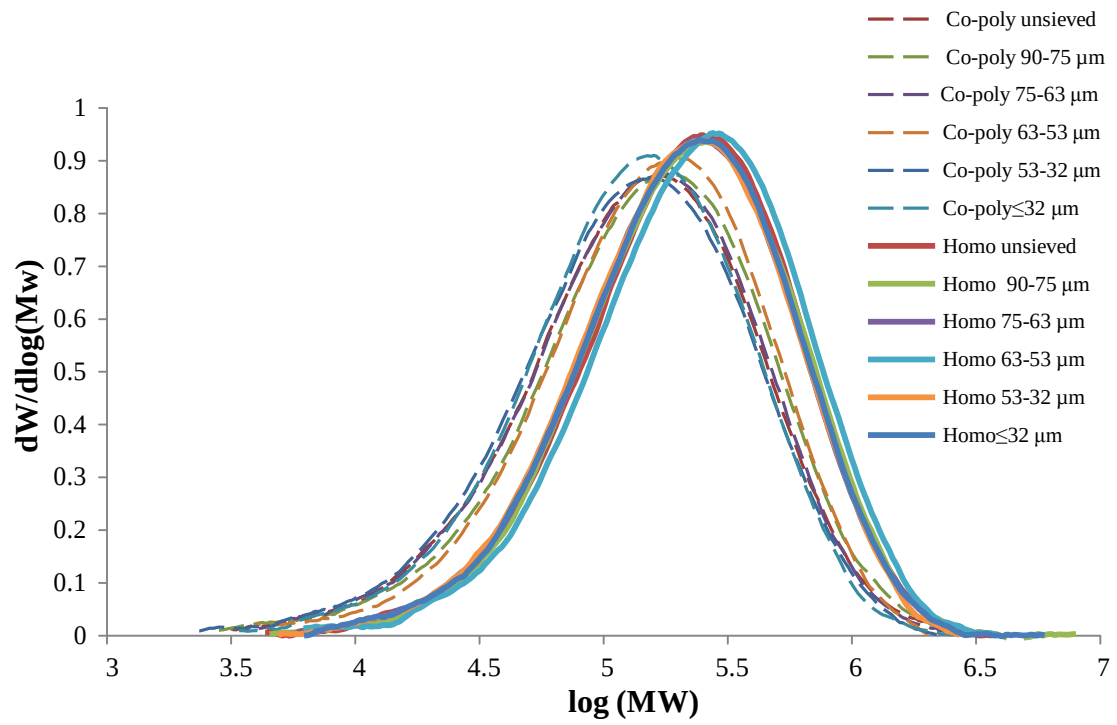

Figure 5.3: MWD of homo-polymers and copolymers produced from Cp_2ZrCl_2/PMAO with different particle sizes from silica 955W

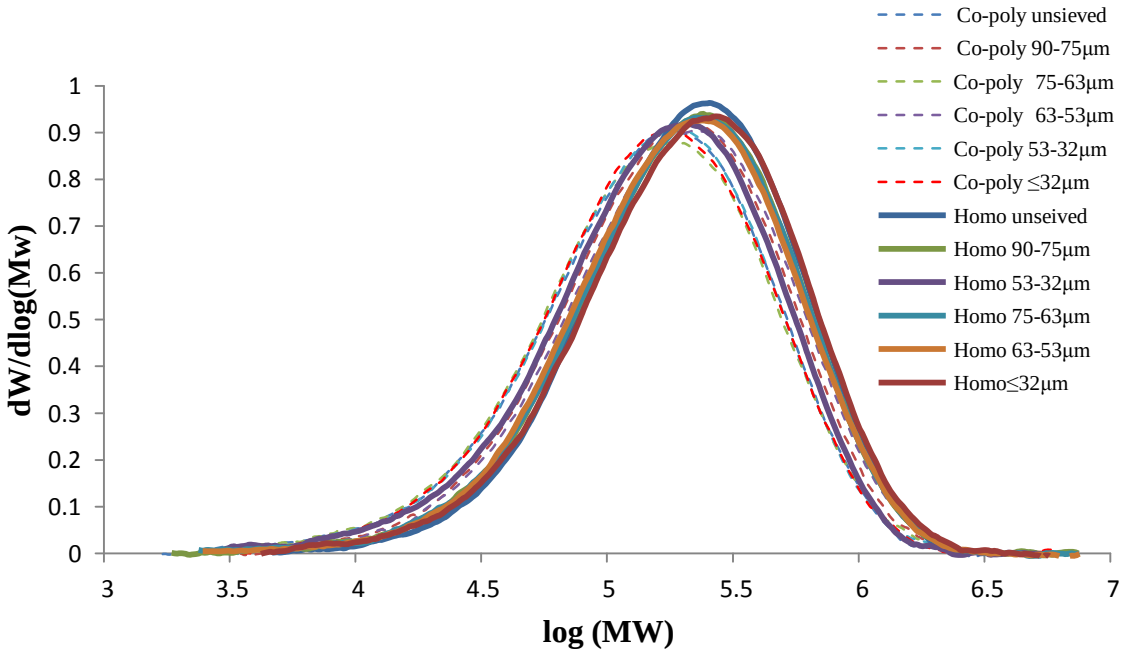

Figure 5.4: MWD of homo-polymers and copolymers produced from Cp_2ZrCl_2/PMAO with different particle sizes from silica ES-70

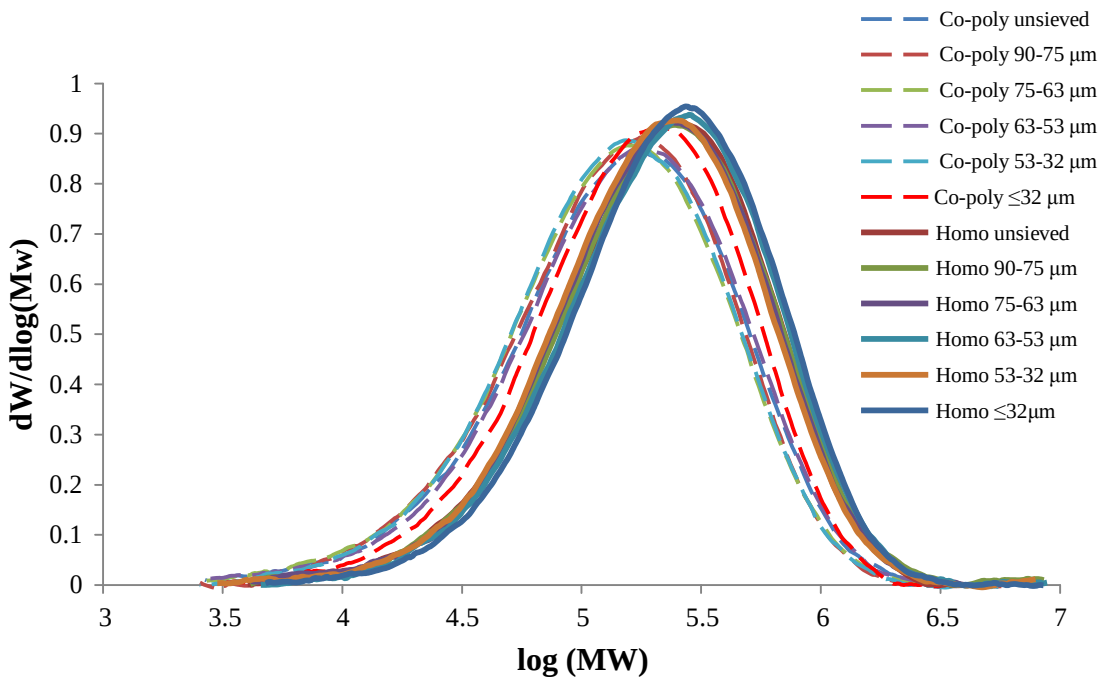

Figure 5.5: MWD of homo-polymers and copolymers produced from Cp_2ZrCl_2/PMAO with different particle sizes from silica 2408HT

In Chapter 4, the effect of different cocatalyst types on ethylene polymerization kinetics and polyethylene particle morphology was investigated. Herein, GPC analyses for the same products are shown in Table 5.6. The Cp_2ZrCl_2 produced polymers with relatively similar MWD with each silica type even with different alkylaluminum compounds, as shown in Figure 5.6. The results suggest that catalyst supported on silica 2408HT makes polyethylene with slightly broader PDI with all tested cocatalysts. The only noticeable difference is that the polymers made using TEAL as a co-catalyst tend to produce slightly lower *Mw*, *Mn* with all of the silicas, as shown in Figures 5.7, 5.8, and 5.9. This may indicate that the TEAL has different chemical behavior during the polymerization than other alkyl aluminums and produce sort of a different MWD.

Table 5.6: PDI, Mw, and Mn of polymers produced from (Cp_2ZrCl_2/MAO) with different co-catalysts and different silica types

Silica	Co- catalyst	PDI	Mw	Mn
2408	TIBAL	2.81	314000	112000
2408	TEAL	3.06	295000	96000
2408	TOAL	2.89	355000	123000
2408	TMA	3.06	422000	138000
ES-70	TIBAL	2.7	294000	109000
ES-70	TEAL	2.7	312000	115000
ES-70	TOAL	2.61	371000	142000
ES-70	TMA	2.49	385000	154000
955-H	TIBAL	2.61	320000	123000
955-H	TEAL	2.72	294000	108000
955-H	TOAL	2.94	364000	124000
955-H	TMA	2.57	339000	132000

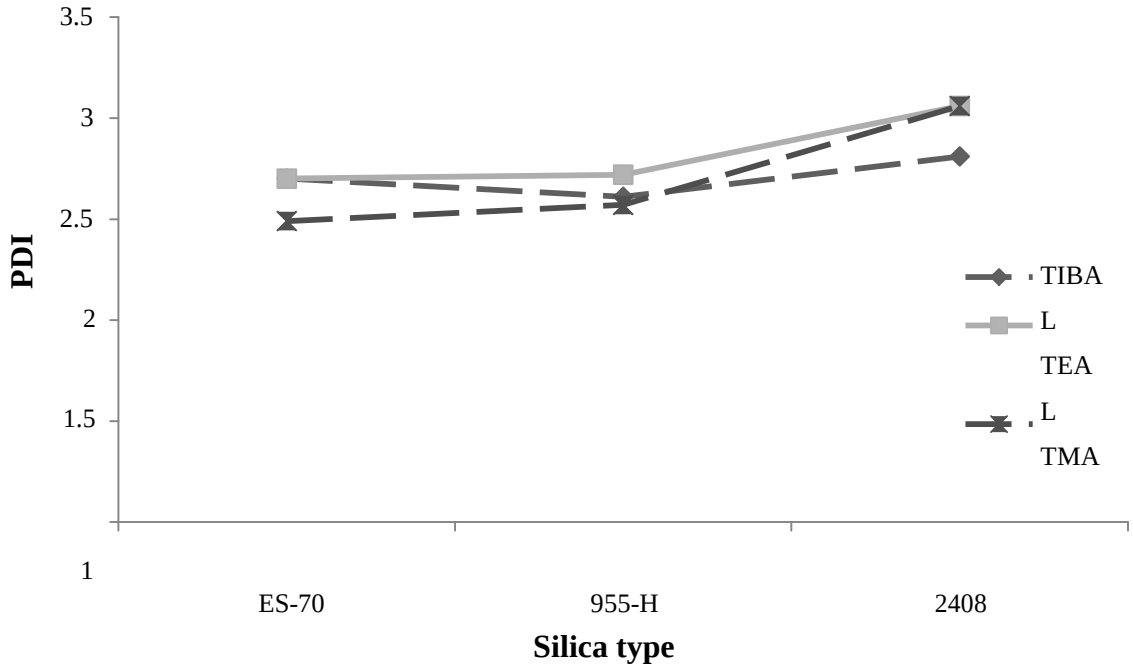

Figure 5.6: PDI of polymers produced with different co-catalysts and different silica types

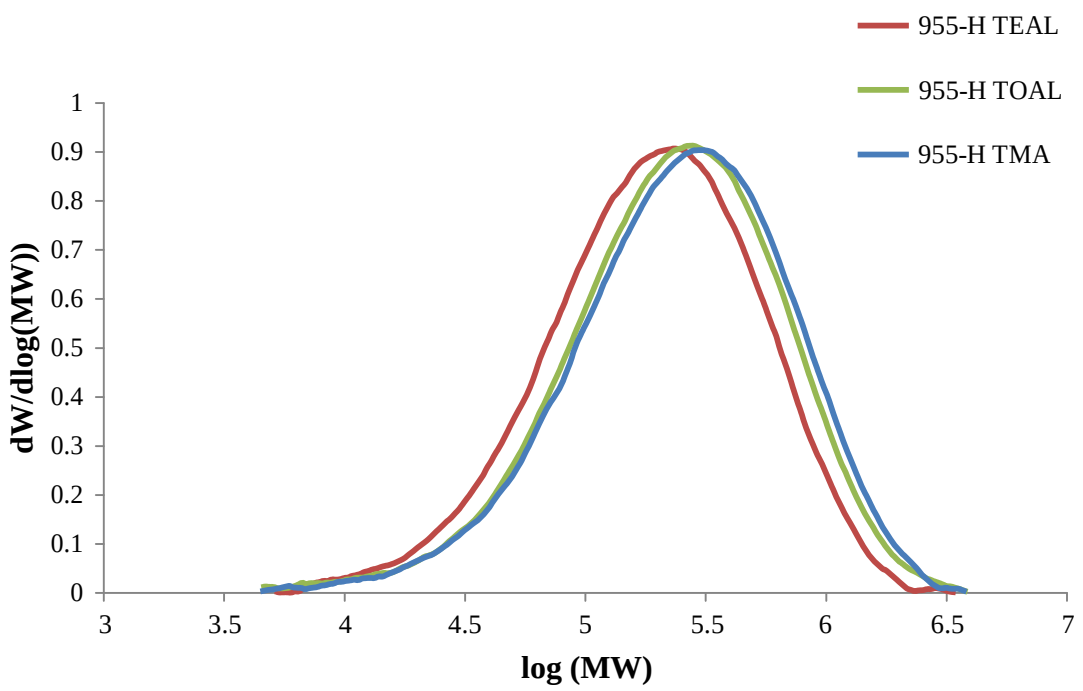

Figure 5.7: MWD of homo-polymer produced from catalyst supported on silica 955W with different co-catalyst types

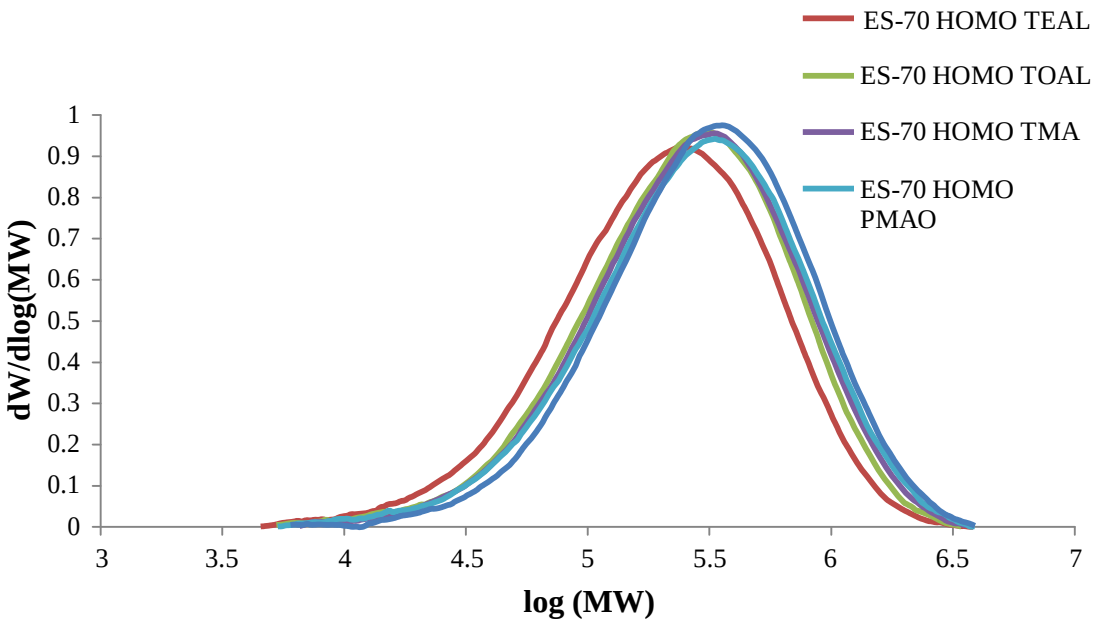

Figure 5.8: MWD of homo-polymer produced from catalyst supported on silica ES-70 with different co-catalyst types

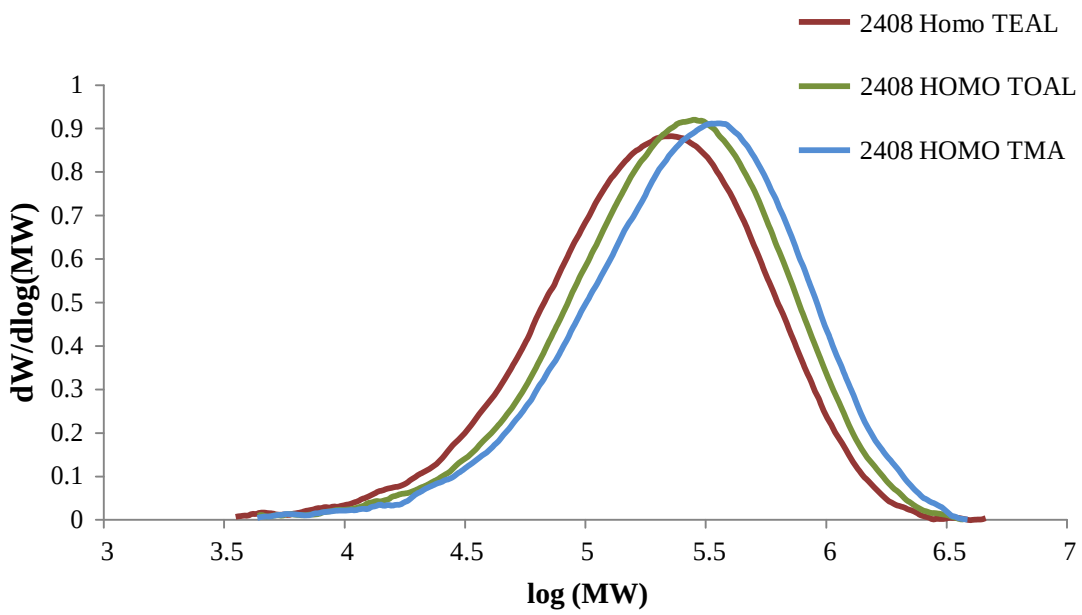

Figure 5.9: MWD of homo-polymer produced from catalyst supported on silica 2408HT with different co-catalyst types

5.2.2 CEF Analyses

The CEF results also showed that the type and size of the silica particles used to support Cp_2ZrCl_2 had no effect on the crystallization behavior of the resulting homopolymers, as shown in Figures 5.10 and 5.11. Since, these homopolymers had no short chain branching (SCB) and CEF fractionate the polyethylene according the SCB.

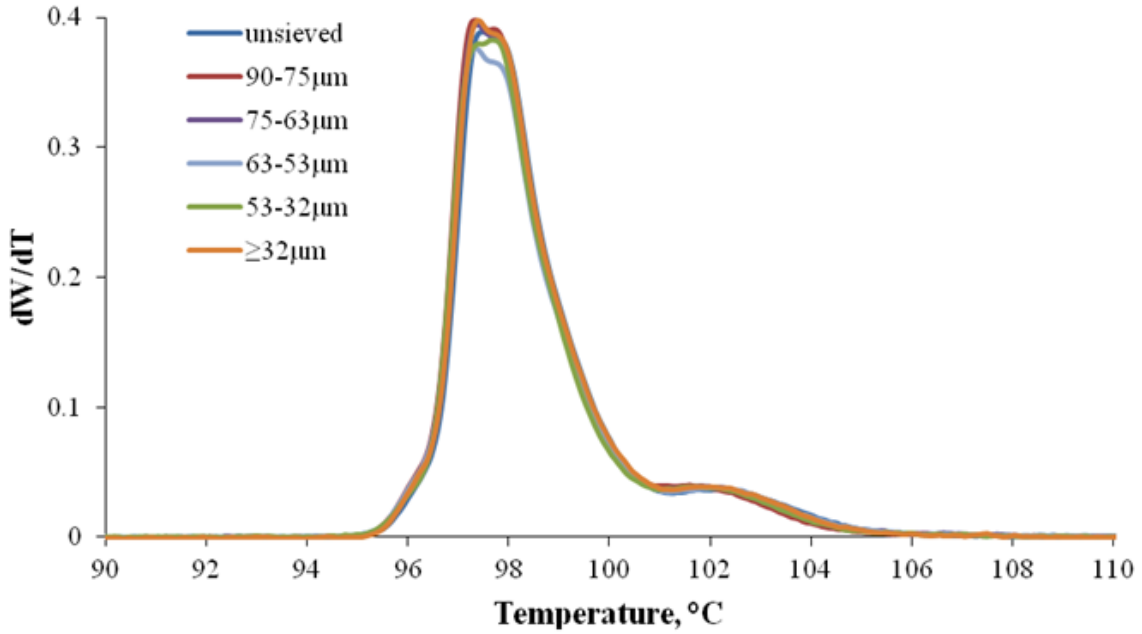

Figure 5.10: CCD of homo-polymers produced with catalyst supported on ES-70 silica [Rxn Temp.: 75 C, C_2Press: 190 psig, Cat.: Cp_2ZrCl_2/PMAO, Scav: TIBAL]

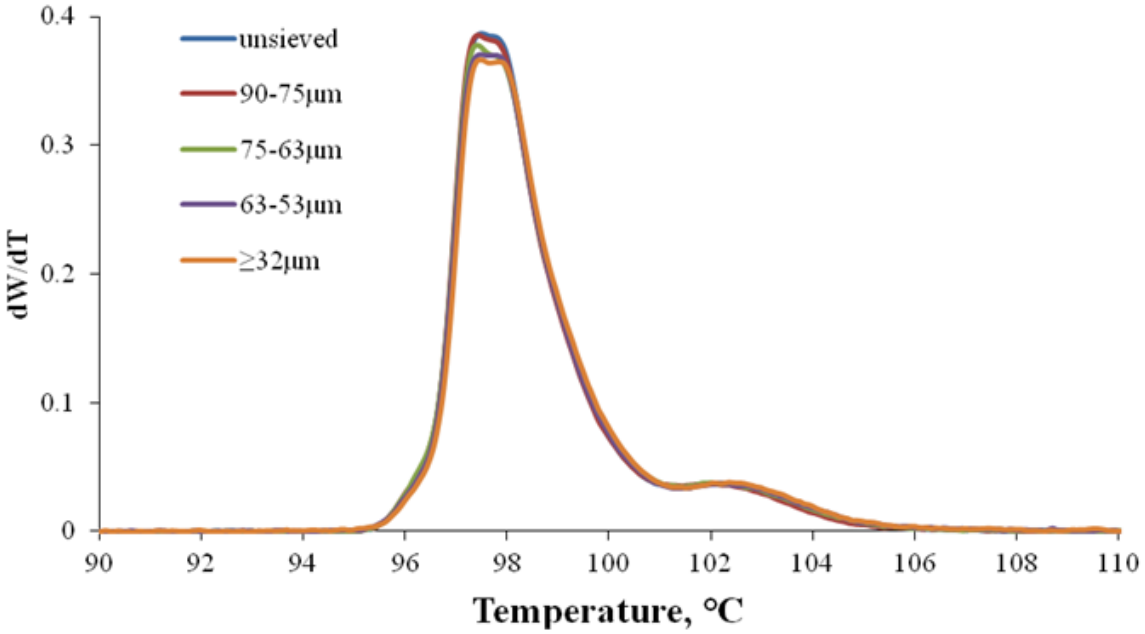

Figure 5.11: CCD of homo-polymers produced with catalyst supported on 2408HT silica [Rxn Temp.: 75 C, C_2Press: 190 psig, Cat.: Cp_2ZrCl_2/PMAO, Scav: TIBAL]

Therefore, copolymerization was needed to study the effect of the silica support on CCD based on the SCB in the produced polymer. As mentioned in chapter 4, different levels of 1-hexene was tested and Figure 5.12 shows the CEF analyses for these copolymers. As expected, the results show that the crystallinity depends strongly on the level of comonomer in the copolymer. Another interesting point is the fact that the high temperature shoulder appeared in the homopolymer samples, but it disappeared as more and more comonomer is incorporated.

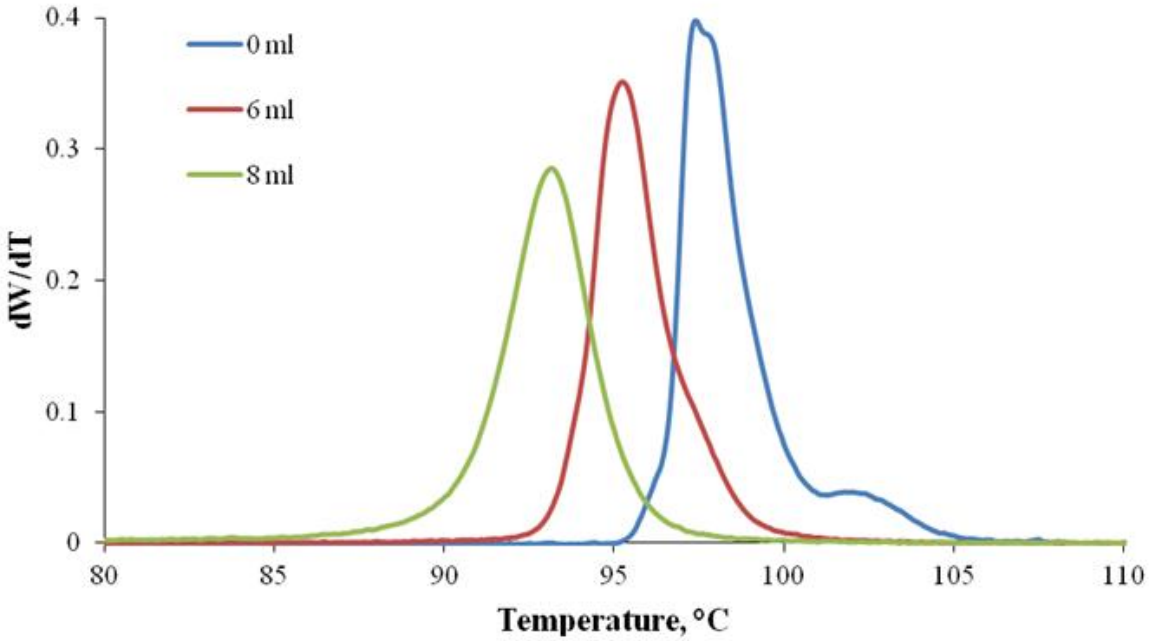

Figure 5.12: CCD of polymers produced from catalyst supported on ES-70 with three different 1-hexene levels [Rxn Temp.: 75 C, C_2 Press: 190 psig, Cat: Cp_2ZrCl_2/PMAO, Scav.: TIBAL]

Figure 5.12 compares the CEF profiles of the samples (homopolymer, 6ml and 8ml of 1-hexene) equivalent to (0 mol/L, 0.32 mol/L, 0.43 mol/L) concentration respectively. The CCDs of the polymers produced with Cp_2ZrCl_2/PMAO supported on ES-70 silica tend to broaden as the comonomer content increases, as also seen in TREF and CRYSTAF

analyses [75, 76], and as expected theoretically. For the homopolymer sample, a small peak was observed at high temperature (102 °C) when the sample was analyzed using the fast cooling rate of 1 °C/min. At this cooling rate, the highest molecular weight fraction of the homopolymer resin is separated first from the other lower molecular weight fractions. This anomalous effect can be eliminated by using slower cooling rates [73], but is not relevant for copolymer samples.

Slight differences in the CCDs of copolymers produced on the different silicas are presented in Figure 5.13. Catalyst supported on silicas 955W and 2408HT made polymer with slightly broader CCD than that supported on ES-70, perhaps because their higher pore volume and surface area (and some variation in surface chemistry) affect the diffusion of the MAO and Cp_2ZrCl_2 during the catalyst supporting process. On the other hand, silica ES-70, which has the lowest pore volume and surface area, produced a polymer with narrowest CCD, as well as with slightly narrower MWD, perhaps pointing towards a higher uniformity of this silica support surface.

The CEF results also indicated that the copolymer produced with Cp_2ZrCl_2 supported on ES-70 has slightly higher comonomer incorporation (lower CEF elution temperatures) than that made with 955W and 2408HT supports, but the reasons for this phenomenon are not clear from the data acquired during the present investigation.

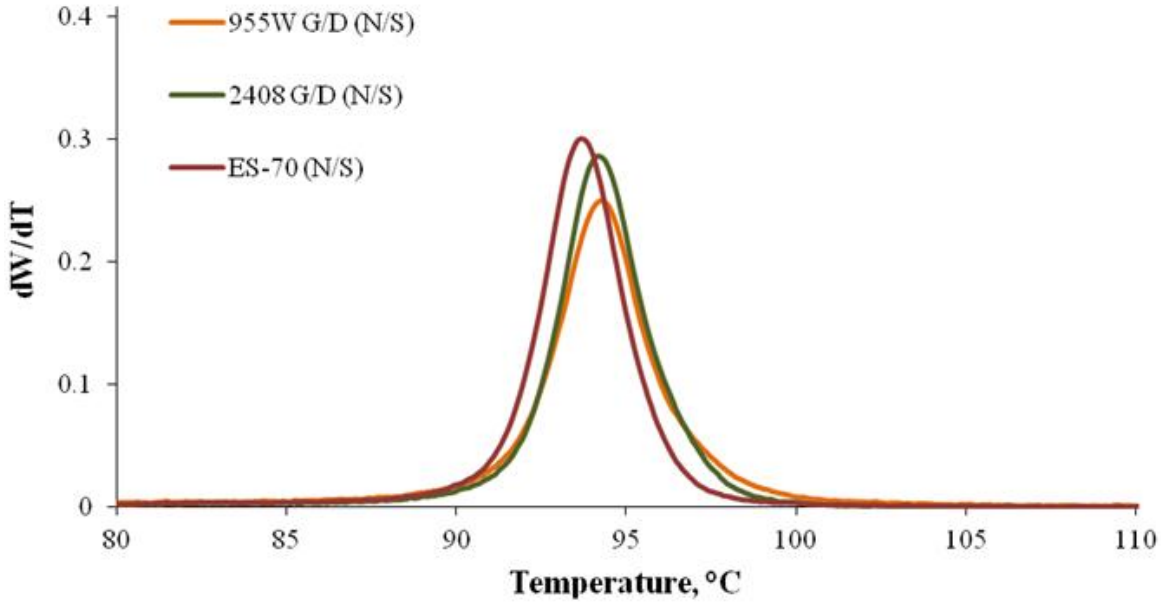

Figure 5.13: CCD of copolymers copolymers produced with catalyst supported on catalysts supported with different silica types [Rxn Temp.: 75 C, C_2Press: 190 psig, Cat: Cp_2ZrCl_2/PMAO, Scav: TIBAL]

The second part of this investigation was to explore the influence of the silica support size on CCD. As mentioned above, a fixed amount of 1-hexene was used with all of the experiments and all the other conditions remained the same as in the reference run defined in Chapter 4 in order to study the effects of the support size.

CEF results in Figures 5.14-16 show two reasonably well-defined curve families: one for the large diameter particles, and another for the smallest diameter particles (53-32µm and ≥32µm). The CCD for the polymer made with the catalyst supported onto the unsieved silica particles coincide with that of the large diameter particles. The difference is less distinct for Cp_2ZrCl_2 supported on silica 955W, where only particles with diameters smaller than 32 µm had a different CCD from the rest. In all, polymer made with the two smallest particle sizes had narrower CCDs with peak temperatures shifted towards higher

temperatures, indicating lower 1-hexene incorporation. The differences in the pore volume and other physical properties between these cuts might affect the loading of the Cp_2ZrCl_2 and/or MAO during supporting, or the diffusion of 1-hexene during polymerization which may create a concentration gradient across the catalyst particle leading to this behavior [79] [78].

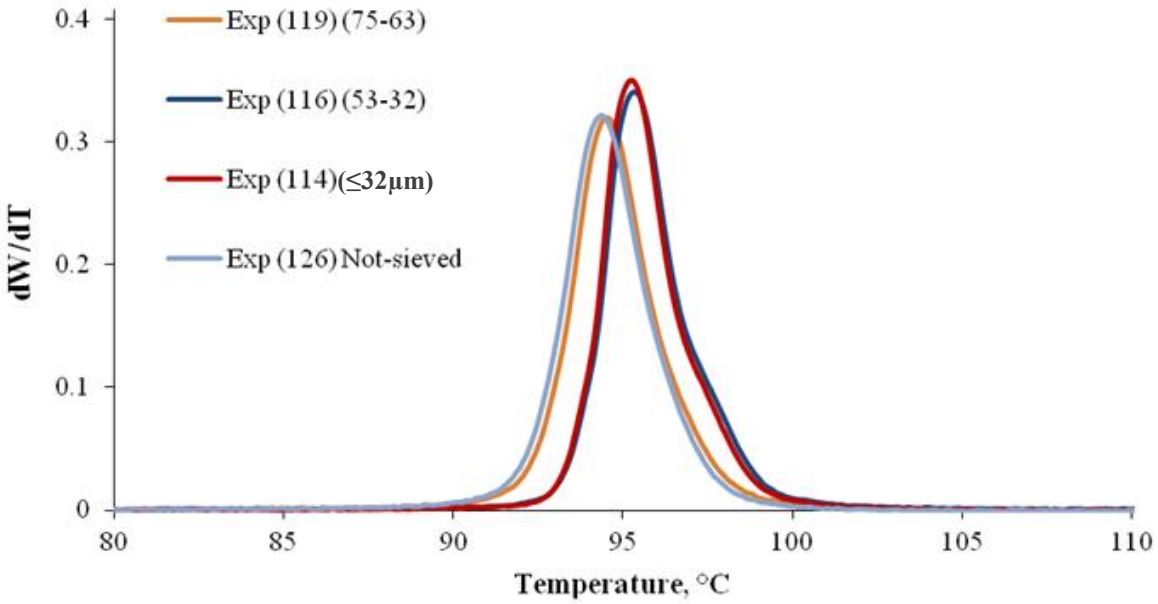

Figure 5.14: CCD of copolymers produced with ES-70 silica having different particle sizes cuts [Rxn Temp.: 75 C, C_2 Press: 190 psig, Cat.: Cp_2ZrCl_2/PMAO, Scav: TIBAL]

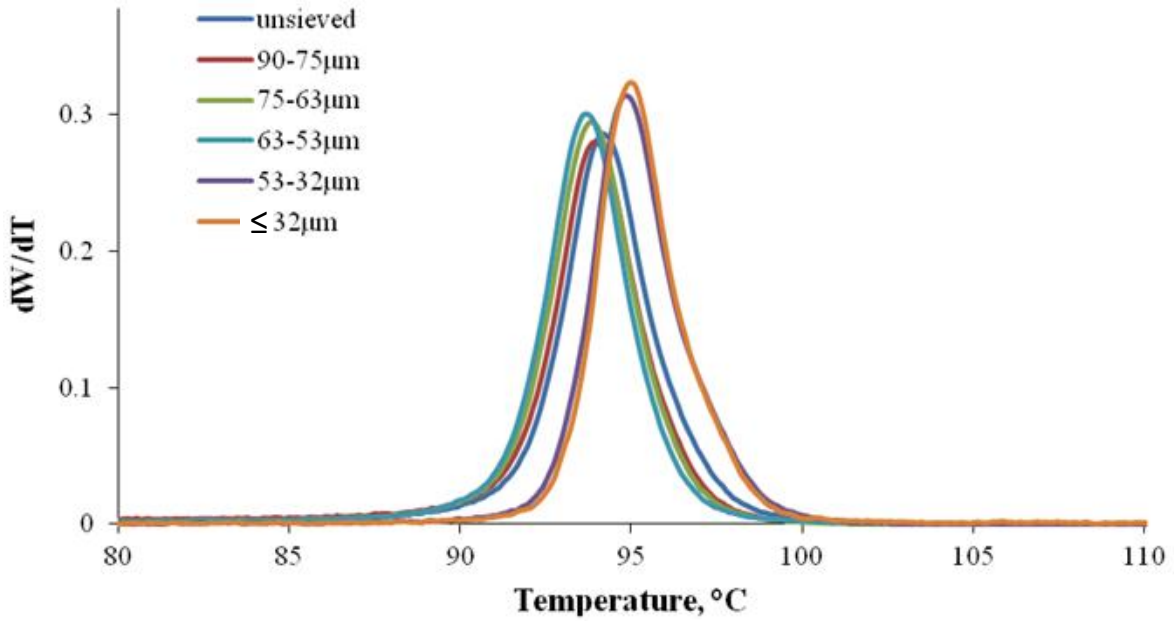

Figure 5.15: CCD of copolymers produced with catalyst supported on 2408HT silica having different particle sizes cuts [Rxn Temp.: 75 C, C_2Press: 190 psig, Cat: Cp_2ZrCl_2/PMAO, Scav: TIBAL]

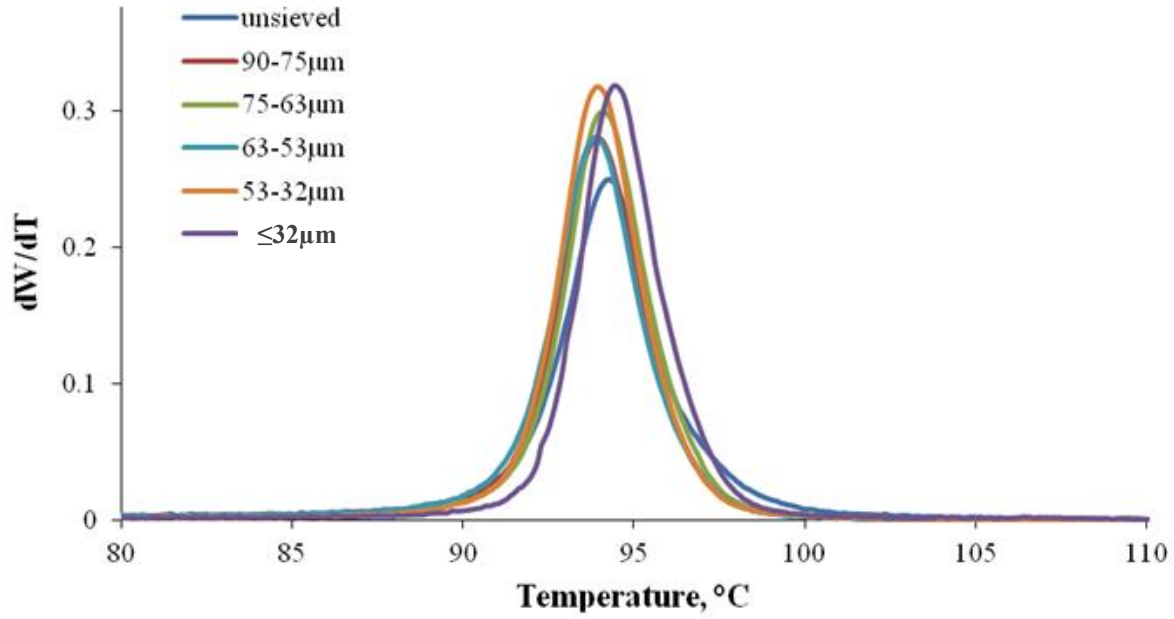

Figure 5.16: CCD of copolymers produced with catalyst supported on 955W silica having different particle sizes cuts [Rxn Temp.: 75 C, C_2Press.: 190 psig, Cat.: Cp_2ZrCl_2/PMAO, Scav.: TIBAL] .

Finally, CEF was used to investigate whether cocatalyst type influenced polymer CCD. Analyses were performed on catalysts supported on 955W, using selected cocatalysts polymerized under the same conditions. The results are shown in Figure 4.18. Clearly, changing alkyl aluminums under fixed experimental conditions with Cp_2ZrCl_2 supported on silica 955W had no appreciable effect on the CCD.

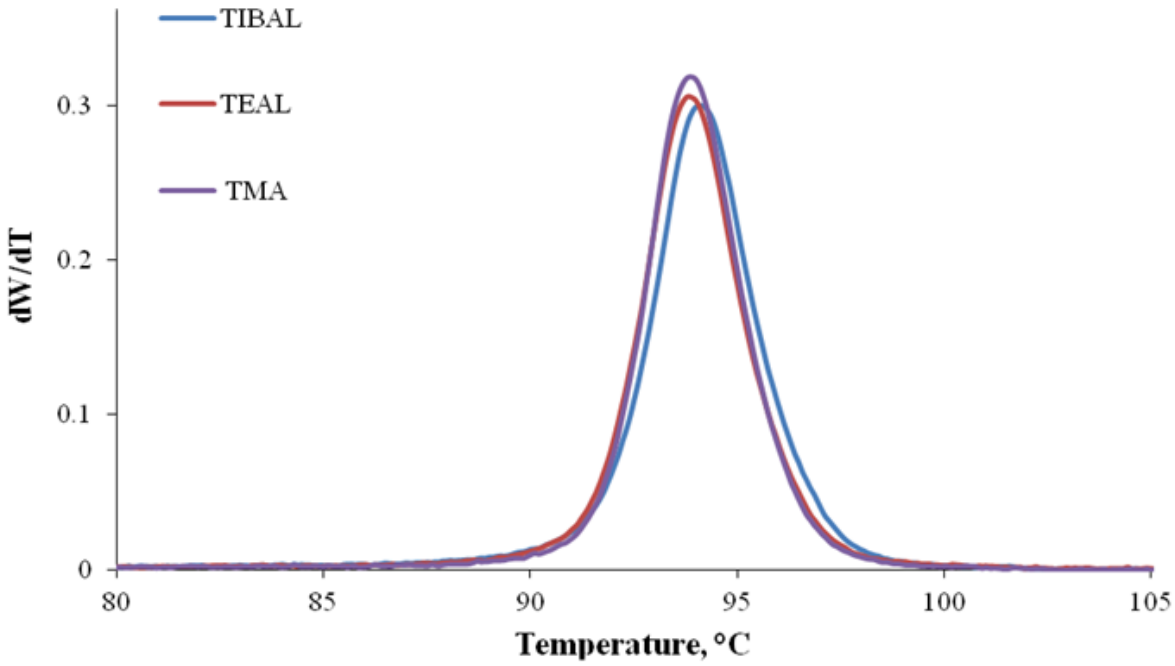

Figure 5.17: Comparison in CCD between co-polymer produced with catalyst supported on 955W silica with different co-catalysts [Temp.: 75 C, C_2Press: 190 psig, Cat: Cp_2ZrCl_2/PMAO]

5. 3 Conclusions

In this chapter, we investigated the impact of the catalyst support and co-catalyst type on the microstructure of the polymers produced in Chapter 4. A single site catalyst (Cp_2ZrCl_2) was supported on different silica types with different particle sizes. All the catalysts were prepared with the same technique, and then also polymerized under the same conditions to explore the effects of the support on PDI, Mn, and Mw.

The experiments indicated that the silica types had no clear effect on M_n, M_w and consequently PDI. The effect of different co-catalysts was also studied with the different silicas. Once again, there was no apparent effect on the PDI. However, when TEAL was used as a co-catalyst, slightly lower values of Mw and Mn were observed for each of the different supports. This suggests that chain transfer to TEAL is more prevalent than the other alkylalumina. Also, Cp_2ZrCl_2 supported on 2408HT tend to produce polymers with a slightly broader MWD than other silicas with all of the used cocatalysts.

The CEF results did not show any difference in the CCD of the homopolymers. In the case of copolymers, there were very slight differences in the CCD as a function of the silica type. However, it was interesting to note that the CCD of the small particle cuts were narrower and shifted to a higher temperature (i.e. less comonomer) than all of the other cuts. Finally, the co-catalyst type had no effect on the CCD under the same polymerization conditions.

Chapter 6

Conclusions and Recommendations

During this research many physical supporting techniques were tested to find out the optimum technique for supporting Cp_2ZrCl_2 on used pours silicas. Many supporting temperatures, time, and Al/Zr ratios were tested to achieve the best activity, morphology control, and reactor processability. The experiments showed good reproducibility with relatively good activity. The same supporting technique was implemented to all of the silicas.

The BET was used to measure pore volume and surface area of the silicas. The BET results indicated that, ES-70 had the lowest pore volume and surface area. The BET also showed that, the particle size of the silica slightly affects the pore volume and surface area. In addition, it had been found that, the smallest cut had the lowest pore volume and surface area.

ICP was used to measure the metal loading in the catalyst in order to understand the effects of the silica type and size on it, and how that will affect the activity and product morphology. The ICP results showed that, the silica 955W had the highest level of Zr loading corresponding with its high activity. Also, findings indicated that the silica with high pore volume and more surface area, allowed more Cp_2ZrCl_2 and MAO to diffuse

within it. Also, 955W silica had the lowest average particle size that may increase the metal loading. This was supported by the results that indicated that the smallest cut of the 955W silica had the highest Zr load and activity.

TGA results pointed out that each silica had different levels of hydroxyl groups. Also, it indicted that the detachment mechanism of the hydroxyl groups varied with the pore volume and surface area. The experiments concluded that, the silica with low pore volume tends to lose the OH group slowly, at a relatively high temperature. In addition, different silica particle size did not show a clear effect on the removed mount of the hydroxyl groups.

Different silica types generated different kinetic profiles. The ES-70 showed more induction time to reach the highest activity, which could be related to less surface area and pore volume, as it was approved in the literature [17, 18]. The induction time at the beginning of the reaction could be due to more monomer diffusion resistance and slower fragmentation. Findings concluded that, the silica with high pore volume and surface area such as 955W tends to have high activity. The same thing was noticed with all of the 955W cuts with different particle sizes, that they had this high activity.

A general behavior was noticed with all of the three silica types, that all of the cuts with different particle sizes had similar activity, except the smallest cuts ($\leq$ 32 µm) which had

a much higher activity. These findings matched the literature [67]. Smaller particle sizes have higher activity due to less diffusion resistance, and more surface area which exposed more active sites on silica with the same catalyst loading.

The effects of the silica types were also clear on the morphology of the produced polymers. Two main factors had the major influence on resin morphology: first is the physical property of the silica support in terms of the pore volume and surface area. The second is the catalyst activity and active sites/activator distribution through the particles. A high degree of fragmentation was noticed in the 2408HT product, which generated more fines that produced a high bulk density. While, ES-70 silica showed different fragmentation with less big deep cracks in the particles that could be related to its small pore volume. The 955W silica had a higher pore volume than the other silicas. However, it still had more controlled fragmentation associated with high activity and bulk density.

The highest activity was achieved with MAO, but with very bad morphology and severe reactor fouling. Both TMA and TOAL produced higher activity than TEAL and TIBAL, however with poor morphology and low bulk density.

The morphological analysis showed that TEAL produced the best morphology with the highest bulk density. Also, the TEAL product had a smoother surface compared with the

TOAL and TMA products. Rough polymer surfaces were always associated with a leaching problem during polymerization, and producing lower bulk density. All the silica types responded similarly to each type of co-catalyst.

This research investigated the effects of the catalyst support on the kinetics and micro properties of produced polymers. A single site catalyst (Cp_2ZrCl_2) was supported on different silica types with different particle sizes to explore the effects of the support on PDI, Mn, and Mw. The experiments indicated that, the silica type and silica size had no clear effect on the MWD, Mn, and Mw. However, more comonomer response was noticed with silicas having high pore volume and surface area. This may be due to less comonomer diffusion resistance and more chain transfer to comonomer that was reflected on the MWD, and was clearer in the Mn. Thus, different co-catalysts had no effect on the PDI. However, TEAL tends to produce lower Mw and Mn with all of the silica types, indicating more chain transfer to co-catalyst with TEAL.

Different silica types indicated sort of an effect on CCD. The differences in CCD matched the differences in the MWD of these polymers. This variation in CCD and MWD could be related to the pore volume of the silica. Silicas with higher pore volume tends to produce broader CCD and MWD, which may be related to higher comonomer concentration inside the particle due less mass transfer resistance. Also, it seems that the smallest cut from all of the silica types had narrower CCD, indicating less comonomer

incorporation and corresponding with the small pore volume in these cuts. The co-catalyst type had no effect on the CCD under the same polymerization conditions.

6.1 Recommendations

The physical properties of the silica support have showed a significant effect on the catalyst performance and polymer properties. Silica 955W had the best performance and it seems to be the best silica among the three silicas used. It produced the best activity and morphology and had the best operational features. Smaller particle sizes produced higher activity, therefore the silica average particle size and particle size distribution have to be very well controlled during the silica manufacturing to suit the targeted application. Silica with smaller average particle size is recommended with slurry processes; since there is no heat transfer limitation and particles are carried over as in the gas phase process. Different alkyl aluminums showed different kinetics and morphology control. Based on the experimental results, TIBAL and TEAL are recommended as co-catalysts with supported Cp_2ZrCl2 on silica.

Each silica type should be dehydrated based on its physical properties. TGA is considered one of the best recommended techniques to understand the dehydration behavior. Therefore, the dehydration profile will be designed based on the TGA analysis. Also, CEF is a powerful new technique to study and understand the response of the catalyst to the comonomer. Also, the CEF technique is a highly reproducible, that can perform experiments in a short time compared to other conventional techniques.

References

1. http://www.sriconsulting.com
2. Frosch, R.A. and N.E. Gallopoulos. Sci. Amer., **1989**, 261, 144-152.
3. Galli, P. and G. Vecellio. Prog. in Poly. Sci., **2001**, 26,1287- 1336.
4. Galli, P. and G. Vecellio. Jour. of Poly. Sci., **2004**, 42, 396-415.
5. Tannous, K. and J.B.P. Soares,. Macro. Chem. and Phy., **2002**. 203, 1895-1905.
6. Romano, U. and F. Garbassi,. Pure and App. Chem., **2000**, 72, 1383-1388.
7. Xie, T.Y., et al.,. Indus. And Eng. Chem. Res., **1994**, 33, 449- 479.
8. Andersson, L.H.U., B. Gustafsson, and T. Hjertberg,. Polymer, **2004**. 45, 2577-2585.
9. www.chemsystemscom, Chem. Sys. Prep Prog., **2008**, PREP, 07/08-1.
10. www.lyondellbasell.com, *Hostalen Process and Services.*
11. Sever, J.R, J.C Chadwick, R. Duchateau, and Friederichs. Chem. Review, **2005**, 105, 4073 – 4147.
12. Choi, K.Y. and W.H. Ray,. Jour. of Macro. Sci. Rev. in Macro. Chem. and Phy., **1985,** 1-55.
13. Severn, J.R., et al.,. Chem.Rev., **2005,** 105, 4073- 4147.
14. Schuster, C.,ExxonMobil high pressure technology for LDPE, Technology licensing executive summery **2006**.
15. Ihler, R.K, Polym. Sci. **1970**, 8, 2637.
16. McDaniel, M.P.. D.R. Witt, E.A. Benham, J. Catal, **1998**, 176, 344.
17. McDaniel, M.P., k.S. Collins, J. Polym. Sic. **2008**, 47, 845-865.
18. Severn, J.R., J.C. Chadwick, Tailor-Made Polymer, Wiley-VCH, **2008**.
19. Ellsworth, G. A. , U.S. Patent 3,526,603, **1970**.
20. Patrick, W.A., U.S. Patent 1,297,274, **1979**.
21. Iler R.K. The Chemistry of Silica, Wiley, **1979**, 886.
22. Breslow, D.S., N.R. Newburg. Amer. Che. Soc., 79, 5072 – 5073.
23. Fink G., B. Steinmetz, J. Zechlin, C. Przybyla, B. Tesche, *Chem. Rev.* **2000**, *100*, 1377-1390.

24. Exxon, U. S. Patent 4701432(**1986**), Exxon Chemical Patents Inc., inv.: C. Howard, Welborn.
25. Patent Cooperation Treaty PCT/US94/07232(**1994**), Mobile Oil Corp., L. O., Frederick, Yip-kwai.
26. Chen, E. Y. X. and T. J. Marks. Chem. Rev., **2000**, 100, 1391 – 1434.
27. Sinn, H., W. Kaminsky, and W. Hoker. Macro. Symposia 97, **1995**, 1995.
28. Srinivasa, R.S., S. Sivaram. Prog in Poly. Sci., **1995**, 20, 309 – 367.
29. A.R., R.A. Newmark, W.M. Lamanna, and J.N. Schropfer. Polyhedron,**1990**, 9, 301 – 308.
30. Siedle, A.R., R.A. Newmark, W.M. Lamanna, and J. Stevens, and M. Ryan. Macro. Symp., 66, 215 – 225.
31. Zurek, E. T., Ziegler. Prog. Polym. Sci., **2004**, 29 107–148.
32. Sugano, T., Matubara, T. Fujta, and T. Takahashi. Jour. of Molec. Cat., **1993**, 82, 93 – 101.
33. Resconi, L., S. Bossi, L. Abis. Mcro., **1990**, 23,, 4489 – 4491.
34. Giannetti, G., P. Pino, G. Mazzanti, and U. Giannini. Our. Of Amer. Che. Soc., **1985**, 79, 2975 – 2976.
35. Chien, J.C.W., B. Wang. Jour. of Poly. Sci., **1988**, 3089 – 3102.
36. Tritto, I., R. Donnetti, M.C. Sacchi, P. Locatelli, and G. Zannoni. Macromolecules, **1997**, 30, 1247 – 1252.
37. Exxon, U. S. Patent 4701432(1986), Exxon Chemical Patents Inc., inv.: C. Howard, Welborn
38. Schneider H.; G. T. Puchta; F. A. R. Kaul; G. R. Sieber; F. Lefebvre; G. Saggio; D. Mihalios; W. A. Herrmann; J. M. Basset *J. Mol. Catal. A: Chem.* **2001,** *170*, 127-141.
39. C. Alonso, A. Antiñolo, F. C. Hermosilla, P. Carrión, A. Otero, J. Sancho, E. Villaseñor, *J.Mol. Catal. A: Chem.* ***2004****, 220, 286-296.*
40. S. Collins, W. M. Kelly, D. A. Holden, *Macromolecules* **1992**, *25*, 1780-1785.
41. L.M.T. Simplicio; F. G. Costa; J. S. Boaventura; E. A. Sales; S. T. Brandão *J. Mol. Catal. A. Chem.,* **2004,** *216*, 45-50.

42. U. S. Patent 5635437(1997), Exxon Chemical Patents Inc., inv.: T. J. Burkhardt, W. B. Brandley.
43. Laurence, R.L. and M.G. Chiovetta. Poly, Reac. Eng., **1983**, 74, 111.
44. Abboud, M., P. Denfi, and K.H. Reichert. Macro. Mate. And Eng., **2005**, 290, 558 – 564.
45. U. S. Patent 5767300(**1998**). LG Chem, inv.: B. Y. Lee.
46. Hoechst, U. S. Patent 5767300(1998).
47. L. H. Dubois; B. R. Zegarski, J. Am. Chem. Soc. **1993**, 115, 1190-1191.
48. Choi Y., J. B. P. Soares The Canad. Jour. Of Chem. Eng. **2011**, DOI: 10.1002/cjce.20583.
49. European Patent 839836(**1997**). Repsol, inv.: A. M. Lafuente, P. L. Canas, J. S. Royo, B. G. Begona, M. F. M. Nunez, C. M. Marcos.
50. D. H. Lee, H. B. Lee, S. K. Noh, B. K. Song, S. M. Hong, *J. Appl. Polym. Sci*. **1999**, *71*,1071-1080.
51. Jang, Y.J., K. Bieber, C. Naundorf, N. Nevov, M. Klapper, K. Mullen, D., D Ferrari, S. Knoke, and G. Fink. E-polymer, **2005**, 013, 1 – 13.
52. Abboud, M., P. Denfi, and K.H. Reichert. Macro. Mate. And Eng., **2005**, 290, 558 – 564.
53. Conner, W.C., S.W. Webb, P. Spanne, and K.W. Jones. Macromolecules, **1990**, 32, 4742 – 4747.
54. Jones, K., P, Spanne, S.W. Weeb, W.C. Conner, R.A. Beyerlein, W.J. Reagan, and F.M. Mautzenberg. Nucl. Inst. And Meth. In Phy. Res., **1991**, B56/57, 427 – 432.
55. Ferrero, M.A., R. Sommer, P. Spanne, K.W. Jones, and W.C. Conner. Jour. of Poly. Sci.,31, 2507 – 2512.
56. Tisse V.F., F. Prades, Ch. Boisson, T.F.L. McKenna. Macromol. Chem. Phys., **2010**, *211*, 91.
57. DiMartino, A., J.P. Broyer, R. Spitz, G. Weickert, T.F. McKenna. Macromol. Rapid. Commun., **2005**, 26, 215-220.
58. Tioni E., R. Spitz, J.P. Broyer, V. Monteil, T.F.L. McKenna. AIChE J, **2011**, DOI: 10.1002/aic.12576.

59. Zheng, X., Madri S., Chadwick J. C., J. Loos. *Macro.* **2005,** *38,* 4673-4678.
60. Ferrero, M.A., E. Koffi, R. Sommer, and W.C. Conner. Jour. of Poly. Sci., **1992**, 30, 2131 – 2141.
61. Alizadah A., F. L. McKenna. Review article. to be published soon.
62. Webb, S.W., Weist E.L., Chiovetta M.G., Laurence R.I and Conner W.C. The Canad. Jour. Of Chem. Eng., **1991**, 69, 665 – 681.
63. McDaniel, M.P. Jour. of Poly. Chem. Eng., **1981**, 19, 1967 – 1976.
64. McDaniel, M.P. Advance in Cat, **1985,** 33, 47 – 97.
65. Kumkaew P., Wanke S.E., Prasertham P., and Kaliguine S. Jour. of App. Poly. Sci., **2003**, 87, 1161 – 1177.
66. Kumkaew P., Wu L., Wanke S.E., Prasertham P. polymer, **2003**, 11, 4791 – 4803.
67. Fink, G., B. Steinmetz, J. Zechlin, C. Przybyla, and B. Tesche. Chem. Rev., **2000**, 100, 1377 – 1390.
68. Floyd, S., Choi, K.Y, Taylor, T.W., & Ray, H.W. *Jour. of Appl. Poly. Sci.*, **1986**, 31, 2231-2265.
69. Patent Cooperation Treaty PCT/US94/07232(**1994**), Mobile Oil Corp., L. O., Frederick, Yip-kwai.
70. Stefánsson A, I. Gunnarsson, N. Giroud. *Anal. Chim. Acta, **2007,*** 582, 69–74.
71. Mermet, J. M. *J. Anal. At. Spectrom, **2005**,* 20, 11–16.Brunauer, S., P. H. Emmett and E. Teller. *J. Am. Chem. Soc.*, **1938**, 60, 309.
72. Monrabal, B., J. Sancho-Tello, N. Mayo, L. Romero. Macromol. Symp. **2007**, 257, 71–79.
73. Alghyamah, A. and J. B. P. Soares, , *Macromol. Symp.*,accepted **2011**,
74. Alghyamah, A. and J. B. P. Soares, , *in preparation.*
75. S. Anantawaraskul, J. B. P. Soares, P. M. Wood-Adams, *Adv. Polym. Sci.* **2005**, 182, 1.
76. D. M. Sarzotti, J. B. P. Soares, A. Penlidis, *J. Polym. Sci., Part B: Polym. Phys.* **2002**, 40, 2595.
77. Yiannoulakis, H., A. Yiagopoulos, C. Kiparissides. Chem. Eng. Sci., **2001,** 56 917 – 925.